IMPACT FRACTURE OF AUSTENITIC STAINLESS STEELS

by

Cynthia E. Kornegay

Thesis submitted to the Graduate Faculty of the
Virginia Polytechnic Institute and State University
in partial fulfillment of the requirements
for the degree of

MASTER OF SCIENCE

in

Materials Engineering

APPROVED:

M. R. Louthan, Jr., Chairman

W. R. Hibbard

N. E. Dowling

July, 1985

Blacksburg, Virginia

Acknowledgements

The author would like to express her sincerest gratitude to Dr. M.R.Louthan, Jr., for his many contributions and suggestions throughout this undertaking. His constant help, faith, and wit over the past year of graduate school and four years as an undergraduate were very inspirational and are greatly appreciated.

The author also wishes to extend her thanks to Dr. W.R.Hibbard and Dr. N.E.Dowling for their helpful suggestions and for serving as committee members. Also, thanks are due to Dr. R.E.Swanson for his initial help with this thesis and to Dr. H.R.Forkner for his understanding, listening ear.

Thanks are also in order for: for her speedy help in preparing the thesis, for assisting in impact testing, for helpful suggestions, and finally to for her constant cheer.

Finally, the author wishes to express her deepest thanks to her parents. nd to her fiance . Their encouragement and love was instrumental throughout each stage of this endeavor.

TABLE OF CONTENTS

LIST OF FIGURES

LIST OF TABLES

INTRODUCTION

Industry is constantly searching for improved materials for use in highly demanding applications. The materials chosen must withstand a wide range of temperatures and extended exposure in aggressive environments, including hydrogen gas. Because of the risk of catostrophe if brittle failure occurs, careful material selection is imperative. Austenitic stainless steels may be a likely choice for hydrogen service because their behavior in high pressure hydrogen ranges from no apparent damage to relevent, but generally small ductility loss (13). Because of this variation in behavior, a single category cannot be established to encompass all austenitic steels and studies must be performed on each type of steel to determine its behavior under specific circumstances. Two steels being currently under consideration for use in hydrogen are Armco 21-6-9 and Tenelon, both are fully austenitic stainless steels which may be used over a wide range of temperatures, including service at liquid nitrogen temperature.

Austenitic stainless steels may be processed by high energy rate forging (HERF) to vastly improve strength (33). Proper forging conditions may produce steels with yield strengths above 690 Mpa while maintaining adequate ductility as well as the other desireable characteristics of stainless steels. Studies have also shown that the HERF process can increase the resistance of austenitic steels to hydrogen damage (33, 38). Currently, very high strength austenites have not been used extensively in service because more elaborate testing must be performed to qualify this steel. However, extensive tensile tests of HERF 21-6-9 have been performed (33, 38).

The tensile data for HERF stainless steels include studies of hydrogen effects on mechanical properties; however, very little impact testing data is available. In general, tensile behavior studies have demonstrated that 21-6-9 stainless steel samples precharged with, or tested in hydrogen environments suffer losses in ductility and/or fracture stress (38). Investigators found significant ductility losses in nineteen different heats of 21-6-9 stainless steels tested in high pressure hydrogen (7). These tests and most other studies have been conducted under conditions favoring dynamic hydrogen redistribution during the test (10). According to many

investigators such hydrogen redistribution by dislocation transport plays a critical role in the hydrogen induced degradation of austenitic stainless steels, yet a study of the hydrogen effects on the impact behavior of 304L stainless steel contradicted the need for redistribution (14). Extensive embrittlement was evident in the impact tests at temperatures where hydrogen relocation during testing could not occur (21).

Currently, most investigators will agree that hydrogen embrittlement of austenitic stainless steels is a function of the amount and location of absorbed hydrogen (39). Calculations on hydrogen charged 304L samples found that the hydrogen content was greater in the HERF samples, and that the HERF samples were slightly more susceptable to hydrogen damage (14). Thus, although the need for absorption is well recognized, the role of redistribution has not been established. Therefore, a study was performed on 21-6-9 and Tenelon to evaluate the importance of hydrogen redistribution or hydrogen embrittlement. This important study was conducted over a range of temperatures so that variations in hydrogen redistribution during testing were possible.

LITERATURE SEARCH

Materials with potential for use in low temperature, hydrogen environments include the austenitic stainless steels 21-6-9 or Nitronic 40 and Tenelon. Both of these austenitic stainless steels may be used in the standard or annealed condition, or in the high-energy-rate-forged (HERF) condition. The HERF process typically improves the mechanical properties of these metals. Widespread research concerning the adverse effects of hydrogen on austenitic stainless steels has shown that the nature of hydrogen induced effects is dependent on the specific material tested and the specific test environment. Thus both service conditions and specimen design variables will influence the hydrogen compatability of metal and alloys (2-7). Test or service conditions such as temperature (5), stress state (6, 25, 28) strain rate (4), hydrogen exposure pressure (23), and specimen geometry (7), all influence of degree of hydrogen embrittlement. In addition, design variables including strength (7), microstructure (17), and surface condition (13, 25) effect the materials suseptibility to hydrogen induced effects. The HERF process is of particular

interest because work has shown that steels which were processed by the HERF techniques were less susceptible to hydrogen damage than were steels processed by rolling or other or more standard techniques (39).

The effect of hydrogen on the mechanical behavior of austentic stainless steels have been manifested as reduction in strength and ductility, fracture mode changes and sustained load crack growth (1, 5, 6, 8-16, 19-21, 24). These effects will be discussed as will a general overview of the mechanical properties of austenitic steels and the effects of processing variables on those properties.

GENERAL PROPERTIES & PROCESSING

Tenelon is a nitrogen strengthened iron base alloy containing 18% chromium and 15% manganese and 0.4 to 0.6% nitrogen. The chromium (>16%) generally provides stainless steels with their corrosion resistant properties by forming a self-healing continuous oxide layer over the surface (39). The nitrogen is added to improve strength although an adverse effect of nitrogen on hydrogen embrittlement has been reported (10). The manganese additions which act as replacements for nickel,

are made to help stabilize the austenite phase as well as to increase nitrogen solubility and therefore the strengthening potential (10) However, tests have also demonstrated deleterious effect of manganese on the compatibility of steels with gaseous hydrogen (10). Therefore, trade-offs have been made to increase the strength of the steel at the expense of it's resistance to hydrogen embrittlement.

Tenelon is considered a stable steel thus it does not undergo the strain induced transformation to α-martensite that is common in many 18Cr-8Ni stainless steels (13). The α-martensite is an undersireable structure for materials which will experience hydrogen exposure because this structure is highly susceptible to hydrogen induced ductility losses (4, 5, 13, 31, 38). Investigatores have found however, that this transformation to martensite, which was previously thought to be required for hydrogen embrittlement of austentic stainless steels, was not necessary for such embrittlement to occur (5, 38).

Tensile tests of Tenelon demonstrated that cleavage fracture is promoted by the presence of hydrogen (41). Tenelon has a transition from ductile behavior at room temperature to brittle behavior at 78K. The ductile to

brittle transition may be very rapid and large scale or very slow and shallow depending upon the composition, stress state, and strain rate (42). The ductile to brittle transition is sensitive to the carbon and nitrogen content of the alloy (42). Small changes in carbon content can also markedly change the stress corrosion behavior of Tenelon (10). For example if the carbon content is > 0.1% Tenelon has appreciable stress corrosion cracking resistance but if the carbon content is in the range 0.01-0.05% the resistance is low and the increasing carbon content from 0.04 to 0.05% decreases the stress corrosion resistance. Earlier work speculated that their decrease in resistance is due to interactions of carbon with other interstitials such as nitrogen (43). Similar interactive effects may be found on the DBTT.

Fractograph of the low temperature fracture surfaces developed in tensile tests is characterized by mixed transgranular cleavage and ductile rupture. The planar facets on the fracture surface lie along {111} planes which are the twinning and slip planes for this FCC metal (26, 44). During tensile tests on hydrogen free samples at 200 to 350K, ductile rupture was the sole fracture mode observed (41). At lower temperatures microcracks were generally formed along coherent twin boundaries and

occasionally along grain boundaries (41). The planar cleavage like facets observed on the fracture surfaces of samples tested at these lower temperature microcracks along such twin boundaries. The deformation bands also intersect the microcracks and generated the linear markings on the brittle like facet (Figure 1). Usually, the facets and the microcracks do not extend over more than one grain. Thus it is assumed that the grain boundary inhibits transgranular fracture and ductile rupture may initiate in the surrounding grains. Consequently, the fracture surfaces contain facets encompassed by areas of microvoid coalescence (41.)

Tensile testing is the common mode of testing for the compatibility of a metal with high pressure hydrogen. Therefore the effects of high pressure hydrogen on fatigue and impact behavior of stainless steels have not been extensively studied.

The fully austenitic 21-6-9 or Nitronic 40 is also a nitrogen strengthened stainless steel. Its composition differs from that of Tenelon in that Nitronic 40 contains more nickel (7.1% vs 0.2%) and also contains more chromium but less manganese (Table I) (1, 41). The nitrogen content of Nitronic 40 has a major effect on the mechanical behavior. Higher nitrogen contents strengthen

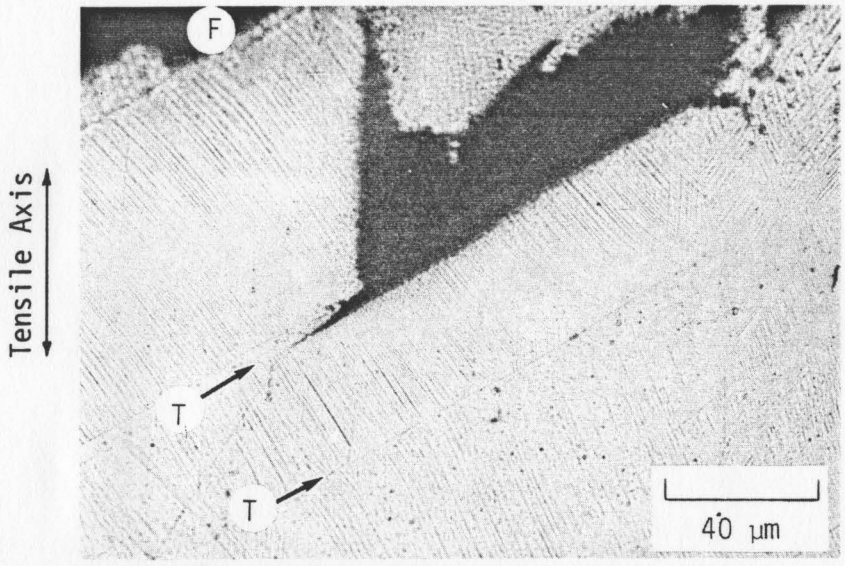

Fracture (F) and Twin Boundaries (T)

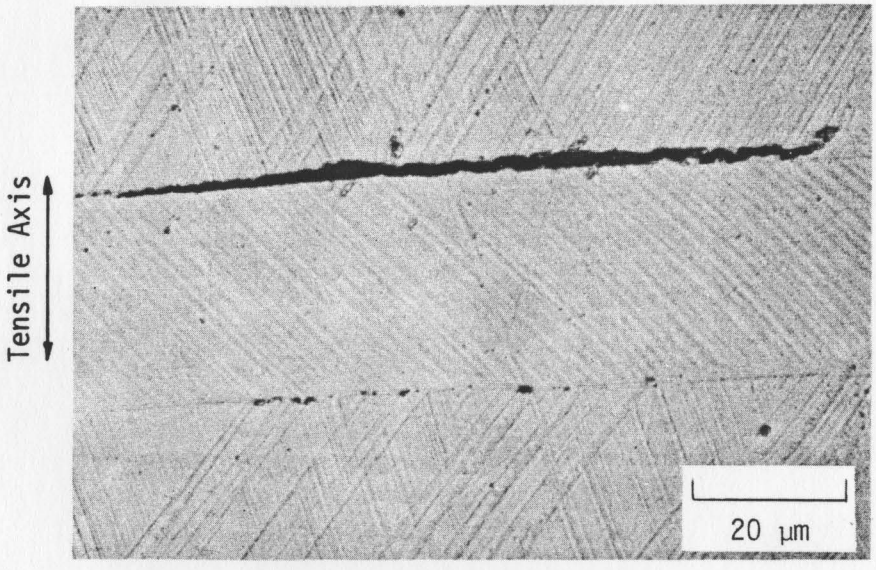

FIGURE 1. Microcracks Along Coherent Twin Boundaries on Longitudinal Section of Fractured Specimen. (11)

TABLE I

Chemical Composition of Tenelon Plate:

Element	Weight %
Chromium	17.44 ±0.06
Maganese	15.31 ±0.20
Nitrogen	0.40 to 0.60
Nickel	0.22 ±0.02
Silicon	0.53 ±0.01
Phosphorus	0.02
Sulfur	0.02
Iron	66.47 ±0.24
Carbon	0.1 maximum

Chemical Composition of Type 21-6-9 Stainless Steel Alloy:

Element	Weight %
Cr	20.20
Ni	7.15
Mn	9.0
Mo	0.20
Cu	0.31
C	0.034
N	0.30
P	0.024
Si	0.74
S	0.005

the alloy and reduces the stacking fault energy, thereby promoting coplanar dislocation motion and a high degree of strain hardening (15, 26). Nitronic 40, however, has a lower nitrogen content than Tenelon and thus because of the importance of interstitials the mechanical behavior of these two steels is quite different.

Tensile tests of 19 experimental heats of Nitronic 40 prepared by a variety of forging processes resulted in studies of samples with a range of strength levels, grain sizes, and microstructures (38). These tests showed that both cold rolling and warm working or HERFing increased the strength above typical annealed values. Microvoid coalescence was the dominant fracture made in all samples which were not charged with hydrogen. However, the working technique and degree of sensitization had major effects on the details of the fracture process (38). Because of processing effects on the distribution of particles which serve as microvoid nucleation sites. When large inclusions were present, large microvoids initiated early in the deformation process and if the distribution of inclusions was directional, tensile instability was promoted or retarded by the inclusion depending on the orientation of the test specimen (38).

HERFing has been a subject included in several investigations (9, 10, 12-15, 21, 30-33, 36, 38-40). The process is a very rapid deformation at elevated temperatures followed by an immediate quench. This process significantly increases the strength of austenitic stainless steels, and thereby expands the useful design range. For austenitic stainless steels, proper HERF processing conditions can double the strength and retaining good ductility as well as the other desireable characteristics of stainless steels (Table II). Additionally, studies have shown that such high temperature deformations can stabilize the austenitic phase (33). Forging by a high energy rate forming process produces a typically cellular dislocation substructure and a very fine grain size (Figure 2). Nitronic 40 exhibits higher strengths in the annealed condition than the 300 series stainless steels because of the nitrogen strengthening and can therefore, because of this intrinsic high strength this steel can be strengthened to an even greater degree via HERFing than the 300 series steels (39). The strength enhancement potential of Nitronic 40 and 22-13-5 by way of a HERF process (32) is sufficient to produce yield strength levels of 120 ksi (827 Mpa) and still retain

Table II (31)

Strengths of Stainless Steels

Material	Condition	Yield Strength* MN/m^2	Yield Strength* ksi	Ultimate Strength MN/m^2	Ultimate Strength ksi
304L	annealed	215	31	575	83
304L	HERF	520	75	675	98
309S	annealed	220	32	595	86
21-6-9	annealed	435	63	690	100
21-6-9	HERF	605	88	795	115
A-286	aged	760	110	1065	154
A-286	HERF & aged	850	123	1105	160
A-286	as-HERF	440	64	750	109

* flow stress at 0.002 plastic strain

Figure 2. Photomicrograph of HERF 316 stainless steel (200X)

High dislocation dense slip bands

High dislocation dense boundaries

Deformed twin boundaries

approximately 21% uniform elongation (32). Metallographic studies showed that the HERFed structure consists primarily of fine twins and a high density dislocation cell structure. In addition, tensile test data show that HERF alloys are more resistant to environmental hydrogen damage than either annealed or cold-worked alloys. This improved resistance has been attributed to the fine structure produced by the forging techniques (40).

Another fabrication variable, sensitization has large scale effects on the mechanical and corrosion behavior. Tensile tests of smooth bar and V-notched specimen showed that a notch reduces the toughness and strength of Nitronic 40, however, the fracture process remained dimpled regardless of the degree of sensitization (45). Most of the mechanical tests were performed at intermediate temperatures (200 to 300K) and very little low temperature data is available. When hydrogen is induced into the steel the deformation and fracture behavior change significantly. These hydrogen induced changes are the subject of the next section of this thesis.

HYDROGEN EFFECTS

A large amount of literature has dealt with the deleterious effects of hydrogen on the mechanical properties of austenitic stainless steels (1, 4-6, 8-17, 20-26, 31-34, 36). However, very little information is available to analyze the hydrogen effects on the impact properties of these steels. Most of the studies that exit deal mainly with the effect of hydrogen on the uniaxial tensile and crack growth behavior. Because this type of investigation composes the majority of literature, a review of some of the relevant studies will be presented. Generally, investigations have shown that stainless steel samples tested in or recharged with hydrogen suffer ductility or fracture stress losses (15, 23). The widespread susceptibility of metals to hydrogen damage is directly related to the easy absorption of hydrogen into metals and the high mobility of absorbed hydrogen. The hydrogen interacts with lattice defects, impurities, and internal boundaries leading to a nonuniform distribution of hydrogen even under equilibrium conditions (40).

Research shows that there is no one physical process that is responsible for hydrogen embrittlement of metals. At least three forms of hydrogen degredation have been identified. They include: hydride embrittlement, hydrogen attack, and hydrogen assisted fracture. Of those three, hydrogen assisted fracture is cause of hydrogen damage in austenitic stainless steels (40). Hydrogen damage is delineated by the existance of a ductility minimum, an inverse strain rate sensitivity, and crack propogation under static load at a stress intensity less than the fracture toughness of the alloy (40). The extent of damage varies greatly depending on the alloy composition, temperature, strain rate, thermomechanical treatment, loading mode, and environment (10, 15, 23, 33, 38, 40).

Hydrogen damage of the Fe-Cr-Ni-Mn class alloys, which include both Tenelon and Nitronic 40, does not correlate uniquely with nickel or equivilent nickel content [Ni + 30 (C + N) + 0.5Mn], as is the case for Fe-Cr-Ni alloys (10, 40). Different alloys produce a wide range of damage susceptibility, Figure 3. The variation in susceptibility may be caused by variations in nitrogen content as documented for Nitronic 40 (22) or by other yet unestablished factors. Higher nitrogen

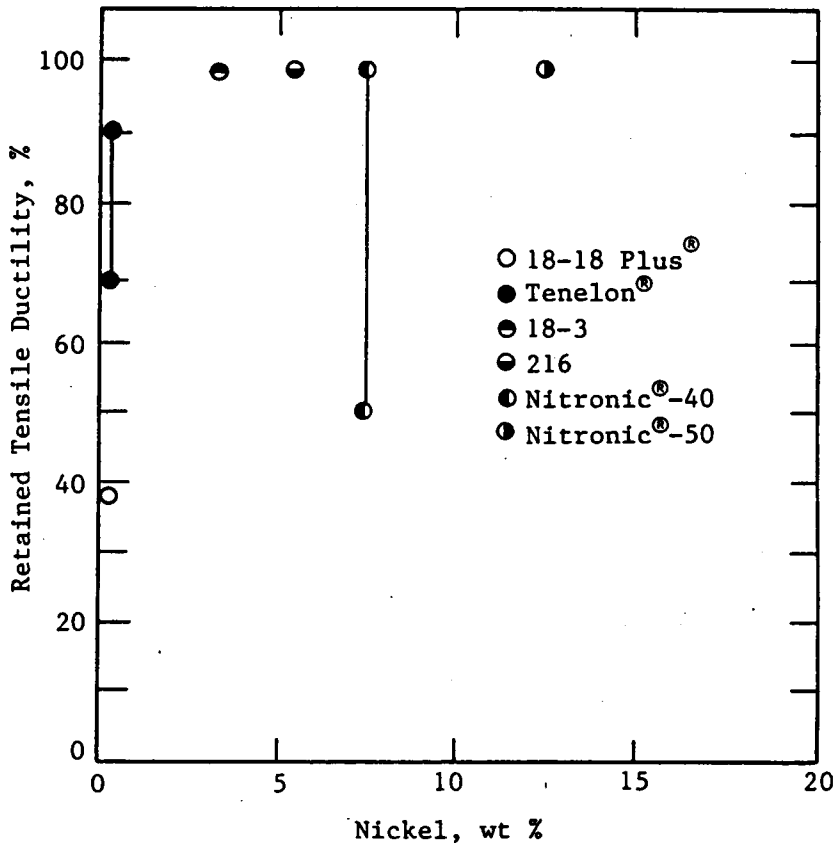

FIGURE 3. Environmental Hydrogen Damage in Fe-Cr-Ni-Mn Alloys at Room Temperature and 69 MPa Hydrogen (40)

contents strengthen the alloy and decrease the stacking fault energy, thereby promoting coplanar dislocation motion (40). Dislocation dynamics have been related to susceptibility to hydrogen damage (24) thus nitrogen may play two roles in the hydrogen induced damage. The higher strength level severely increase damage susceptibility as does coplanar dislocation motion (10). The effect of the other elements on hydrogen embrittlement susceptability of austenitic steels has not been well documented (10, 36, 40).

The temperature dependence of hydrogen damage in stainless steels has been estabilished and is shown schematically in Figure 4. The most severe damage for many austenitic steels occurs at 220-280K (26, 40). Tensile ductility is a minimum for several alloys in this range as evidence in Figure 5 (26, 40). Temperature is also a variable during impact tests in which a ductile to brittle transition takes place. Although not well recognized for the austenitic stainless steels, such transitions are common (23). Hydrogen additions to the metal lattice have been shown to change the DBTT and typically reduce the amount of energy absorbed during fracture (21). This effect will be the major focus of the investigation investigation described in this thesis.

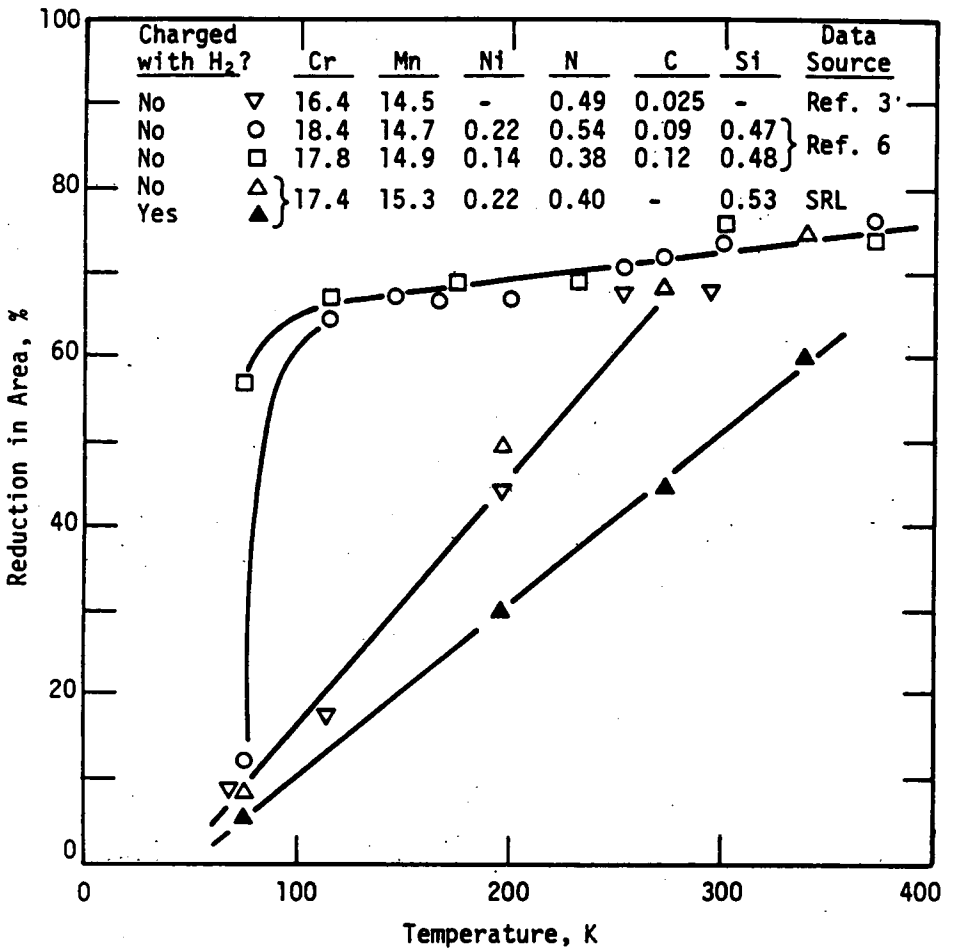

FIGURE 4 Temperature Dependence of Tensile Ductility of Fe-Cr-Mn Alloys (41)

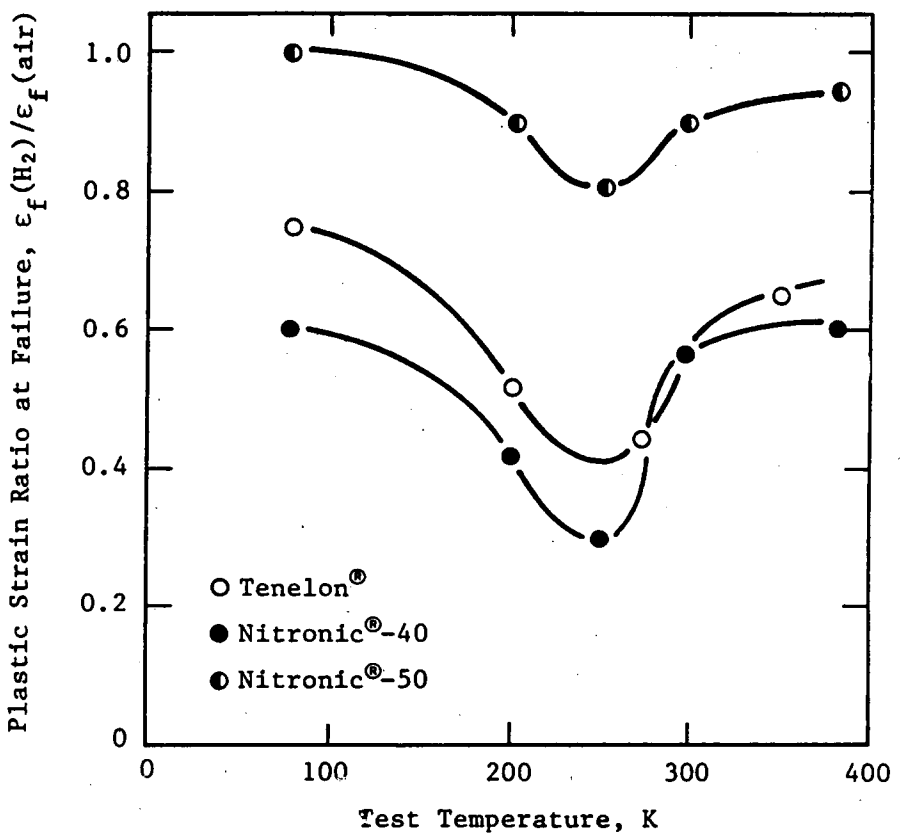

FIGURE 5 **Ductility Minima in Fe-Cr-Mn-Ni Alloys Charged with Deuterium at 69 MPa and 620 K for Three Weeks** (40)

The impact tests also offer evidence for the strain rate sensitivity of the materials. In many studies, the strain rate dependence of hydrogen embrittlement is extremely evident. Tensile tests of tritium charged 304L samples, for example, demonstrated that deformation enhanced tritium release (5) could be correlated with embrittlement susceptibility. A study of 304L showed that the amount of hydrogen transported per unit strain decreases with incresing strain rate (19) as does the degree of embrittlement. These studies all assume that hydrogen redistribution during testing plays a major role in hydrogen embrittlement. However, subsequent tests have proven this redistribution may not be necessary. In a study of the impact behavior of hydrogen charged 304L stainless steel, embrittlement was observed during impact tests. Because redistribution of hydrogen during the short time frame of an impact test is unlikely this impact result suggest that dislocation transport of hydrogen need not occur for hydrogen embrittlement of austenitic steels (21). Extending this idea further however, suggests that redistribution, although not necessary may play a role being it is evident that by decreasing the test strain rate, more hydrogen is capable of segregating to highly strained areas. This extended

localization would be strain rate dependent and cause a change from ductile to fracture of interfaces where hydrogen has segregated. Investigations of 304L saturated with hydrogen by high temperature high pressure experiments showed facets on the fracture surface which were not observed on companion uncharged samples (26). These facets were not as prevelant during impact testing of charged samples thus some additional segregation must have occurred at the slow strain rates.

Another factor effecting a materials hydrogen compatability is its thermomechanical processing history. HERF processes have been shown to decrease hydrogen induced property losses in several 300 series austenitic stainless steels (5, 13, 24, 33, 36, 40, 47). This effect is attributed to the development of a cellular dislocation substructure and the fine grain size. Dislocation behavior in the HERF steels is the characteristic of easy cross-slip conditions even though the alloy may deform by coplanar dislocation motion under normal processing conditions (5, 33). Tensile test data show that at lower test temperatures, the HERF specimen of 304L and Nitronic 40 are only marginally better than annealed parts in terms of ductility but overall the process offers superior hydrogen compatability (4). The

temperature dependent behavior of Nitronic 40 steel HERFed to different strength levels has not been tested in the impact mode. This thesis study was conducted to determine the effect of various degrees of HERFing on temperature sensitive impact behavior and to determine the effects of hydrogen on that behavior. The impact behavior of Tenelon with and without hydrogen was also studied.

METHODS AND MATERIALS

The test specimen for the impact studies were machined from Tenelon and Nitronic 40 austenitic stainless steels having the compositions given in Table I. The typical microstructure of the two as-rolled steels are shown in Figures 6 and 7 and the room temperature mechanical properties are listed in Table III. Modified Charpy V-notch samples (ASTM E23, Type A) of annealed Tenelon and Nitronic 40 were machined of rolled plate and cross-rolled plate respectively. Small holes, 1/16 inch diameter, were drilled in one end of each sample to a depth of half the distance to the notch, (Figure 8). During impact testing at variable temperatures, a thermocouple wire can be inserted into the hole to acquire temperature readings on the specimen at the instant of the test. Nitronic 40, samples were machined from several plates of HERF material which were processed to different strength levels.

The Nitronic 40 stainless steel plate was produced by closed die forging at temperatures in the neighborhood

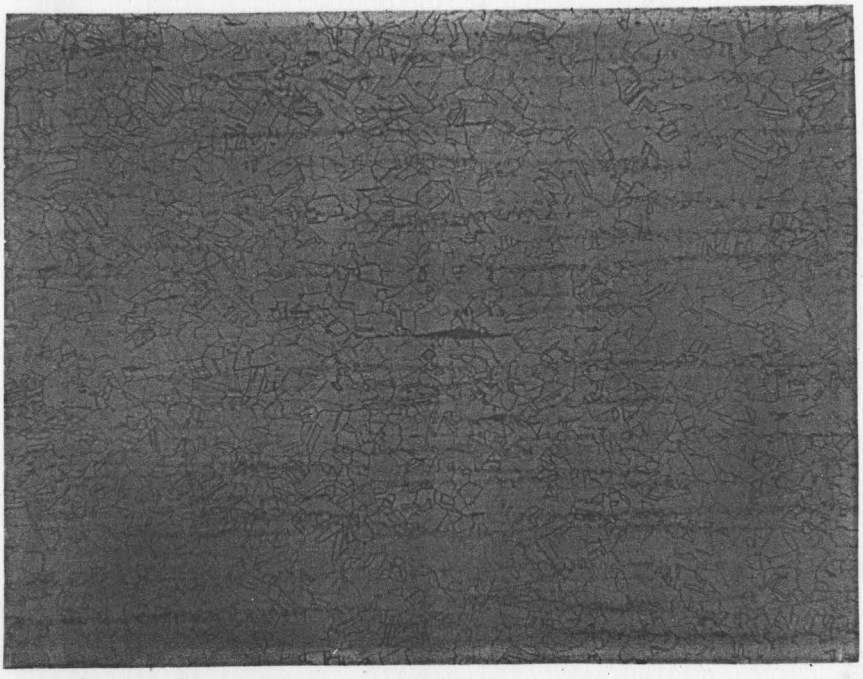

Figure 6. Micrograph of Tenelon's as-received microstructure.

Figure 7. Three-dimensional micrograph of the as-rolled Nitronic-40.

TABLE III

ROOM TEMPERATURE MECHANICAL PROPERTIES

Nitronic 40*

Temp K	Environment	Strength Mpa Yield	Ultimate	Elongation % Uniform	Total
298	Air	400	670	-	58

Tenelon*

298	Air	570	930	-	56

* Tensile A (40)

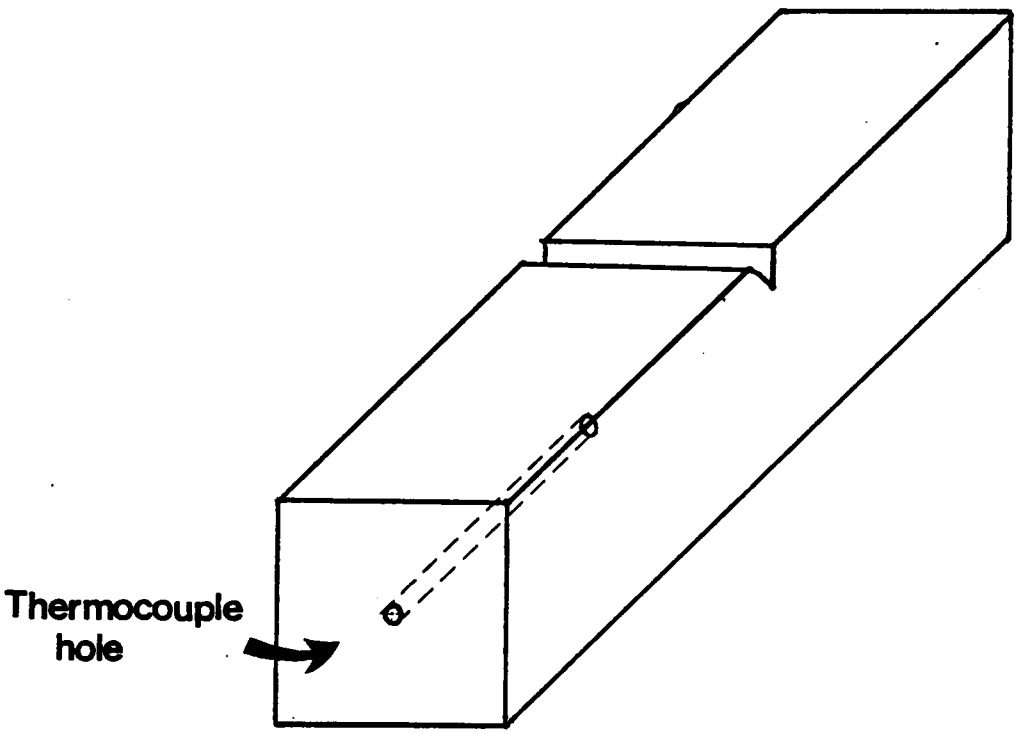

Figure 8. Schematic diagram of the Charpy-V-notch impact sample with drilled hole.

of 980^{o}C, and at deformation rates greater than the speed of sound. The elevated forging temperature effectively raises the toughness of the steel, so that it has adequate ductility to accomodate the substantial strain energy induced in the sample during the HERFing process.

Simple dislocation mechanics and Equation 1, are useful in demonstrating the significance of the high rate at which forging takes place,

$$\gamma' = (b) \cdot x \ (\rho) \ x \ \langle v \rangle \qquad (1)$$

This equation relates the shear deformation rate (γ'), to the Burgers vector of a dislocation (b), the mobile dislocation density (ρ), and the average dislocation velocity <v>, all of which are important to basic dislocation dynamics. Shear strains are produced during HERFing, and compensation must be made for them through increases in the average velocity of the dislocations, or in an increase in the number of mobile dislocations. Using basic energy theories we find that typically the velocity increase occurs before new slip systems can be activated. This is because the energy required to increase the velocity of dislocations moving at speeds less than the speed of sound, is usually less than that

required to activate new slip systems. However, during HERFing, the velocity of mobile dislocations approaches the speed of sound. This velocity is the maximum possible dislocation velocity because it is the speed with which a displacement wave will propogate the steel. Often, the shear strain rate (γ') is too large to be accomodated for entirely through an increase in the average dislocation velocity <v>. Therefore, new slip systems are activated, and as a result the mobile dislocation density (ρ) rises. The very high dislocation density induced by HERFing results in dense slip bands and deformed twins throughout the microstructure. This substructure substantially increases the strength of the steel. A typical micrograph of the HERF material is shown in Figure 9. This specific sample had the highest yield strength, 135 ksi of the steel samples tested. Four sets of samples were HERFed to yield strengths of 135 ksi, 126 ksi, 110 ksi, and 96 ksi. The 96 ksi and 110 ksi yield materials may have the optimal strengths for industry because of their retained toughness.

Hydrogen charging was the next step in the preparation of the samples. Part of each set of samples was thermally charged with gaseous hydrogen by Savannah River Laboratories at 10,000 psi for 28 days at 350^{o}C.

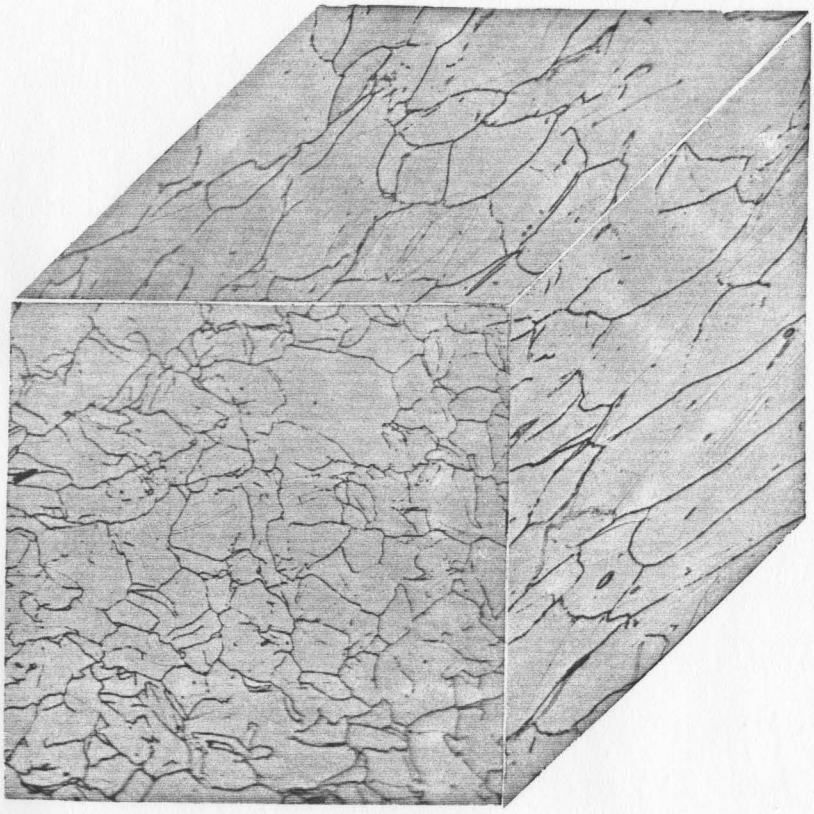

Figure 9. Three dimensional micrograph of HERFed Nitronic-40, 200x.

The concentration of hydrogen in the samples was also tested by Savannah River Laboratories and found to be 86% ppm at the center of the Nitronic 40 samples. The charged samples were then stored at -198^{o}C until tested to ensure minimal hydrogen outgassing, even in the near surface region.

The impact properties of both the charged and unexposed stainless steel, samples were tested on a Dynatup Model 500 instrumented impact machine. The instrumented impact test greatly extends the capabilities of traditional impact testing. In addition to the traditional energy absorbed value, the instrumented set-up allows recording of both load and energy versus time traces. Instrumented impact testing requires several basic components; an impact machine, a load sensor, and a signal display component. The system used in this investigation is shown in Figure 10. The primary purpose of the electronic equipment associated with the instrumented impact machine is to provide an accurate voltage-time signal from the load sensor which is a strain gaged striker. The gages are positioned to sense the compressive force interaction between the pendulum impact machine and the test specimen. The striker as shown in Figure 11 is bolted to the swinging pendulum

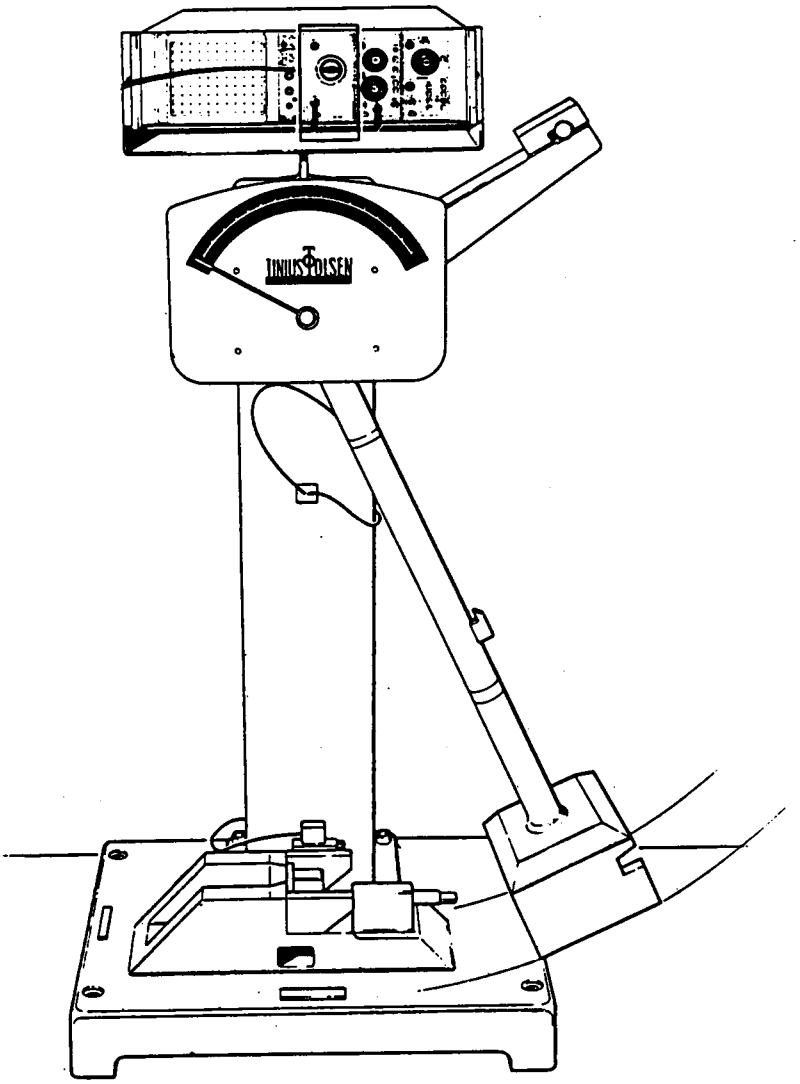

Figure 10. Diagram of the Dynatup Model 500 Instrumented Impact Machine.

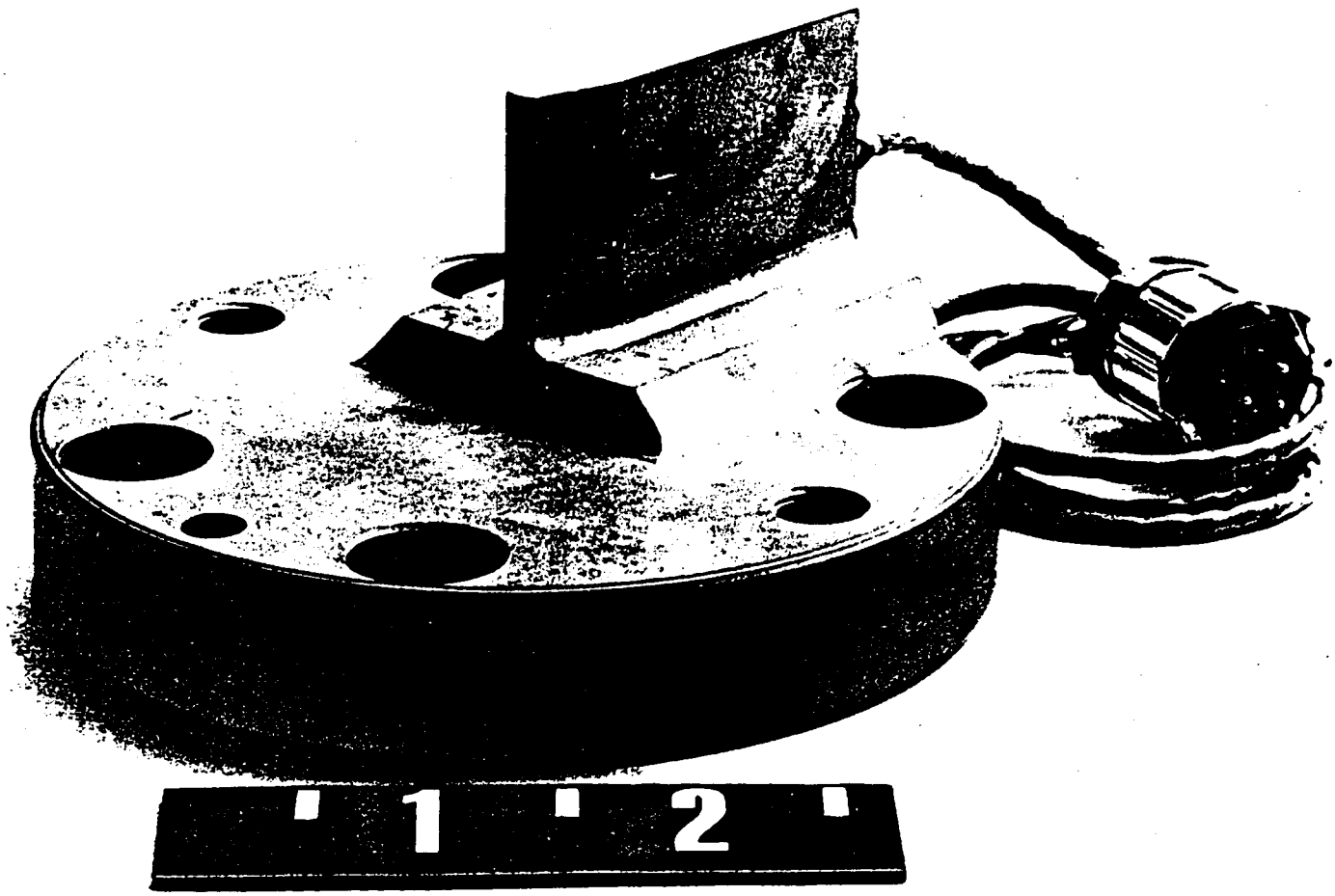

Figure 11. Instrumented Impact Machine striker fitted with strain gages.

arm, Figure 10. The signal from the striker (or tup) represents the load behavior of the specimen during the impact event, and the electronic integration of the signal represents the accumulative energy required to deform and fracture the test specimen. The signal display component in this system consists of a Velcometer and the Velcometer display module. The Velcometer supplies a controlled light beam and photosensor to insure reliable triggering of an oscillographic recorder which then records the load-energy versus time curves. A typical oscilloscope read-out is shown in Figure 12. The information from the read-out can be interpreted by various means.

The samples were stored in liquid nitrogen until test time. The samples were removed one at a time from the liquid nitrogen and a chromel-alumel thermocouple attached to a Doric Trendicator Model 403A, was inserted in the drilled hole to closely monitor the temperature. The wired sample was held back in the liquid nitrogen to stabilize the temperature and then quickly removed and placed in the test set-up with a thermocouple still in place. Depending on which temperature was to be used, the impact test was conducted after different amounts of specimen warm-up. After testing, the samples were

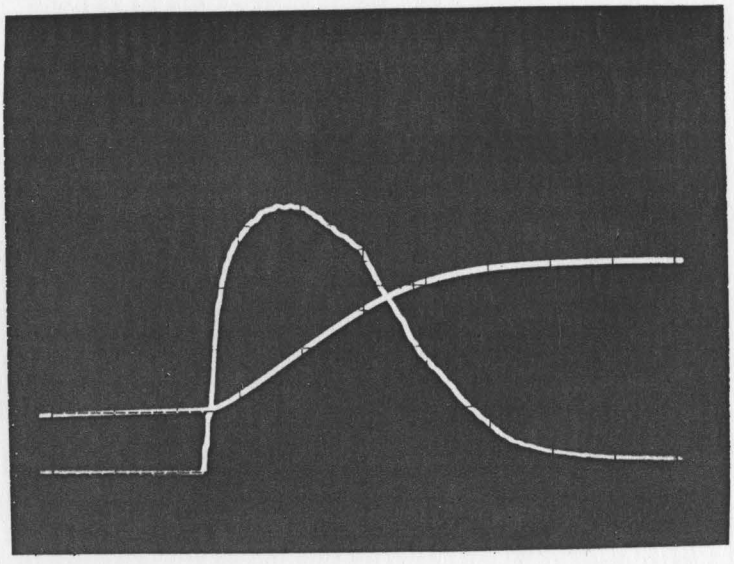

Figure 12. Typical instrumented impact load-energy-time trace.

immediately sprayed with Krylon to protect the fracture surface until the time of the fractographic studies in a SEM. A vibratory bath of acetone was used to remove the Krylon and fractographic studies were conducted on most samples to characterize the fracture surfaces and to determine the effect of HERFing and hydrogen charging on fracture modes.

RESULTS AND DISCUSSIONS

4.1 Nitronic 40 Impact Tests

4.1.1 Non-hydrogen Tests

The beneficial effect of HERFing on the mechanical properties of a stainless steel compared to the standard mill annealing techniques has been demonstrated by several investigators (9, 10, 12-15, 21, 30, 31, 33, 36, 38-40). However, most of these previous tests dealt with the tensile properties of a single heat of HERFed material forged to a given strength level. The study described in this thesis was undertaken to evaluate the effects of the HERF process on several of the impact properties of Nitronic 40 stainless steel forged to different strength levels. Charpy V-notch samples were machined from five batches of material; rolled plate with a yield strength of 135 ksi, 126 ksi, 110 ksi, and 96 ksi.

These sets of samples were impact tested in the temperature range from -198^{o}C to 22^{o}C in an attempt to record the effect of forming on the ductile to brittle transition and fracture behavior even though the HERFed material did not behave in a fully brittle manner even at liquid nitrogen temperature. The results are summarized

in Table IV. Explanation of several of the terms used in the table is in order. Data obtained from the typical impact trace includes the maximum load during the fracture process, the total energy absorbed by the sample, the tearing slope, the energy required to initiate a crack and the energy for crack propogation. Schematic representation illustrating measurement of these parameters is given in Figure 13. The iniation energy is found by assuming that the time to reach the maximum load is also the time for initiation of the cracking process, therefore the E at maximum load is defined as the initiation energy. During a complete failure, the total amount of time is spent in the initiation stage and propogation stage combined. From this simple concept, we see that E of propogation equals ($E_{total} - E_{init.}$). All of the parameters evaluated by the impact test are temperature dependent. A graphical representation of this dependence is shown in Figures 14-20.

The tearing slope is a parameter which was defined for this investigation. Once a failure has been initiated, the size of the tearing slope indicates whether the crack propogated very eaily (a steep slope) or the propogation was slowed by the energy absorption

TABLE IV

Temp. °C	Processing	$E_{max.}$ (ft/lb)	$E_{init.}$ (ft/lb)	$E_{prop.}$ (ft/lb)	Tearing Slope
	cross-rolled				
-198	no hydrogen	33	15	18	-33.3
-169	"	37	12.5	24.5	-20.0
-149	"	0	-	-	
-126	"	48	14.5	33.5	- 7.7
- 75	"	75	28	47	- 5.0
0	"	115	45	70	- 4.0
24	"	115	40	75	- 2.86
24	"	130	40	90	- 2.63
-189	135 ksi HERF	37	14	23	-33.2
-103	"	50	29	21	-20.0
- 50	"	111	42	69	- 8.7
23	"	148	53	95	- 5.3
-197	126 ksi HERF	30	20	10	-28.6
-149	"	50	32	18	-20.0
-101	"	78	33	45	-15.4
- 50	"	142	43	99	- 6.7
0	"	147	52	95	- 5.1
-196	110 ksi HERF	56	-	-	-36.4
-149	"	45	30	15	-28.5
-100	"	104	34	70	-16.7
- 50	"	155	55	100	- 5.4
0	"	230	67.5	162.5	- 3.3
20	"	200	47.5	152.5	- 4.5
-180	96 ksi HERF	60	-	-	
-177	"	64	28.0	36	
-145	"	40	19.5	20.5	
-101	"	46	27	19.0	
- 50	"	125	38	87	
0	"	205	60	145	

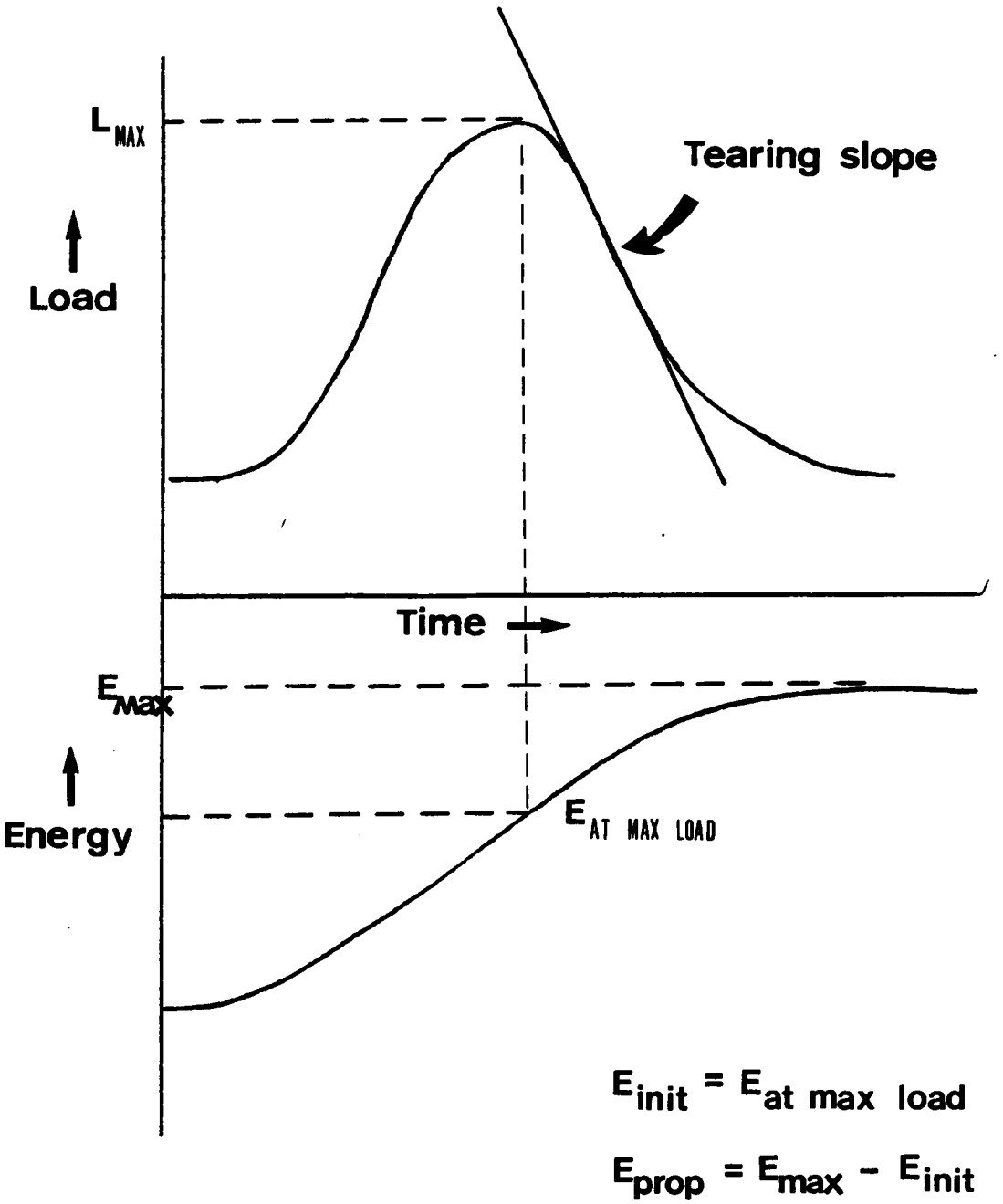

Figure 13. Schematic diagram of the instrumented impact trace.

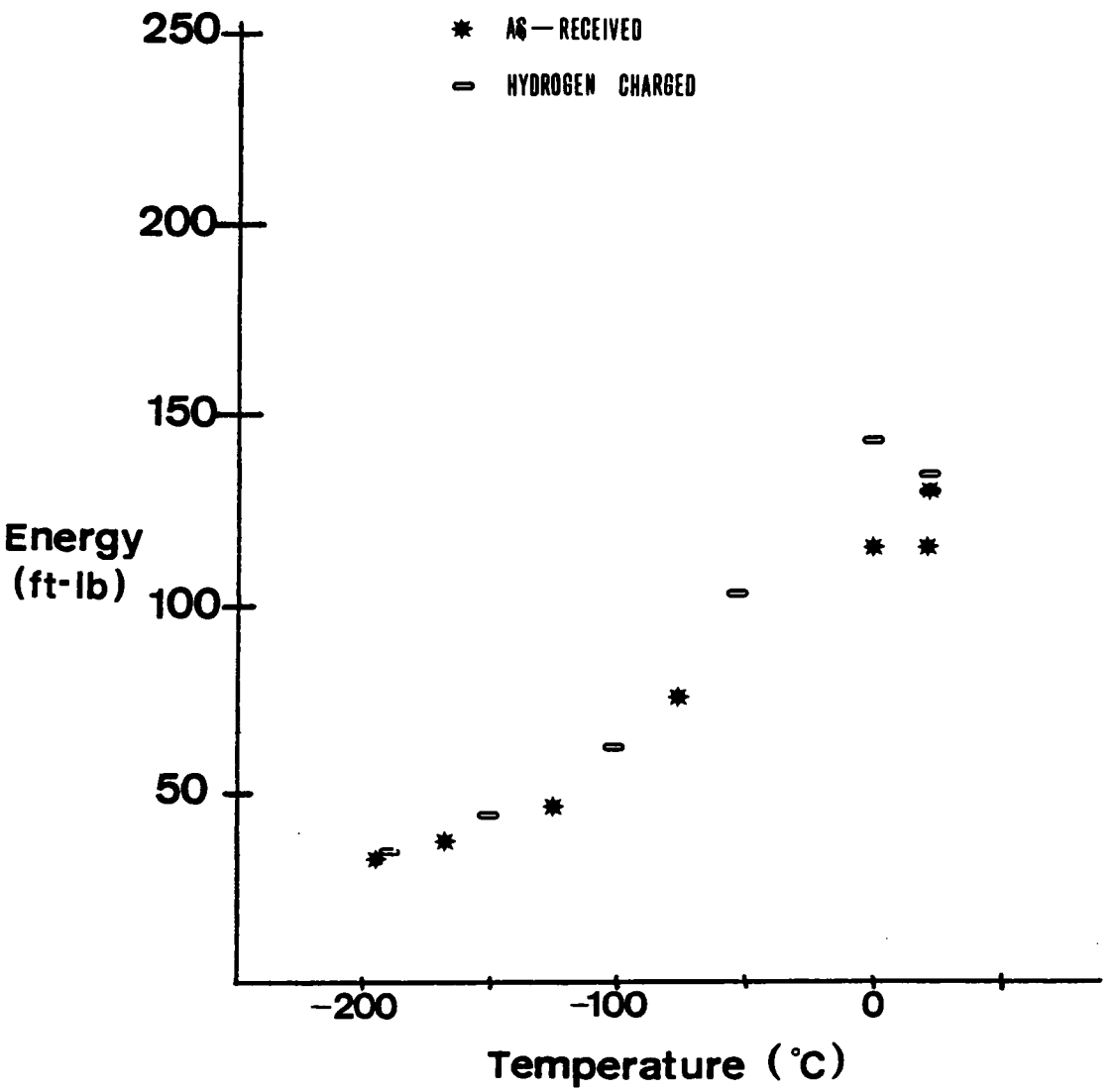

Figure 14. Energy-temperature curve for as rolled Nitronic 40.

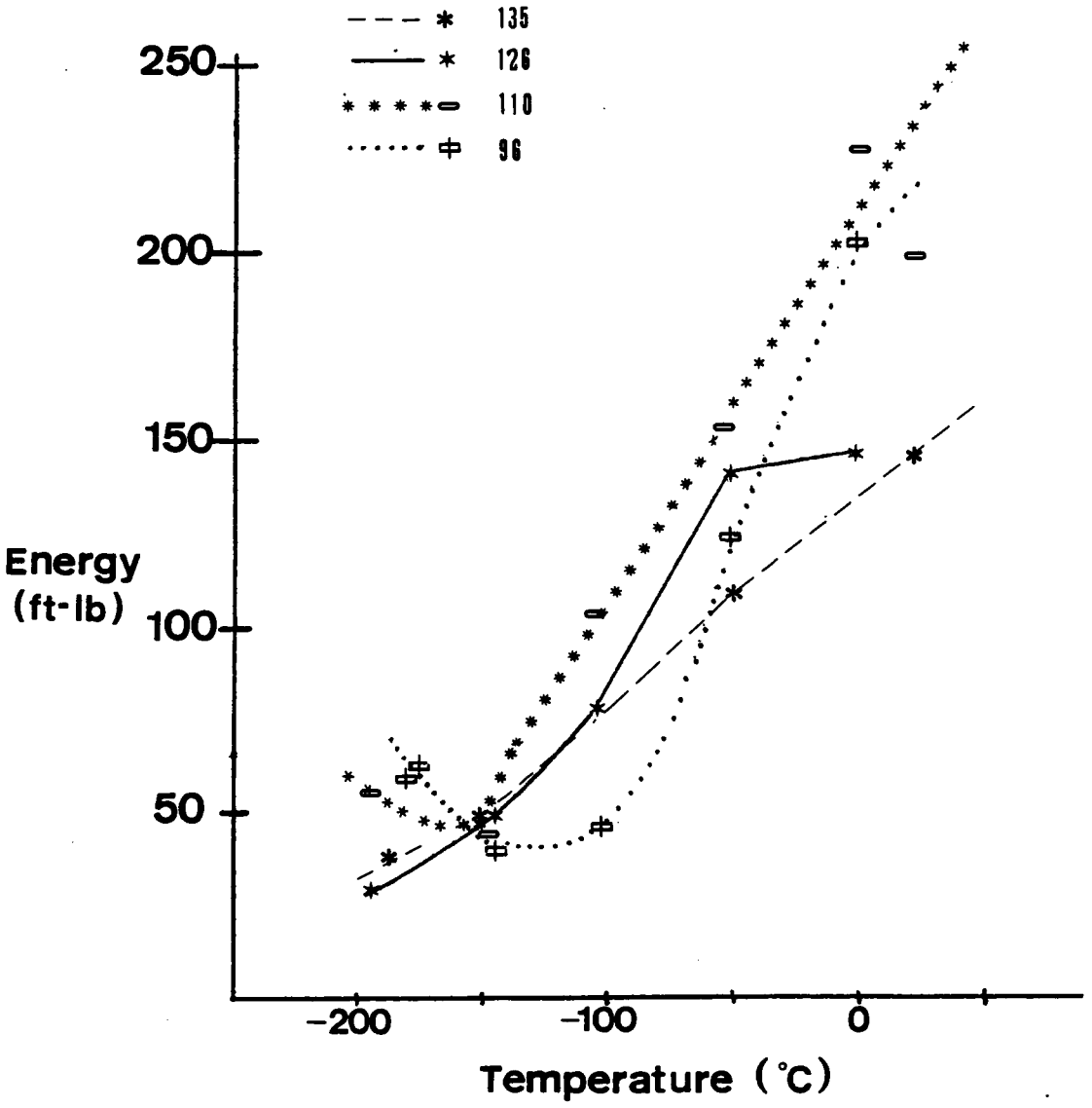

Figure 15. Energy-temperature curves for HERFed Nitronic 40.

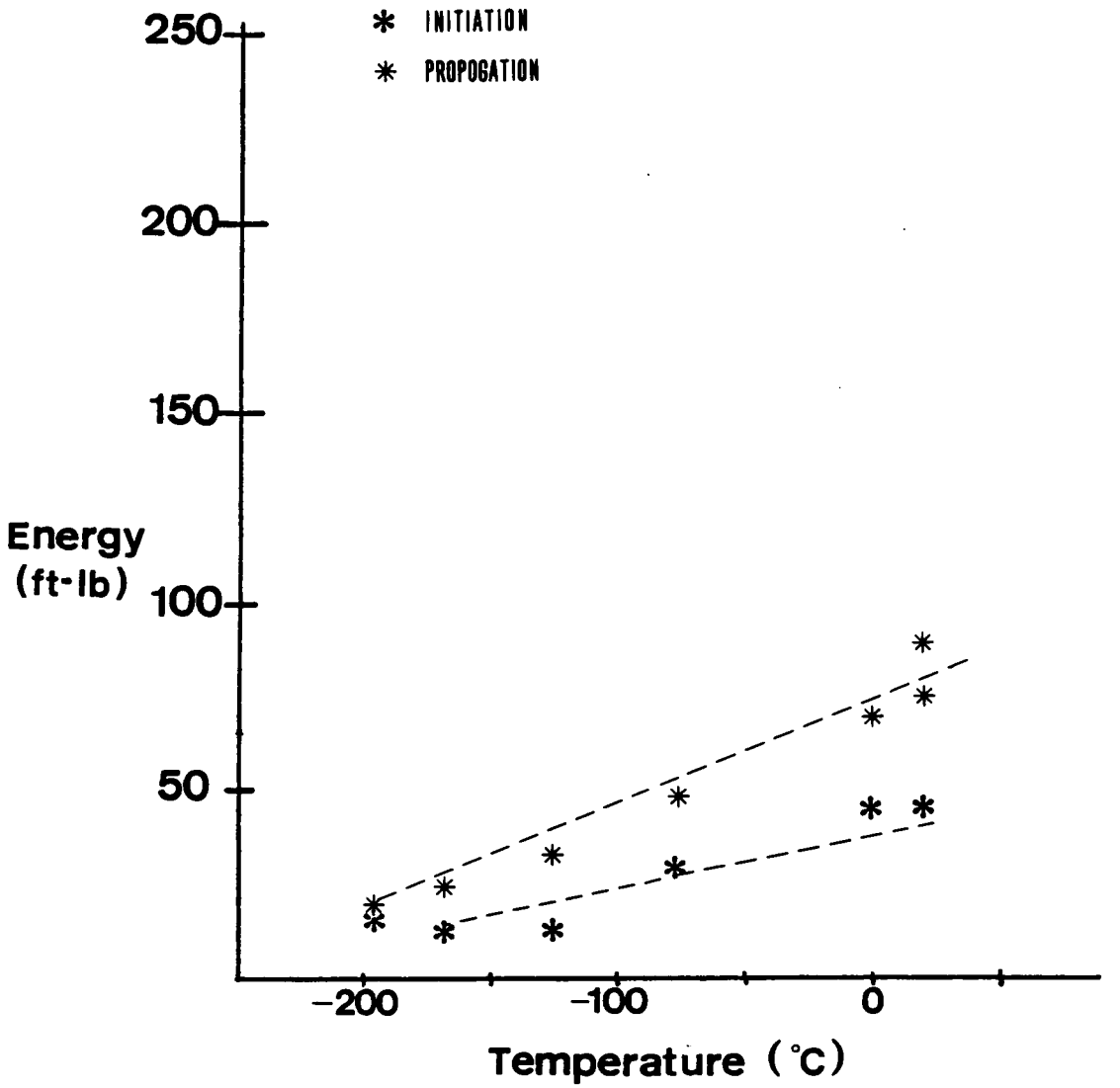

Figure 16. Initiation and propogation energy curves for as-rolled Nitronic 40.

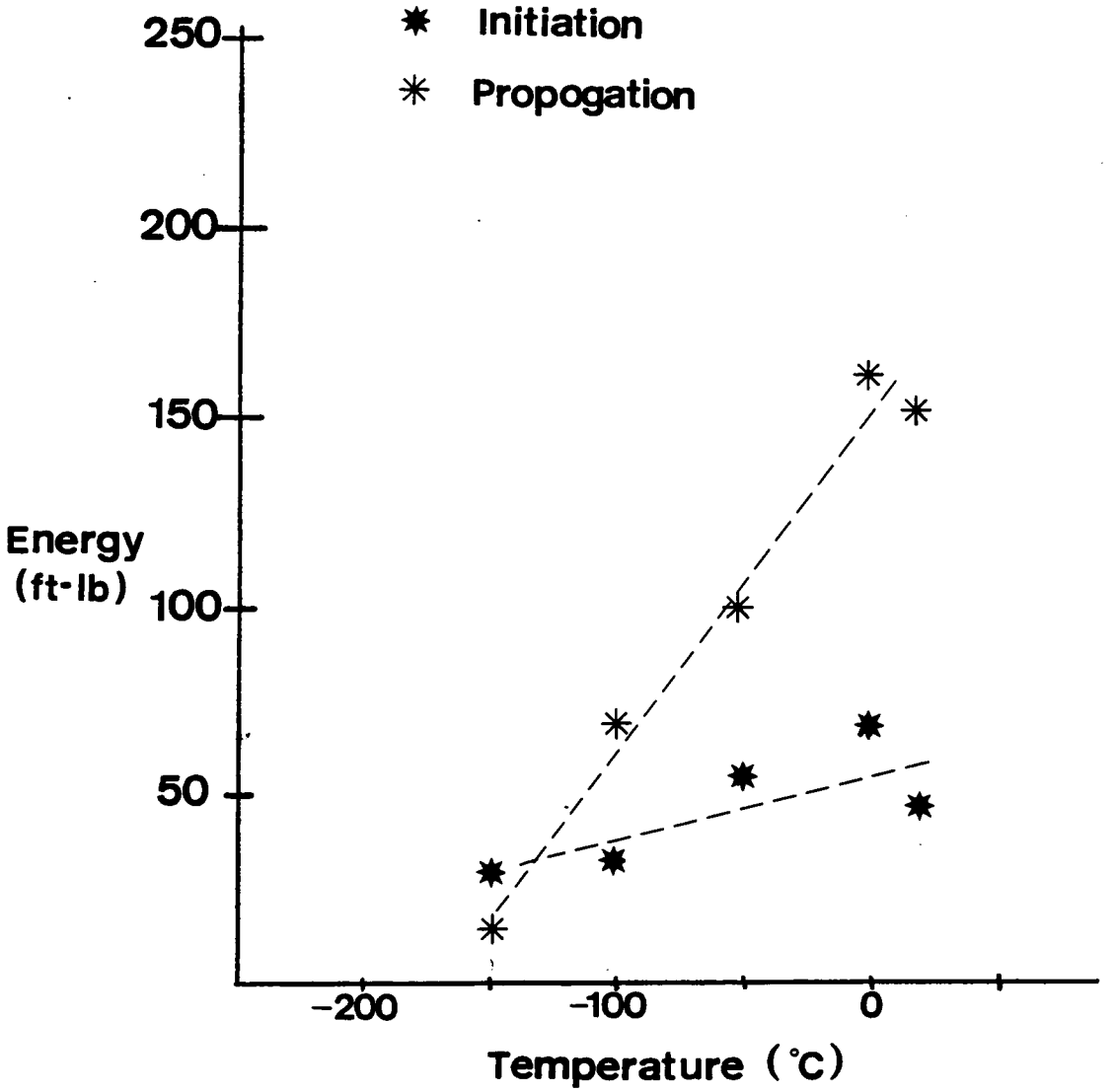

Figure 17. Initiation and propogation energy curves for 110 ksi HERF Nitronic 40.

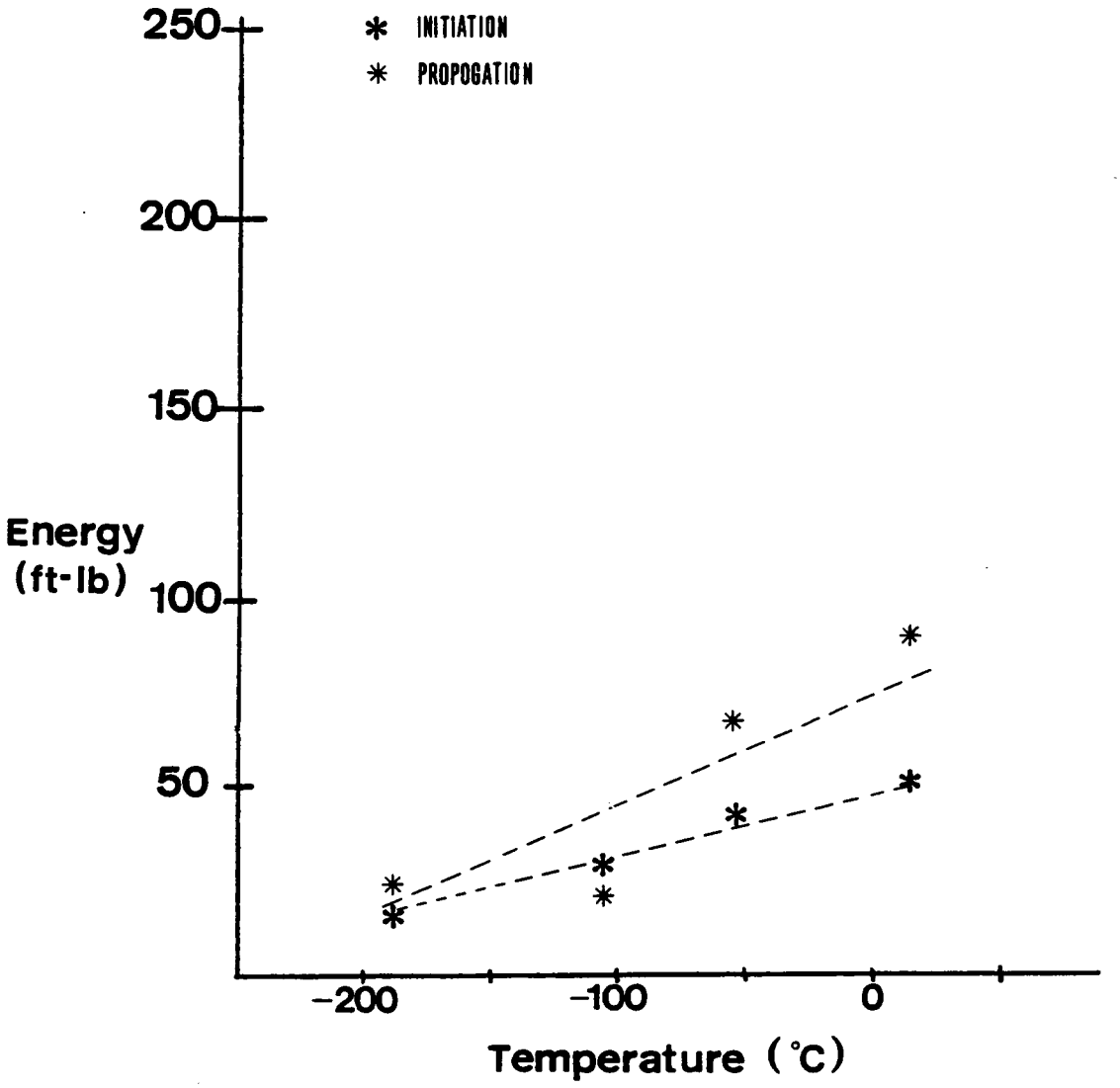

Figure 18. Initiation and propogation energy curves for 135 ksi HERF Nitronic 40.

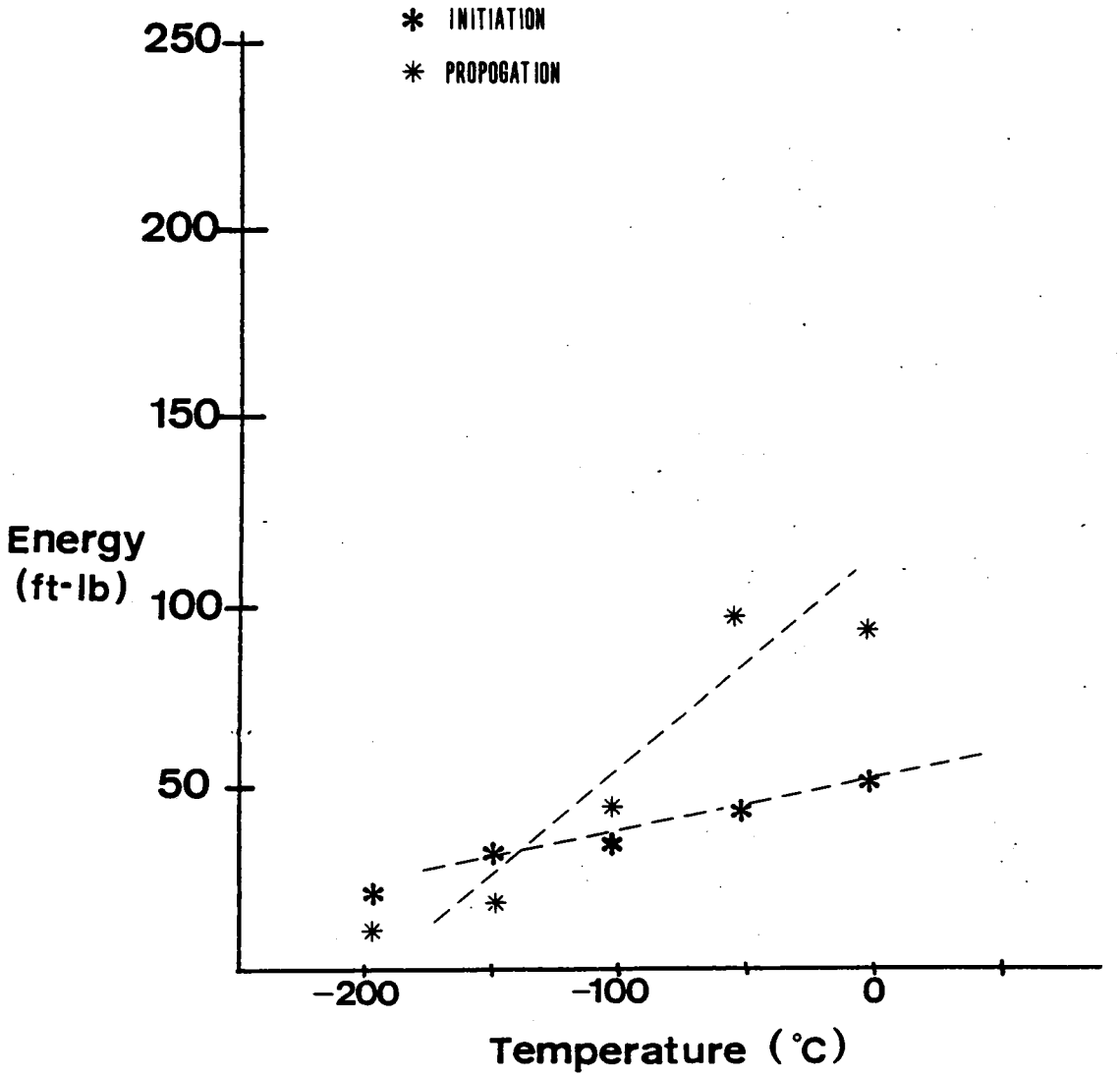

Figure 19. Initiation and propogation energy curves for 126 ksi HERFed Nitronic- 40.

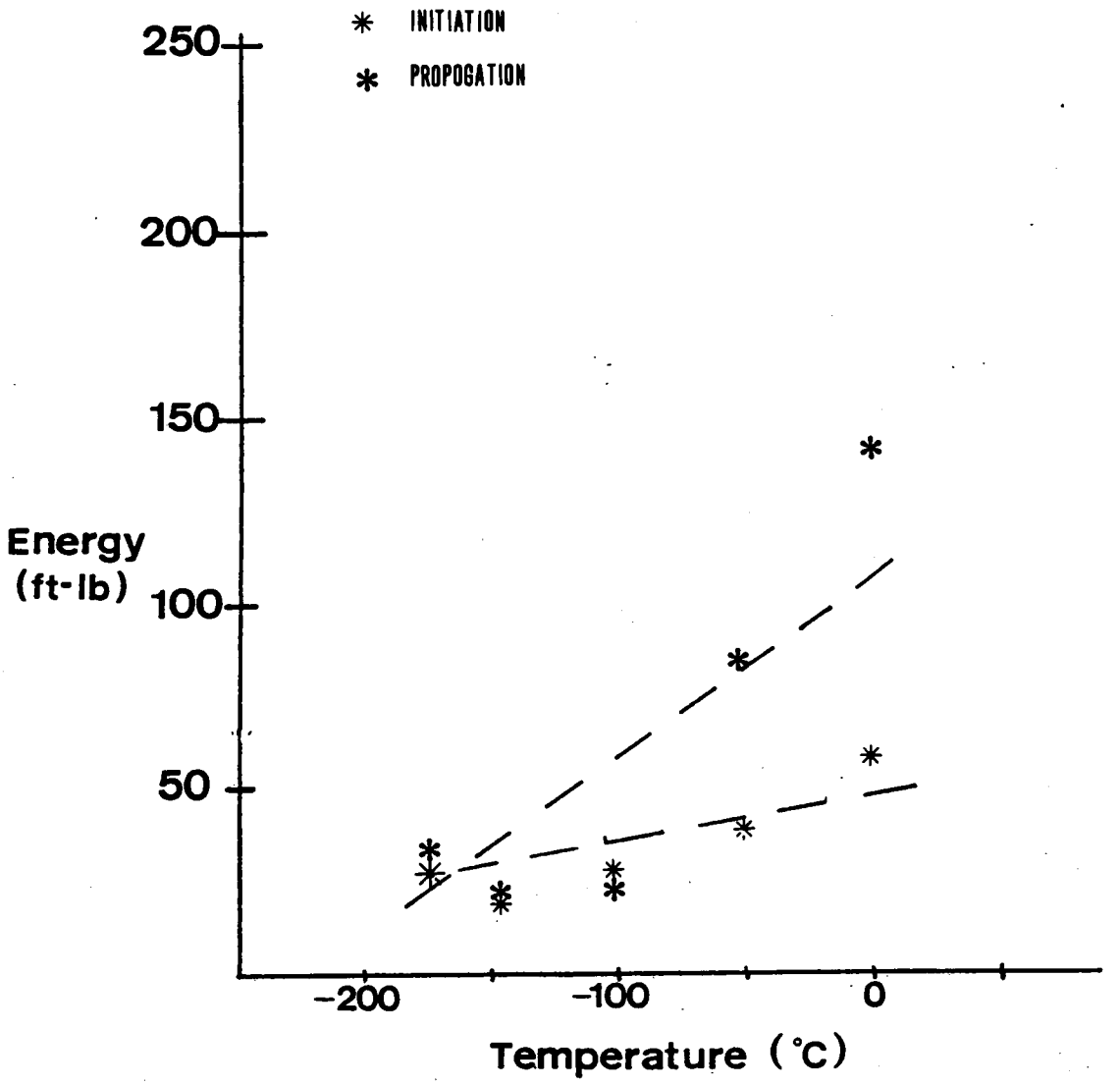

Figure 20. Initiation and propogation energy curves for 96 ksi HERFed Nitronic-40.

capacity of the impact scale (a shallow slope). Temperature has a large effect on the tearing slope because at higher temperatures the more ductile fracture process dominates the behavior, whereas at low temperatures the more brittle fracture processes cause a characteristically steep slope. Simple analysis, therefore, suggests that the tearing slope and the energy of propogation must be related because both deal with the ease of crack growth. Figure 21 illustrates the relationship between the two parameters for the rolled plate. The HERF process alters the relationship between the two parameters. The exact nature of this change was not determined because the testing of different types of materials would be required.

Previous work has shown that fracture is a strain rate dependent process (40. 23). Fast strain rates usually results in a different fracture than slow rate processes. During high rate tests, atom segregation cannot play a part as it would in for example a slow three point bend test. Experiments on tensile samples have shown failures to occur below the typical fracture stress because of atomic segregation to favorable lattice sites. When the strain rate is increased, segregation cannot occur. however the favorable lattice sites still

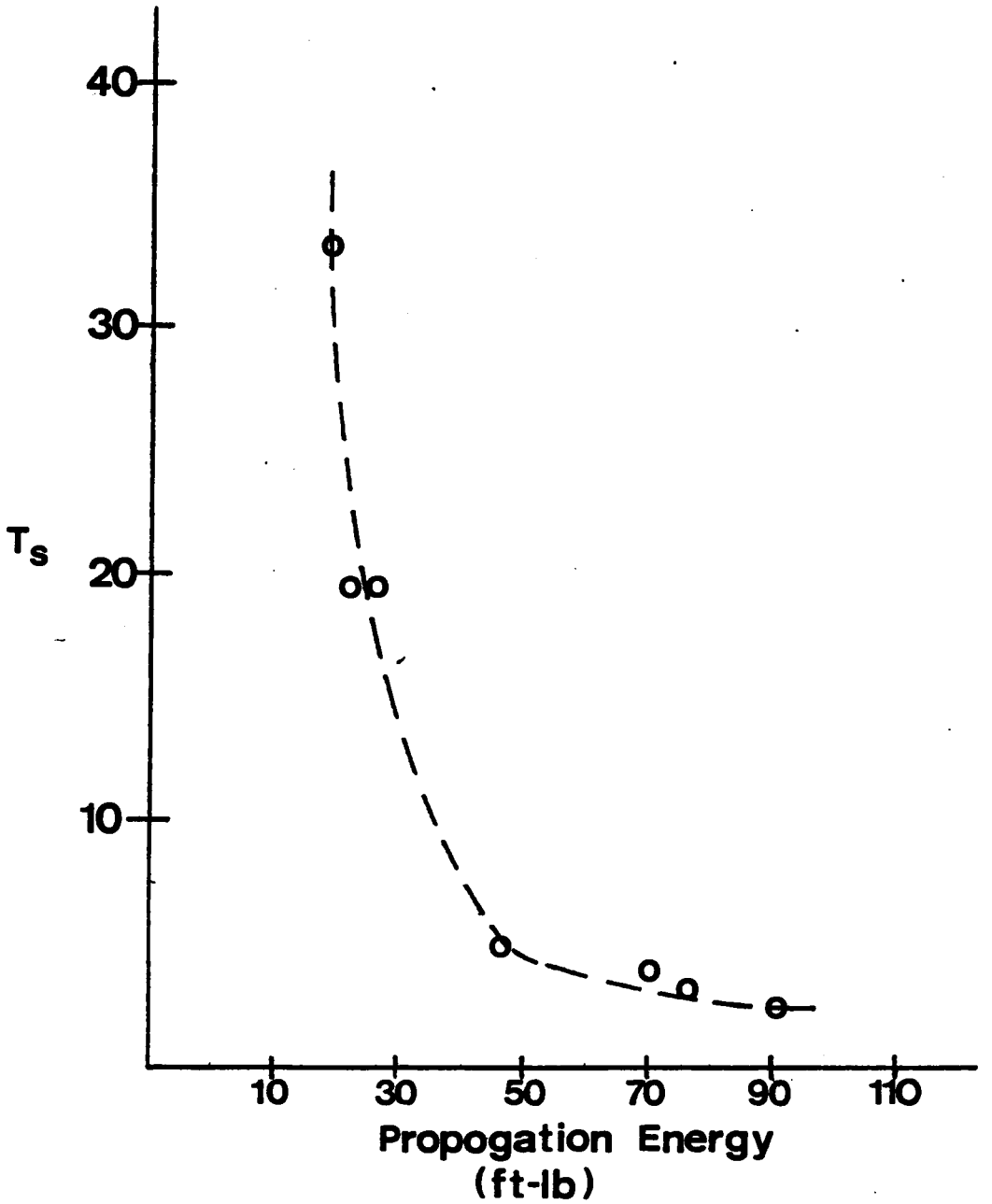

Figure 21. Tearing slope versus E_p for the rolled plate Nitronic-40

exist. The sites will be different for the fabrication differences and will in turn affect fracture at high strain rates. The tearing slope deals with the nature of the fracture.

Typically, a change in fabrication produces two separate effect; 1) raising the strength, and 2) lowering the ductility. When the material condition changes the tests demonstrate that the toughness also changes (Figure 22), however if one examines without reference to the tearing slope a discontinuity exists. If only the strength or max load were to increase, curves given by Figure 23a would result. The integral of these curves or the energy absorbed would be greater for the high strength material. This was not observed. If only the ductility was to decrease, strength remaining the same, the curves in Figure 23b would result. The real life impact situation is inbetween the two given above. On the right half of Figure 22 when the strength is increased the load increases, but the tearing slope does not remain the same, it becomes steeper so that the toughness actually decreases for increasing strength or the ductility decrease effect prevails. On the left half of Figure 22 the toughness increases as the strength increases thus the increased strength effect prevails

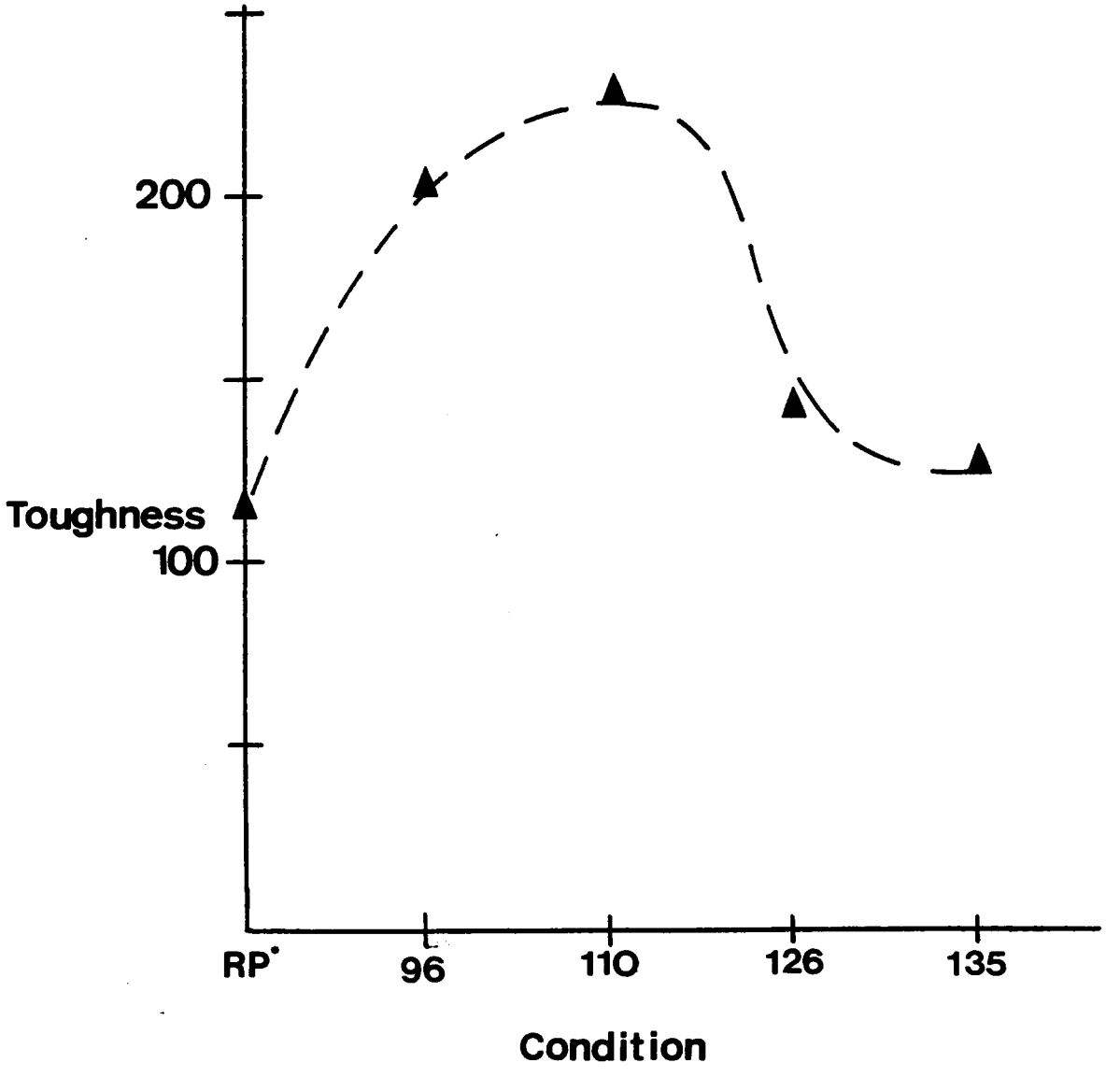

Figure 22. Toughness versus condition.

*rolled plate

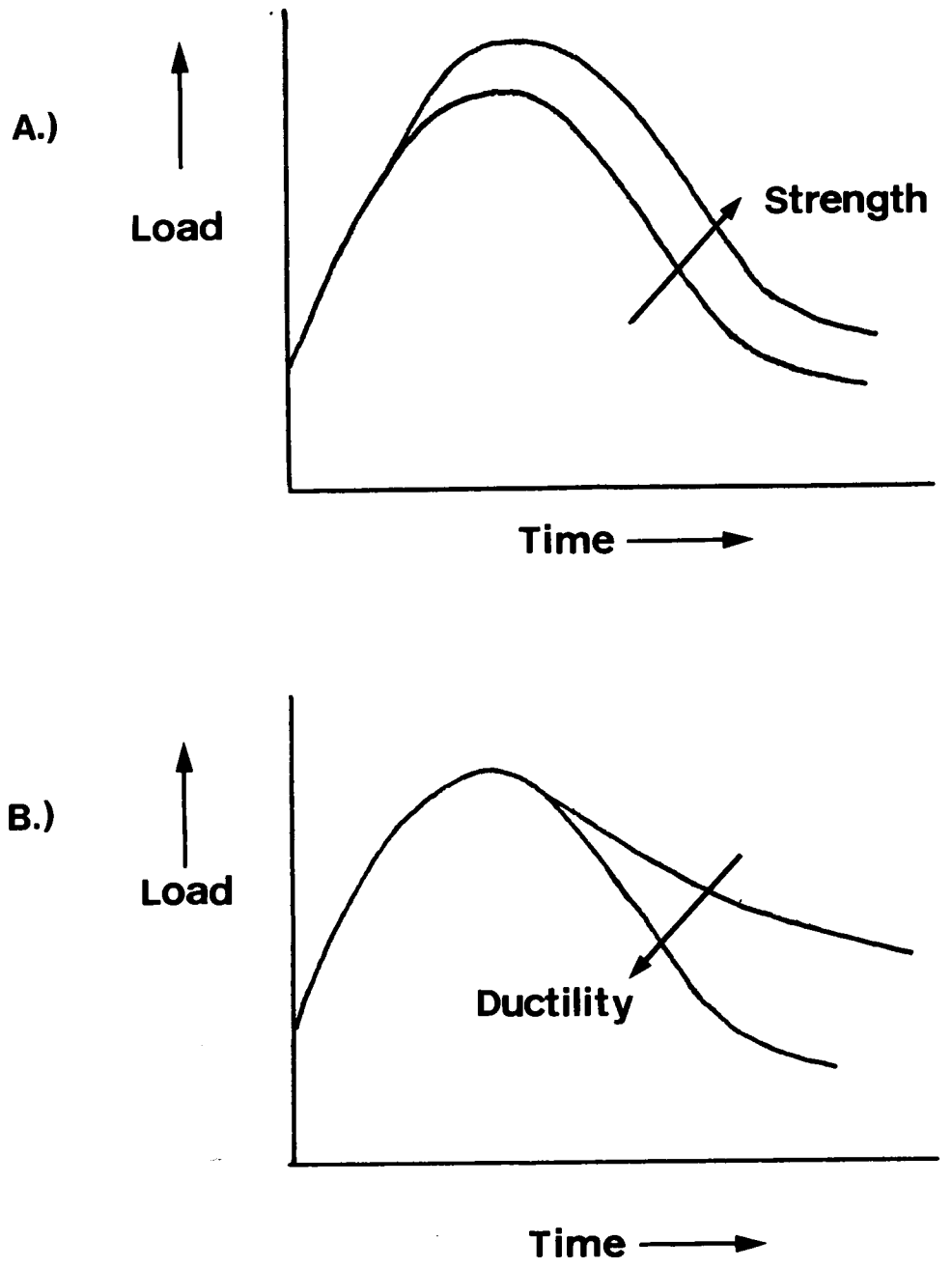

Figure 23. Load versus time curves for different conditions.

with only a slight tearing slope change.

The energy-temperature curves for the various sets of materials were different. Figure 14 illustrates the relationship between temperature and energy absorbed for the rolled plate and like many other austenitic stainless steels, a complete ductile to brittle transition is not evident. In order to achieve brittle behavior, temperatures below the liquid nitrogen temperature must be employed. This lack of a ductile to brittle transition is a good result to observe because brittle behavior is undersireable and any suppression of that type of behavior is worthwhile. The HERF processes acts to change the tendency toward brittle fracture. Even the 135 ksi HERF material has more toughness than the rolled plate, Figure 15, but this material also has the lowest toughness of the four sets of HERFed stainless steels. The tests demonstrate that the 110 ksi HERF material is the toughest material, at all temperatures tested. This material would be the best to have in service because it absorbs a great deal more energy during impact in addition to having a higher yield strength than the typical rolled plate. The 126 ksi and 96 ksi HERF offer the next best set of toughness values. According to the data these two act similarly in that at certain

temperature the 96 ksi absorbs slightly more energy than the 126 ksi and at other temperatures, visa versa. The tests demonstrate that the 110 ksi HERF material is the toughest material, absorbing greater amounts of energy during impact. This material would be the best to have in service because it absorbs a great deal more energy during impact in addition to having a higher yield strength than the typical rolled plate.

These results therefore show that the toughness initially increases as the yield strength is increased by forging. The toughness then reaches a maximum and decreases as the yield strength is increased. When something causes the DBTT to decrease the toughness is rising. The DBTT is caused by a competition between two processes as shown by Figure 24. When the yield strength increases, say from 110 ksi to 135 ksi up to the dashed line (Figure 23) the DBTT would rise. Both the 135 ksi and 126 ksi curves have higher DBTT than the 110 ksi curve. The behavior of the 96 ksi set of material is not consistent with the other results but is explained by observations on previous work (49) which finds that a critical strain rate for HERFing exists. For many materials the elongation to failure increases with strain rate until the critical rate is reached where the

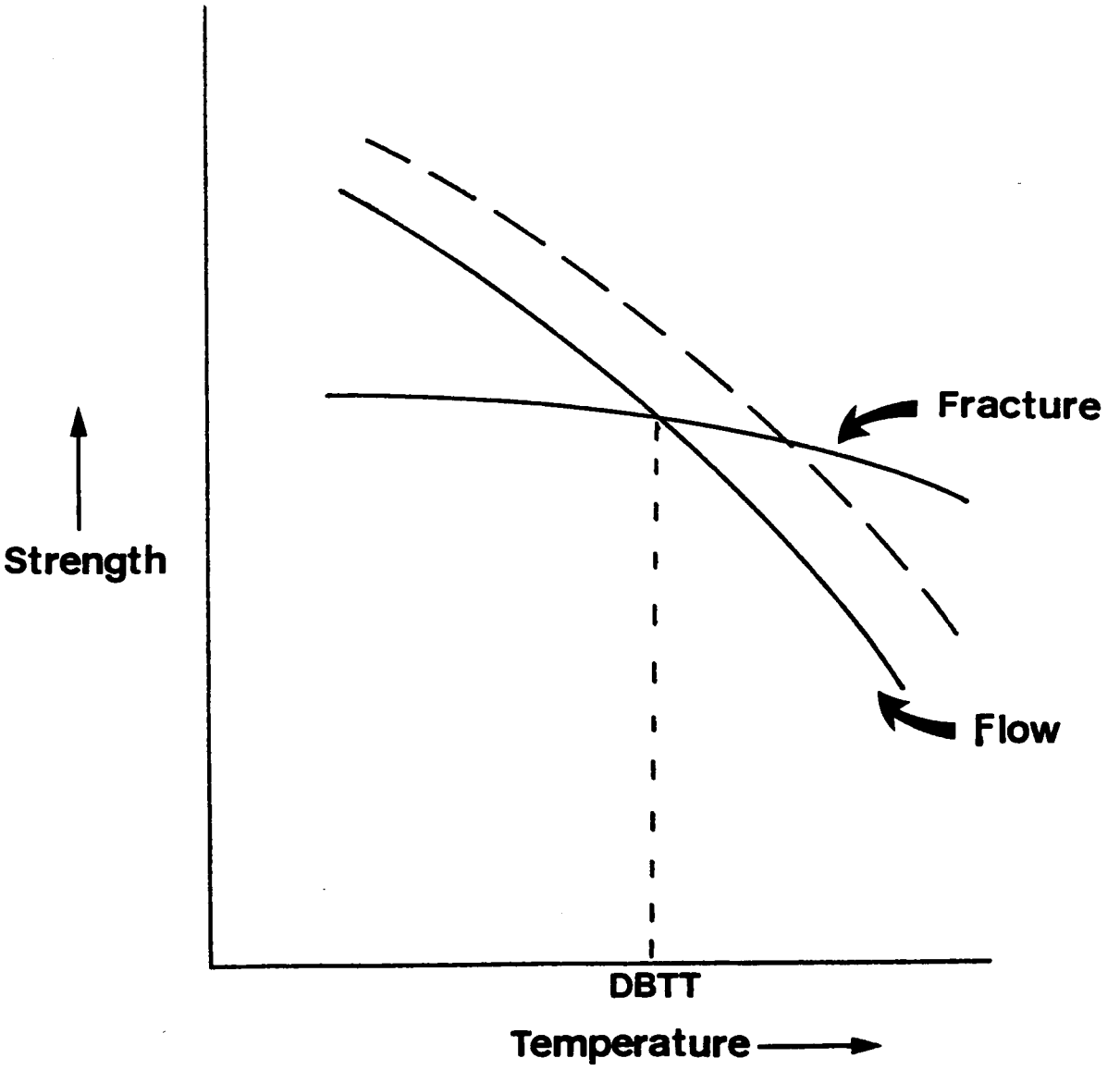

Figure 24. Curve used to determine the DBTT.

ductility or in this case toughness falls off, as is the situation for the 96 ksi HERF.

Another useful concept to develop during impact type testing is the cracking tendency. This would tell an investigator about the nature of the failure. Since the tearing slope changes with processing changes, the energy of propogation (E_p) and the energy of initiation (E_i) were chosen to characterize the cracking tendency. These concepts are studied because in many systems initiation of a crack would be acceptable as long as the propogation stage did not occur. The differentiation between E_p and E_i, and the study of different variables affecting these is helpful in many situations.

Energy of propogation and initiation are temperature dependent as stated earlier and Figure 16 illustrates the relationship for the rolled plate. Several aspects of this curve are of interest. First, the curves show that more energy is employed during the propogation stage than the initiation stage at all temperatures tested. Second, the difference between the two energies increases as the tmeperature rises. Therefore, when the process becomes more ductile, the ease of initiation is not affected as much as the ease of propogation. This is consistent with work performed on notched versus smooth tensile samples.

Think of a notched sample as one in which the initiation has already occurred. When the test temperature is raised, the notched sample should exhibit a greater percentage change in behavior than the smooth samples because the propogation takes up a large percent of the total process time.

When a process variable such as HERFing is added to the experiment the relationship between E_p and E_i changes. At the upper temperature range the changes in energies are the largest, and E_p is the most affected as the large rise in Figure 15 illustrates. Comparing this with the rolled plate curve, the considerable change in the E_p is noted while E_i differs only slightly. For the sets of HERFed material with lower toughness this difference becomes smaller and smaller, as evidence by Figures 18-20. The next step after noting these differences in impact behavior was to see if changes in the fracture process caused the absorbed energy differences.

Scanning electron microscope examination of the fracture surfaces provided more support for the continued use of HERF parts. The rolled plate was dependent on the role of inclusion stringers in its fracture process. Even at a low magnification, Figure 25 demonstrates the

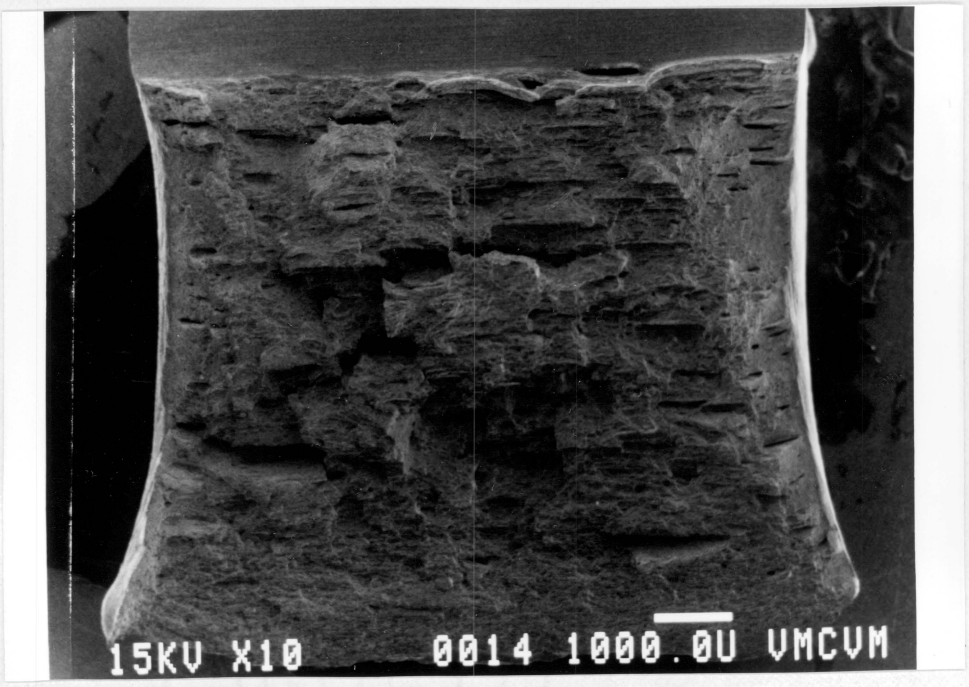

Figure 25. Fracture Surface of a rolled-plate room temperature impact test, 10X.

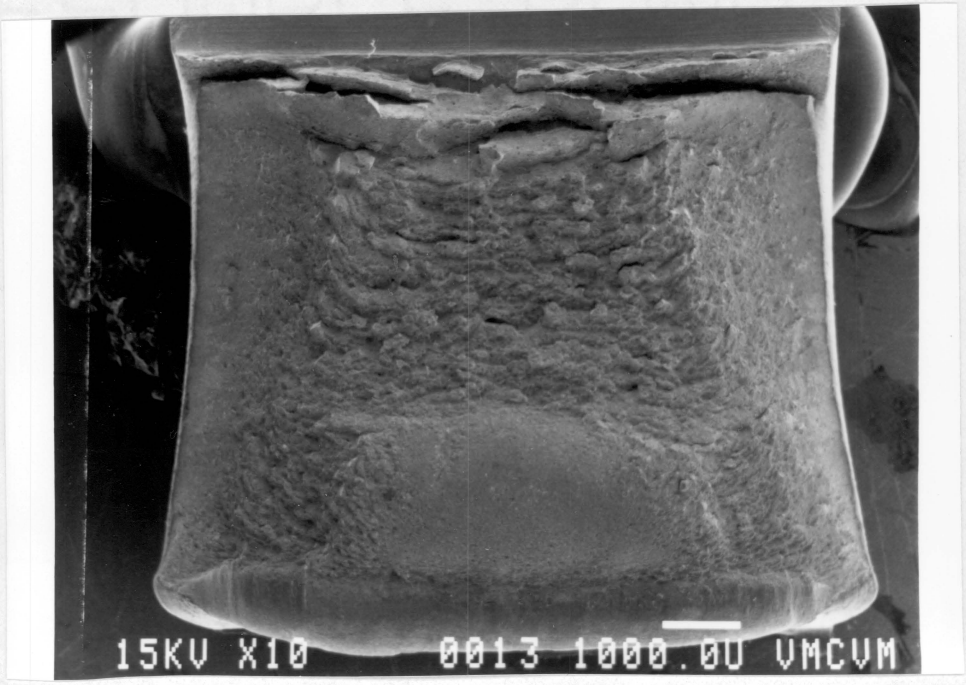

Figure 26. Fracture surface of a HERFed, room temperature impact test, 10X.

nonuniform fracture surface caused by inclusions running along the rolling direction. Also notice that although this sample was tested at the liquid nitrogen temperature, ductility is still considerable as evidenced by the shear lips and dimples. A fractograph of a HERFed sample tested under identical conditions shows that the role of inclusions has been greatly reduced, (Figure 26). Now the surface is smoother, without the discontinuities of the rolled plate which resulted from the crack having to reinitiate at each large inclusion, examples of which will be given later. Samples tested at the upper temperature range, i.e. room temperature exhibit greater amounts of ductility, (Figures 27 and 28). The HERFed sample actually now has shear lips on three sides. Higher magnification of the fracture surfaces show that microvoid coalescence is the dominant mode for both sets of samples although a heterogeneous distribution of microvoid sizes was present. Figure 29 is a 3000X fractograph of the HERFed material whereas Figure 30 is a 300X shot of the rolled plate showing the same fracture mechanism, microvoid coalesence, in addition to pits caused by inclusion action. In some upper shelf temperature samples the ductility is so extensive, the surface takes on a "whipped cream" type appearance

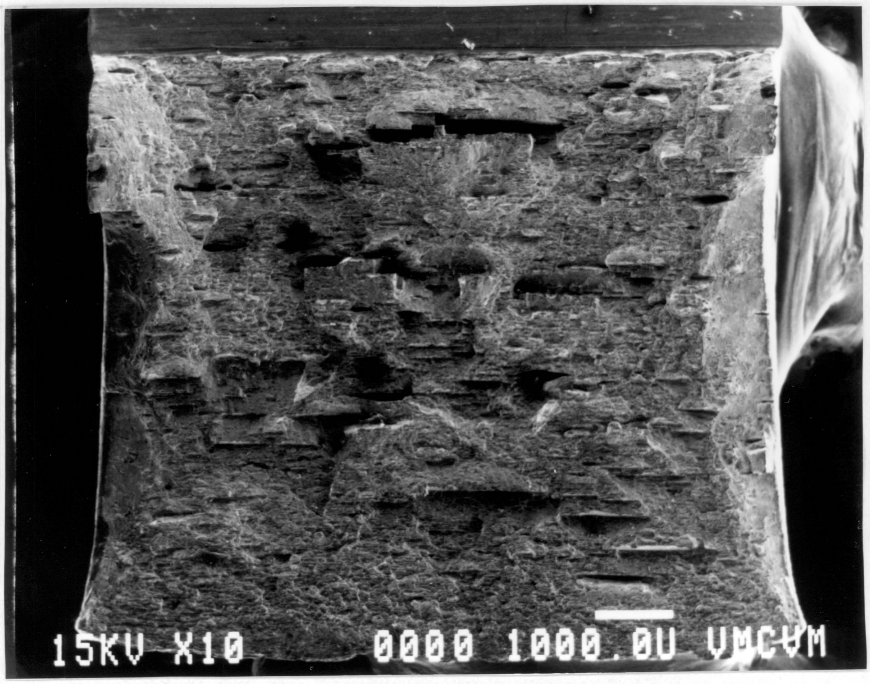

Figure 27. Fracture surface of a rolled-plate, liquid nitrogen impact test, 10X.

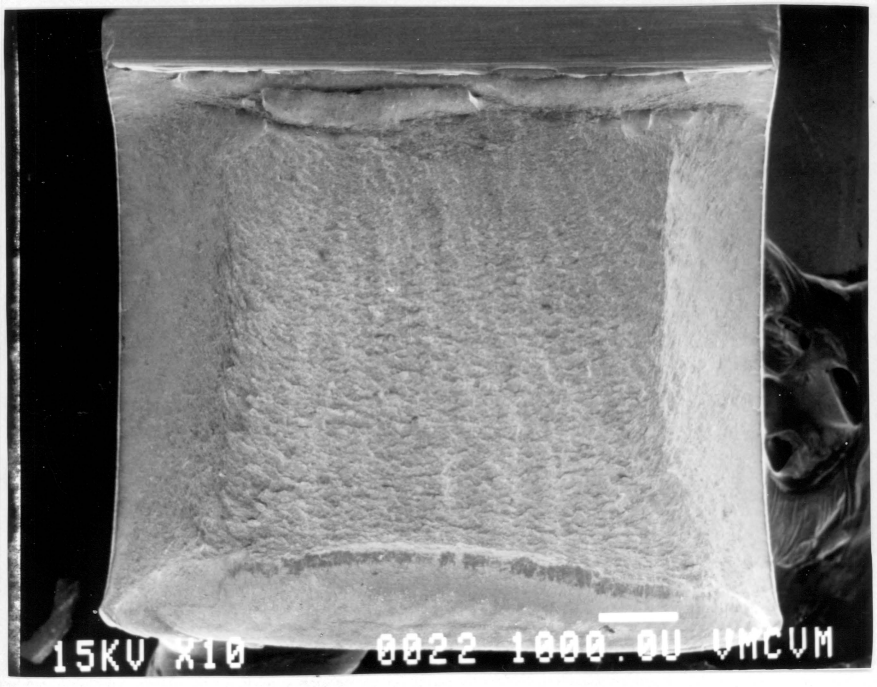

Figure 28. Fracture surface of a HERFed liquid nitrogen impact test, 10X.

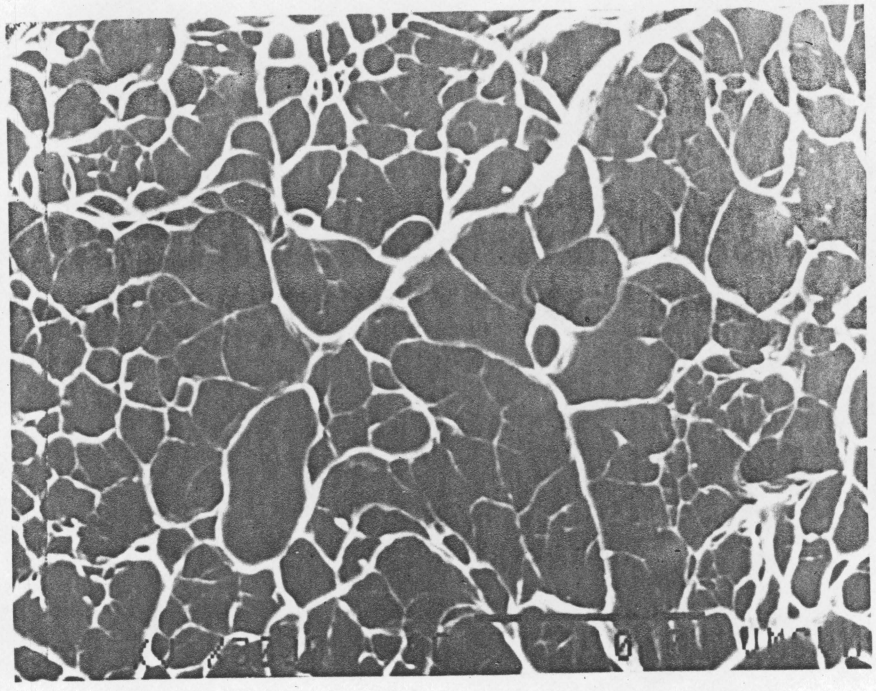

Figure 29. Fractograph of a HERFed impact sample showing microvoid coalescence, 3000X.

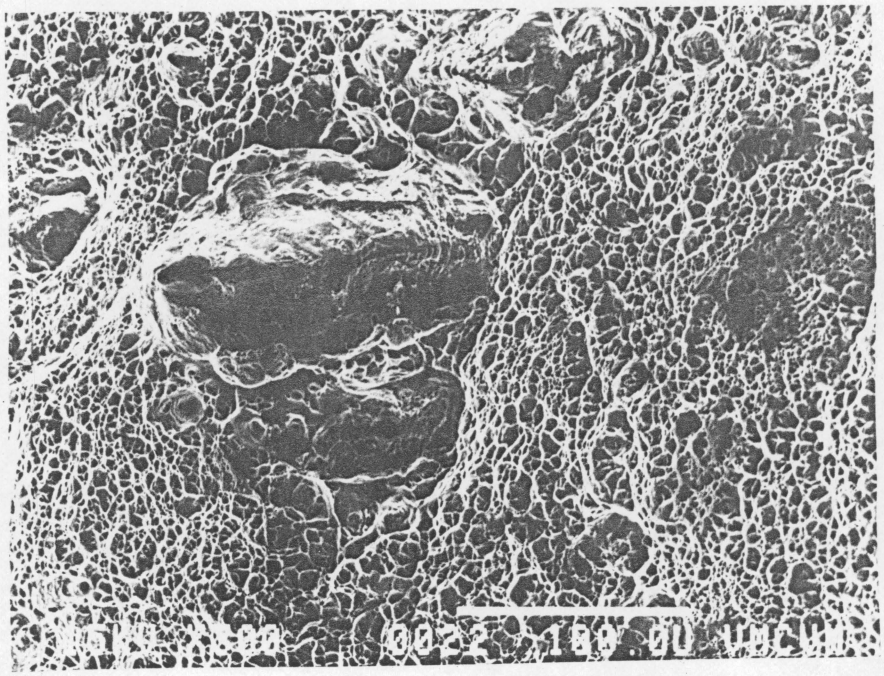

Figure 30. Fractograph on the shear lips of a rolled-plate sample showing microvoid coalescence and the effect of inclusions, 300X.

(Figure 31). The HERFed material still contains the inclusions but the mechanical process tends to randomize the direction of inclusions so that the behavior is more isotropic. Figure 32 shows an inclusion located in the HERFed material but oriented in a direction nonparallel to the crack front.

The progression of fracture is also worthy of examination in the two sets of samples. In the initiation region of both samples, (Figure 33a, b, c) the fractograph exhibits an overload type area. The region is not quite microvoid coalescence but not yet brittle either. The stretch zone consists of flat regions with some tear dimples. As the crack progressed, more dimples were evident until the propogation zone, or the overall fracture process takes over as shown earlier. The reinitiation of crack growth can now be illustrated. A relatively low magnification fractograph of an inclusion hole on the fracture surface shows the typical crack progression (microvoid coalescence) until the hole is intersected (Figure 34a). A closer examination inside the back surface of the hole shows the same type of initiation region found near the notch, (Figure 34b).

Now an examination of the impacted hydrogen charged Nitronic 40 samples is necessary.

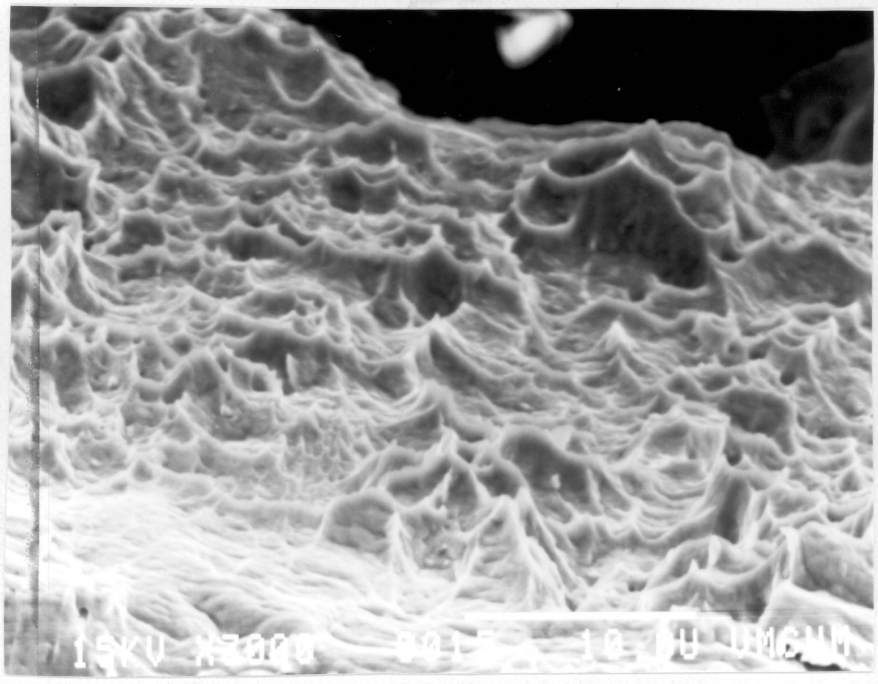

Figure 31. Fractograph of upper shelf ductility manifested as a "whipped cream" type appearance, 3000X.

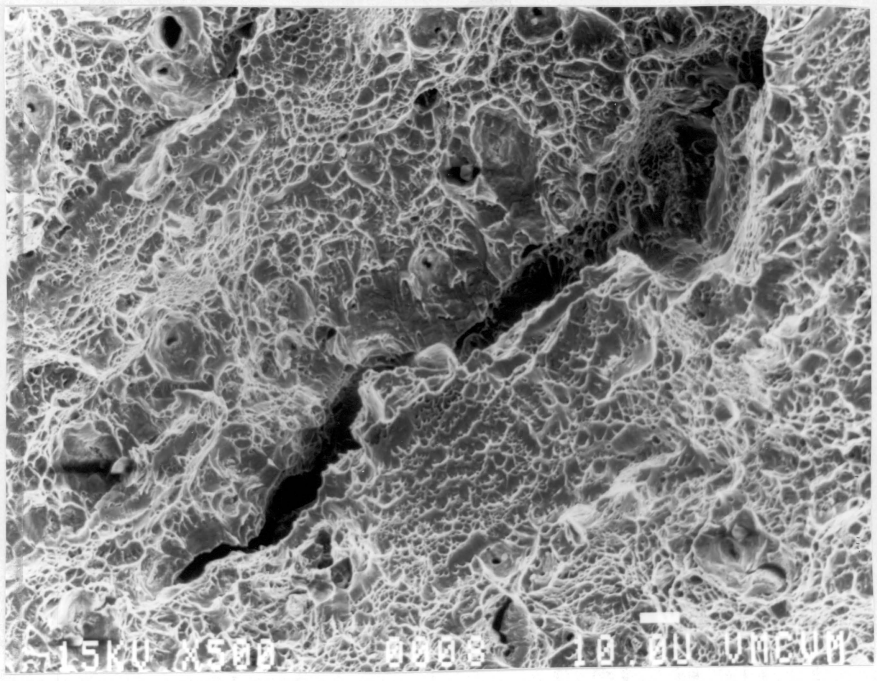

Figure 32. Fractograph from a HERFed sample showing the randomness of inclusion orientation, 500X.

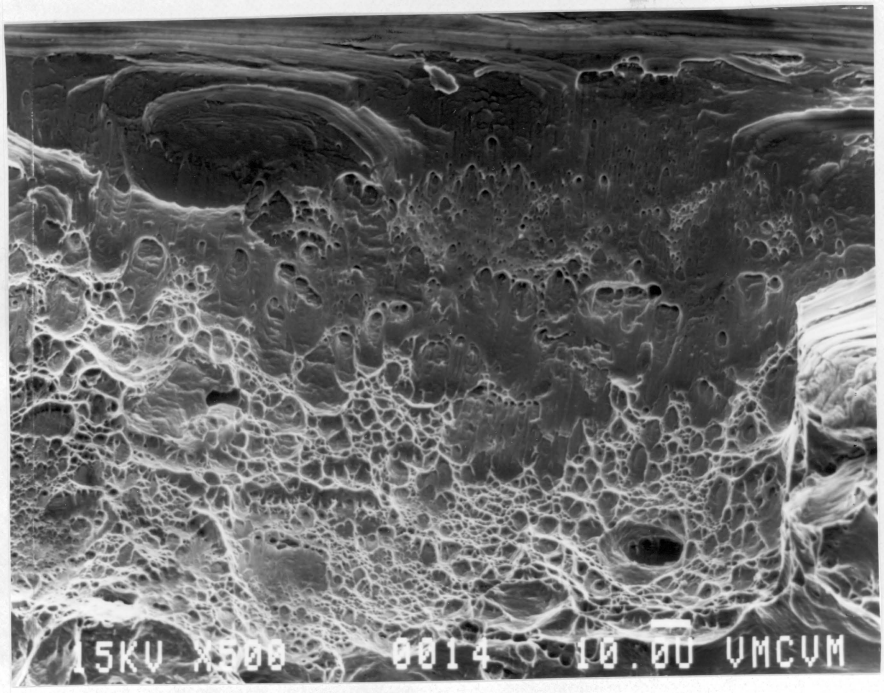

Figure 33a. Fractograph from the notch edge demonstrating a stretch zone and tear dimples on a rolled plate sample, 500X.

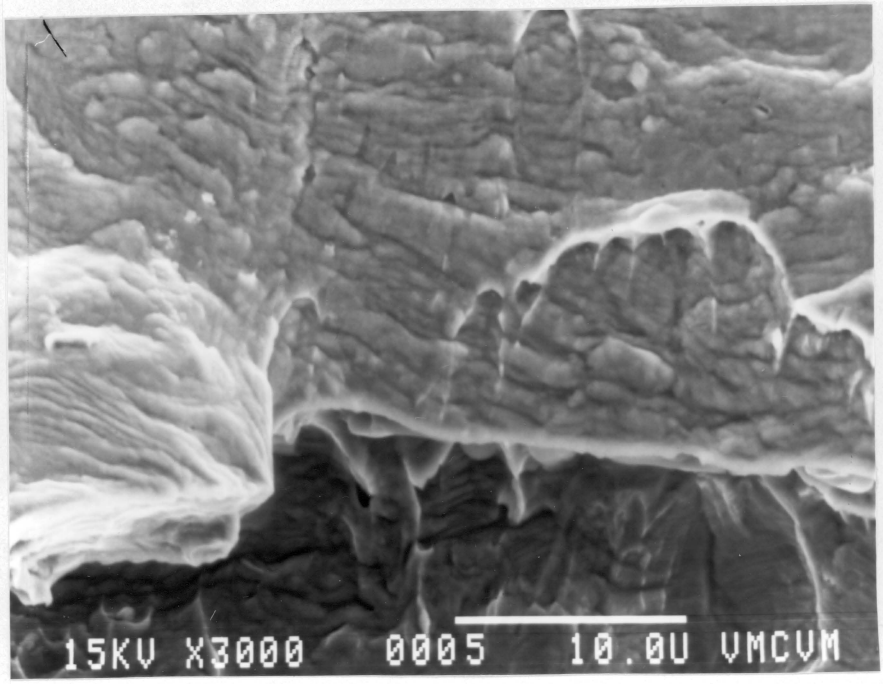

Figure 33b. Fractograph of the same initiation region shown in a.), 3000X.

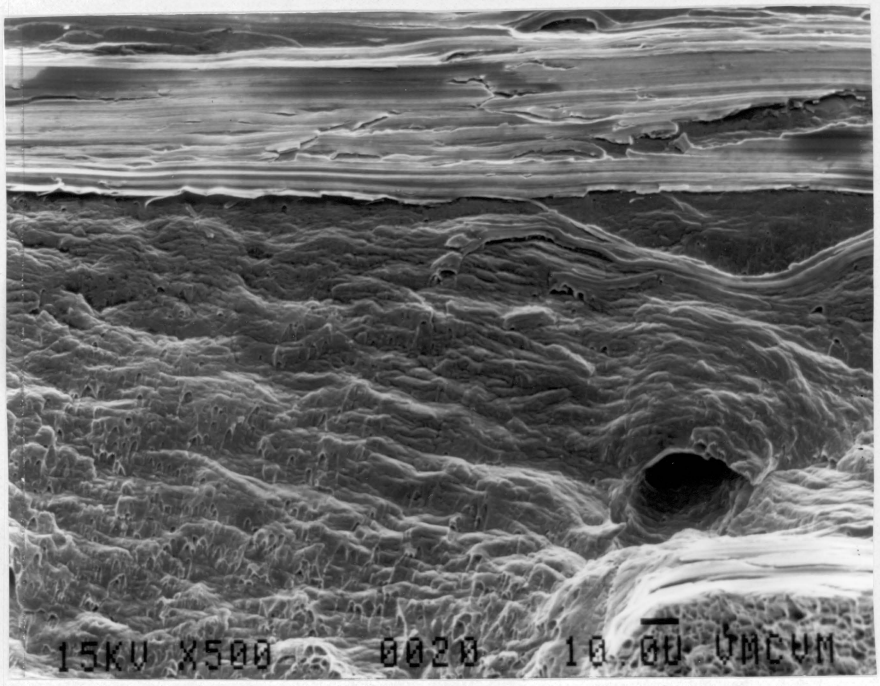

Figure 33c. Fractograph demonstrating the same type initiation region for a HERFed sample, 500X.

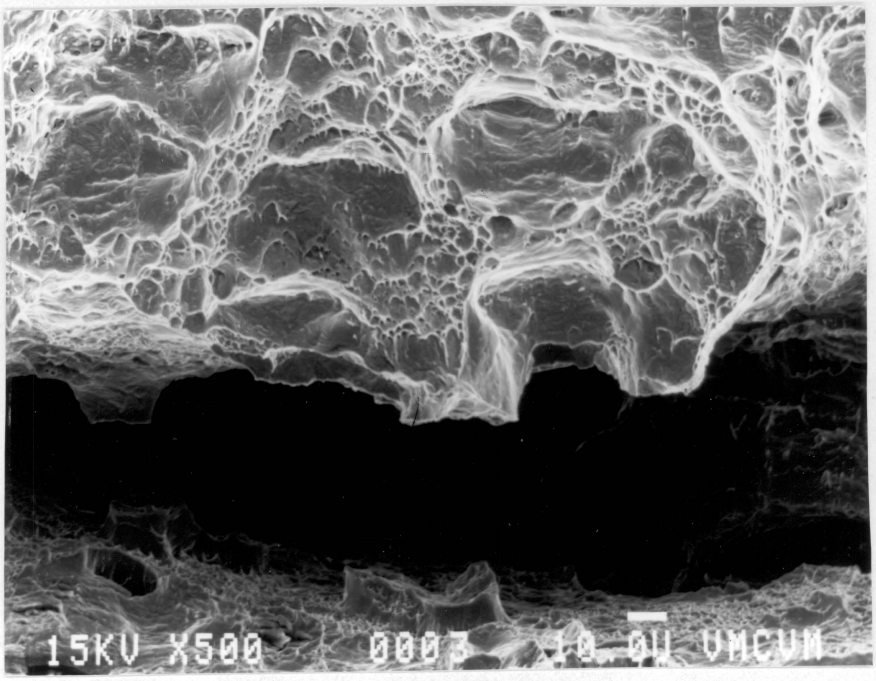

Figure 34a. Fractograph of the rolled-plate and the large pit caused by an inclusion, 500X.

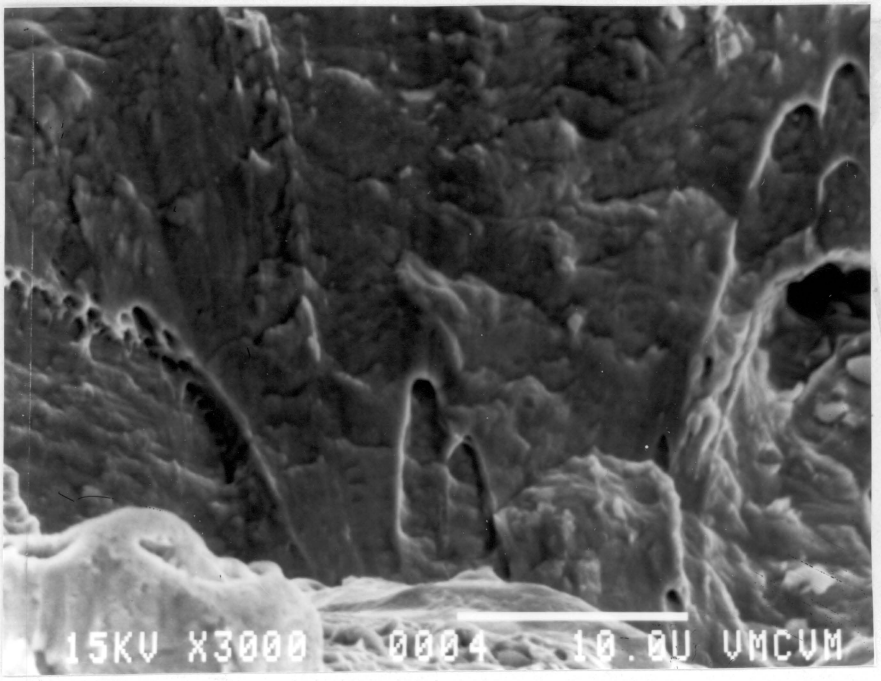

Figure 34b. Fractograph from the back side of the inclusion pit showing reinitiation, 3000X.

4.1.2 Hydrogen Tests

After charging at 10,000 psi Nitronic 40 samples of the same processing were tested in identical circumstances as their companion non-charged samples. The results of impact tests conducted at various temperatures are given in Table V. When compared to the values obtained for the uncharged samples little embrittlement due to absorbed hydrogen is evident (Figures 35 and 36) as manifested in the energy absorption. These tests, however, support previous work (23, 38) finding that interfacial weakening is extremely dependent on the charging pressure, and the exact composition.

Tests performed on Nitronic 40 samples charged at 2000 psi and 20,000 psi demonstrated negligible hydrogen effects at the lower charging pressure and large degrees of embrittlement at the higher pressure (23). A larger hydrogen induced fracture transition was observed in the 20,000 psi charged samples, which were more faceted than the samples charged at 2,000 psi. Fracture mode changes accompanying changes in the pressure of hydrogen charging are well documented (26). Rationale for such a transition begins by requiring that a critical hydrogen concentration develop at an interface and promote failure

TABLE V

Temp.	Processing	E_{max}	$E_{init.}$	$E_{prop.}$
-189	Rolled Plate	35	11	24
-150	"	44	12	32
-100	"	63	20	43
- 50	"	104	35	69
0°	"	145	47	98
22	"	140	45	95
-192	135 ksi HERF	35	13	22
-100	"	34	20	14
- 50	"	95	38	57
22°	"	165	47.5	117.5
-198	126 ksi HERF	37	18	19
-149	"	36	16	20
-100	"	88	22	66
- 50	"	132	38	94
0	"	150	-	-
22	"	180	50	130
-198	110 ksi HERF	46	20	26
-151	"	48	17	31
-100	"	105	36	69
- 50	"	180	50	130
0	"	155	57	98
22	"	183	55	128
-197	96 ksi HERF	42	17	25
-149	"	36	16	20
-100	"	64	28	36
- 50	"	131	40	91
0	"	157	50	107
22	"	185	60	125

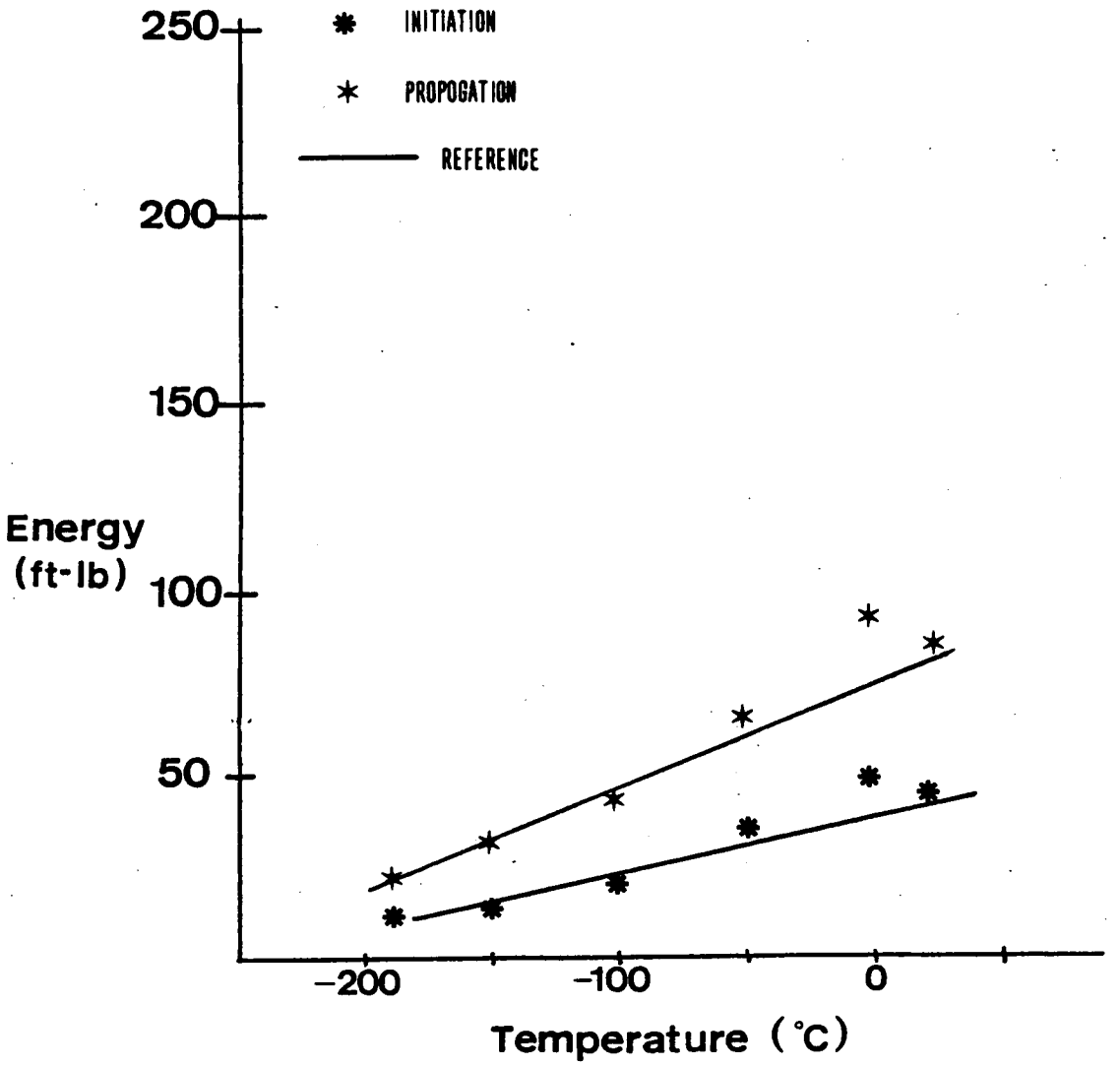

Figure 35. Hydrogen effects on the initiation and propogation energy curves of rolled plate Nitronic 40. Solid line is the no hydrogen reference curve.

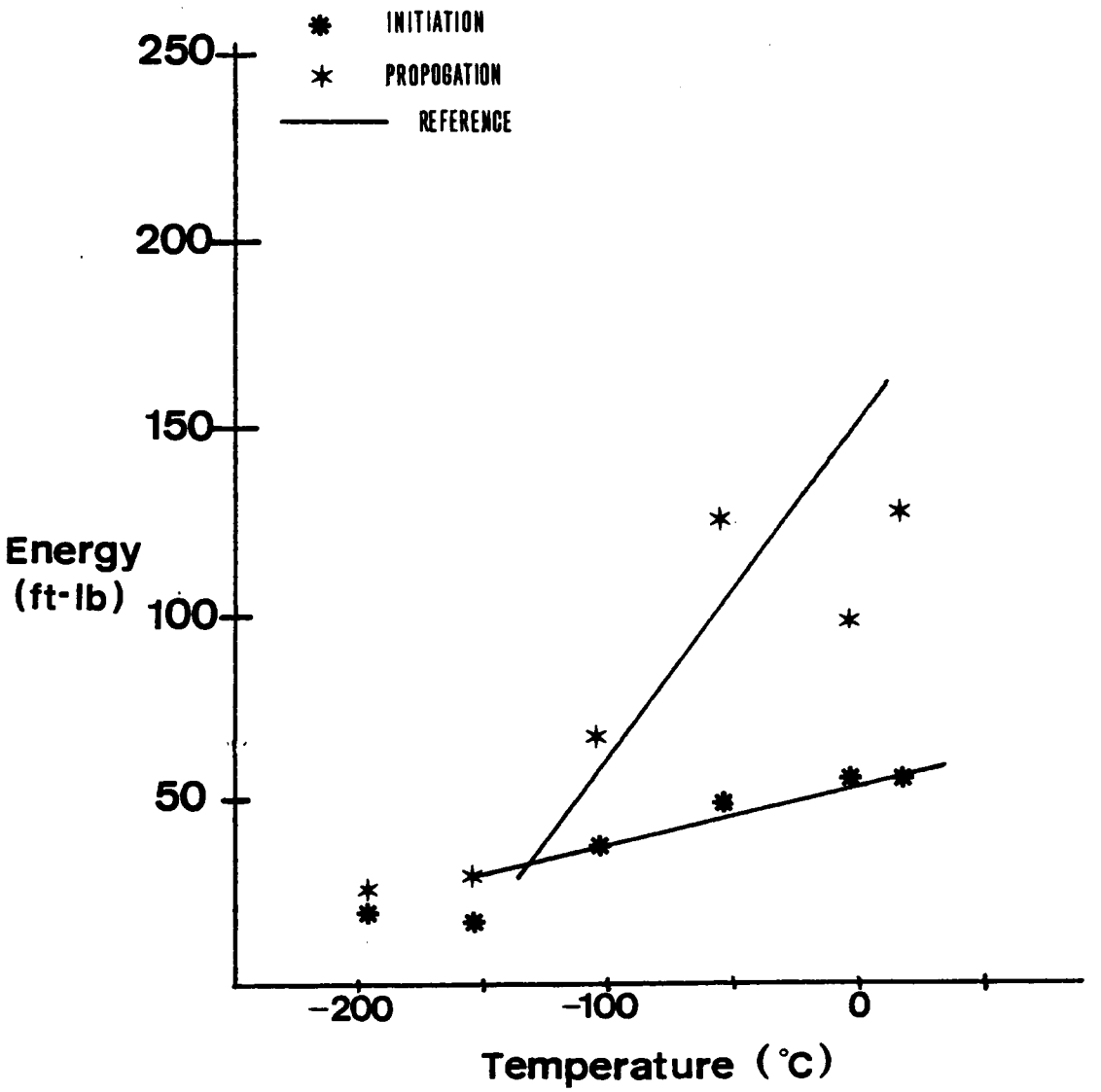

Figure 36. Hydrogen effects on the initiation and propogation energy curves for 110 ksi HERFed Nitronic 40. Solid line is the no - hydrogen reference curve.

of that interface. When this critical hydrogen concentration is reached the interfacial strength will be lowered to the point that interfacial fracture will occur before further plastic strain can develop. Verification of such interfacial weakening was discovered (23) whereby increasing the hydrogen charging pressure increases the degree of faceted fracture associated with a certain sample.

The charging pressure of the current samples is located in between the two stated above, therefore the negligible energy embrittlement found currently can be in part explained by assuming that 10,000 psi is on the lower end of the interfacial weakenging transition. The fractography confirms that this heat of Nitronic 40 is resistant to hydrogen embrittlement in these specific circumstances.

The fracture mode remained ductile with no intergranular or interfacial brittle type fracture observed at the test temperatures. Even at liquid nitrogen temperature the surface maintained microvoid coalesence in the sets of smaples (Figure 37). No substantial change in dimple size was observed and the initiation region was also the same as in the uncharged samples (Figure 38). If a large amount of smaller

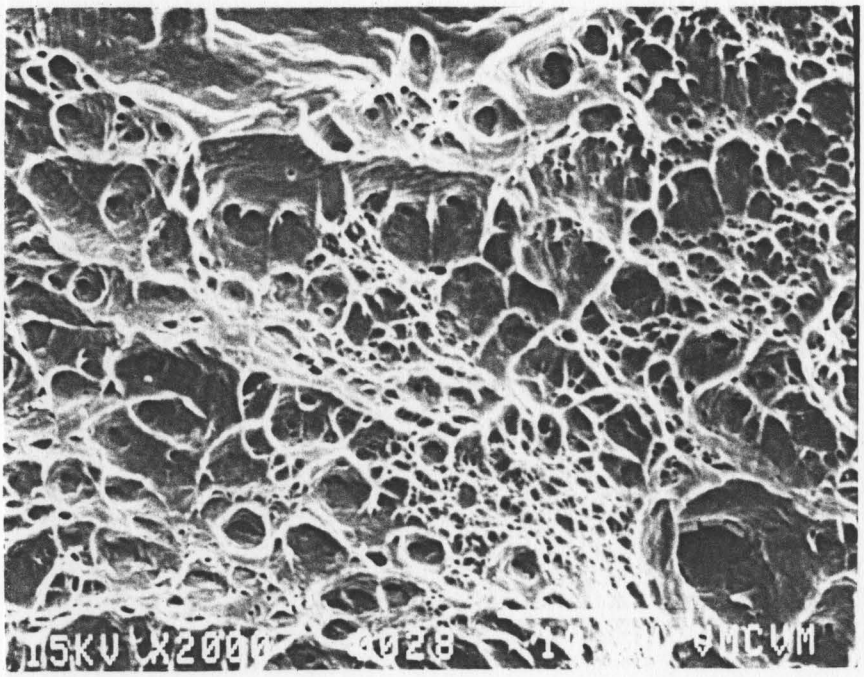

Figure 37. Fractograph of a hydrogen charged, rolled plate sample demonstrating similar microvoid coalescence as the as-received sample, 2000X.

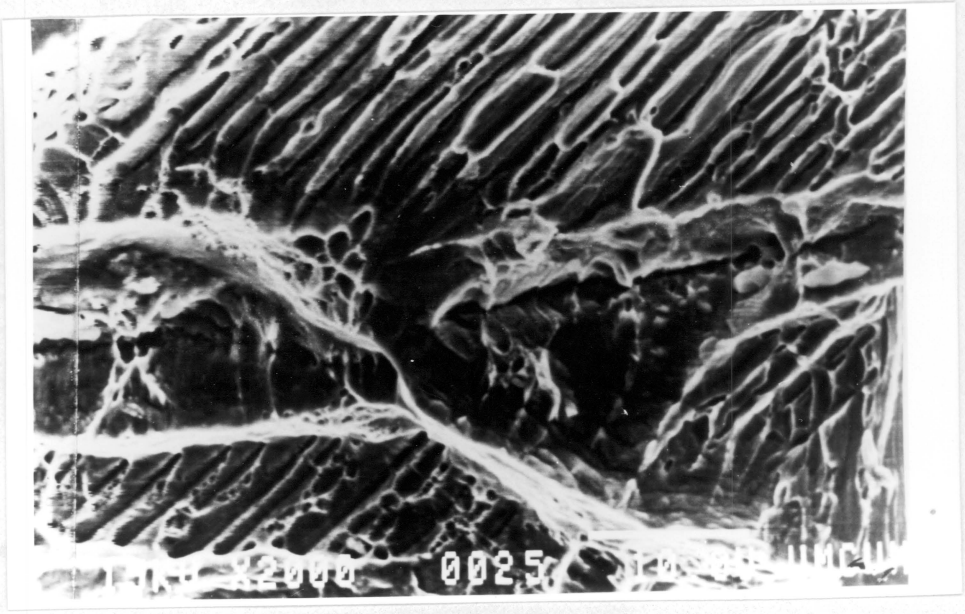

Figure 38a. Fractograph of the hydrogen charged, rolled-plate sample showing the atypical type fracture along preferential interfaces, 2000X.

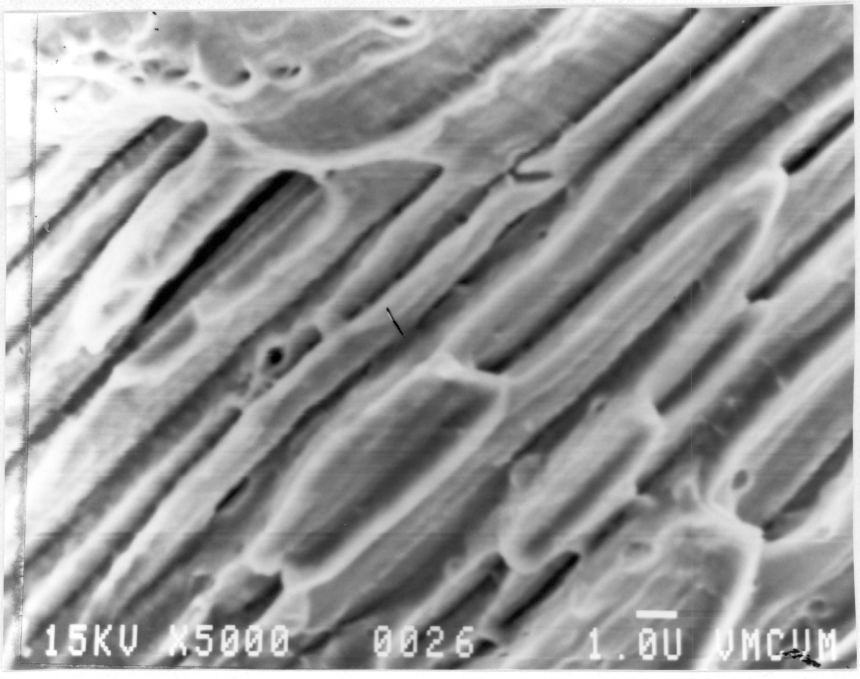

Figure 38b. Fractograph of the same region as a.) at a higher magnification, 5000X.

microvoids were present in the hydrogen charged samples, more evidence of interfacial weakening would be available. The larger number of small microvoids result from hydrogen enhancement of the role of very small inclusions and particles in the fracture process. The only difference in the fracture process took place in the rolled plate samples. Without hydrogen charging these samples exhibit ordinary ductile type fracture over the entire propogation region. When hydrogen is introduced the appearance of a typical type feature is found on several of the rolled plate impact surfaces (Figures 39 and 40). This feature is characterized as ductile fracture along preferential interfaces which is an uncommon phenomena. The rationalization for this occurrance is that the hydrogen weakened the interface to such a degree that it began to fail brittley, however the degredation was not enough to cause a complete brittle failure. The interface let partially go but could not cleave entirely so the process finished in a ductile manner.

Another possible reason for the compatibility with hydrogen under these circumstances is that minor compostional variations between heats of Nitronic 40 can cause more noticeable affects on the hydrogen

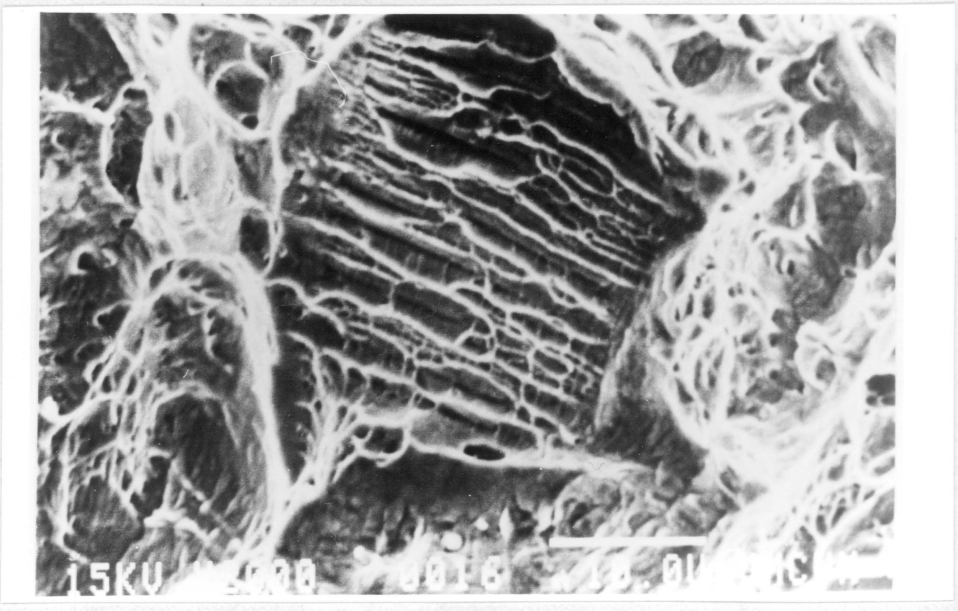

Figure 39. Fractograph giving another example of the strange fracture feature on the rolled plate, hydrogen charged samples, 2000X.

compatibility. The previous tests of Nitronic 40 impact samples were machined from a different heat of material. Slight variations in nitrogen content can cause amplified changes in behavior (36). An investigation of the tensile properties of several heats of type Nitronic 40 found that hydrogen effects on the plastic deformation ofaustenitic steels are similar to the effects of carbon, nitrogen, and other interstitial atoms (38). Alloy additions inhibit dislocation motion and can thereby strengthen the alloy so even one particular alloy so even one particular alloy has enough possible variation in its composition to cause significant variations in behavior.

The hydrogen compatability is good for the high strain rate tests used in this thesis, however the hydrogen compatibility has been shown to change when the strain rate is decreased (27). A suitable extension of this work would be to include slow bend testing at various charging pressures of the same sets of samples.

4.2 Tenelon Impact Tests

The Tenelon rolled plate possessed a relatively uniform grain structure with an average grain size of approximately 30 μm, Figure 41. Inclusion stringers played a major role in the material's behavior because both large (manganese sulfide) particles as in Figure 42 and relatively fine nearly spherical particles shown in Figure 43 were aligned parallel to the rolling direction. These stringers assisted the crack propogation by serving as low energy paths and therefore affected the Charpy V-notch impact behavior. As a result, the orientation of the stringers relative to the notch greatly influenced the fracture dynamics, and is apparent in Figure 44. The samples were subdivided into two groups: Group 1 - samples with the inclusion stringers paralled to the notch and Group 2 - samples with the inclusion stringers "perpindicular" to the notch. The difference in stringer alignment was detected after testing therefore, pairs of hydogen charged and as-rolled specimen with the same orientations were not examined at all temperatures.

Tenelon tested without hydrogen exhibits a DBTT at roughly 280K when Group 2 samples were examined and at roughly 250K when Group 1 samples were examined, Figures 45 and 46. Hydrogen charging caused the samples to lose

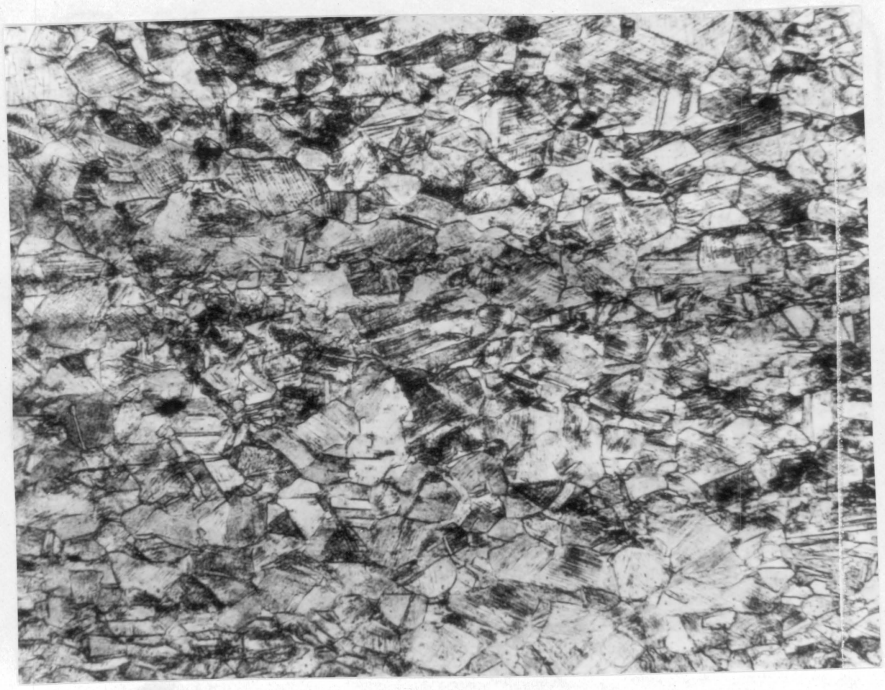

Figure 41. Micrograph of the Tenelon grain structure.

Figure 42. Micrograph showing large inclusions in the as-received Tenelon.

Figure 43. Micrograph showing spread out small inclusions in the as-received Tenelon.

Group 1

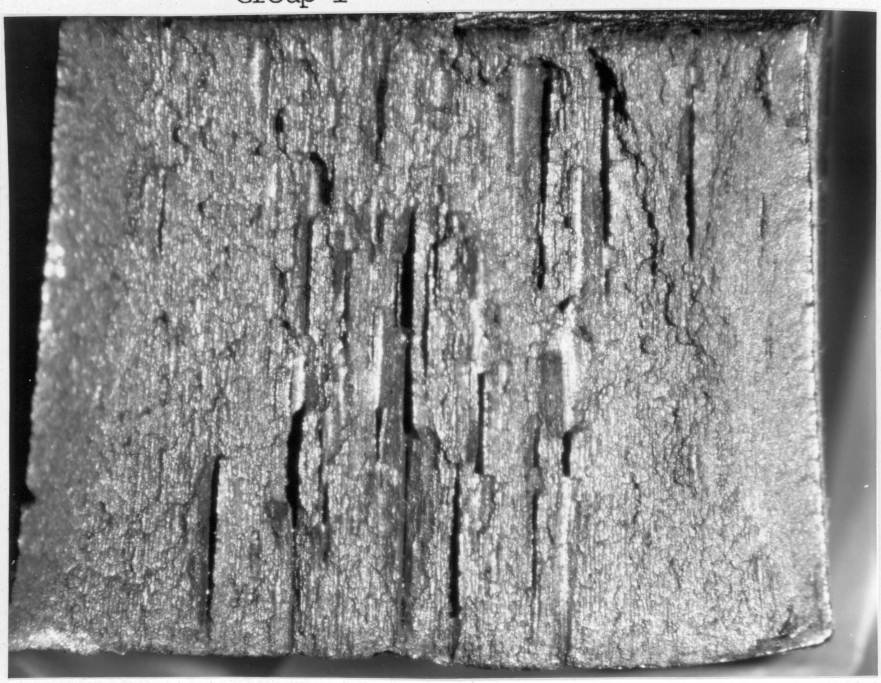

Group 2

Figure 44. Micrographs demonstrating relative orientations in impact fracture surfaces.

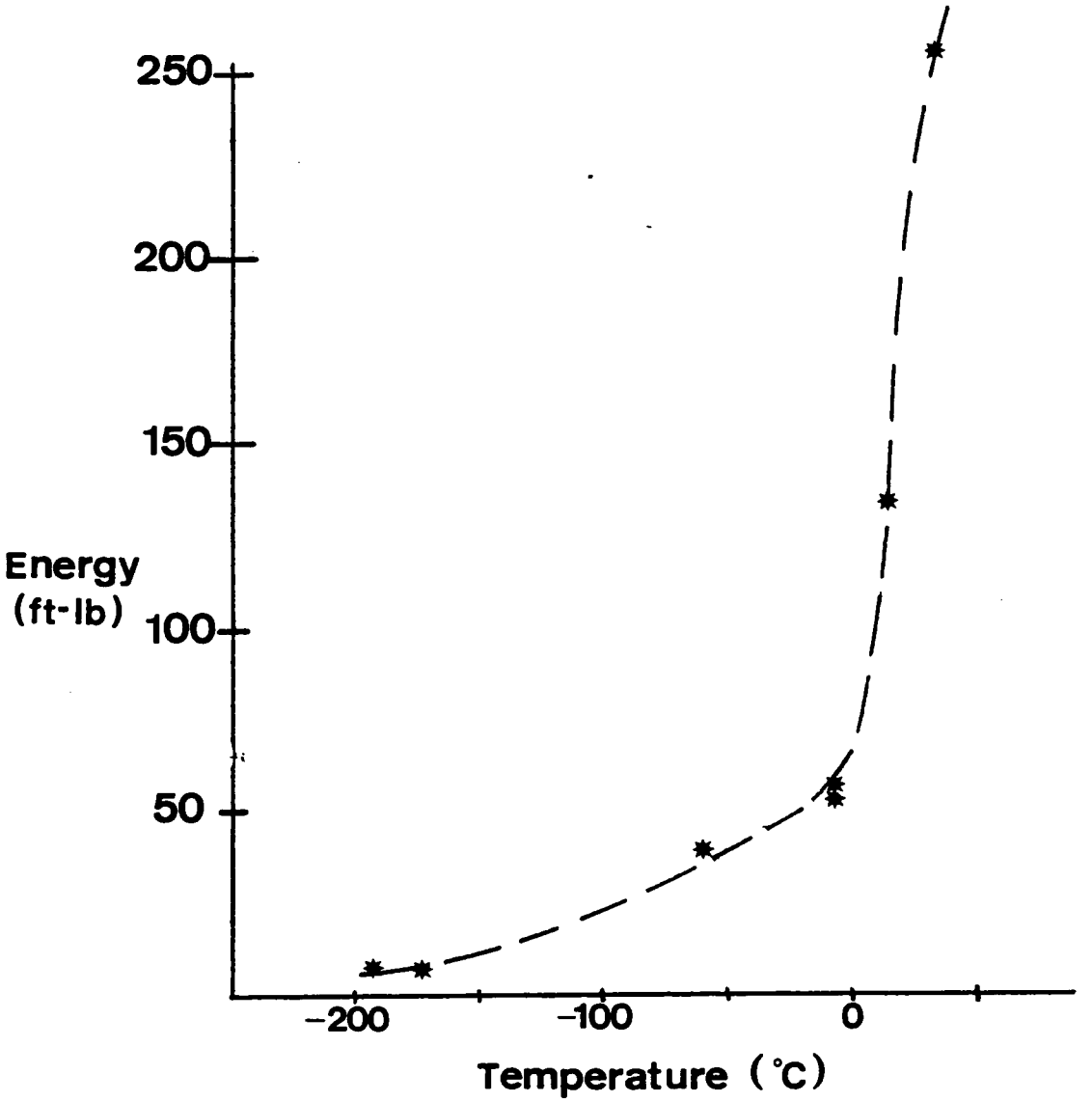

Figure 45. Energy-temperature curve for Tenelon samples in Group 2 without hydrogen charging.

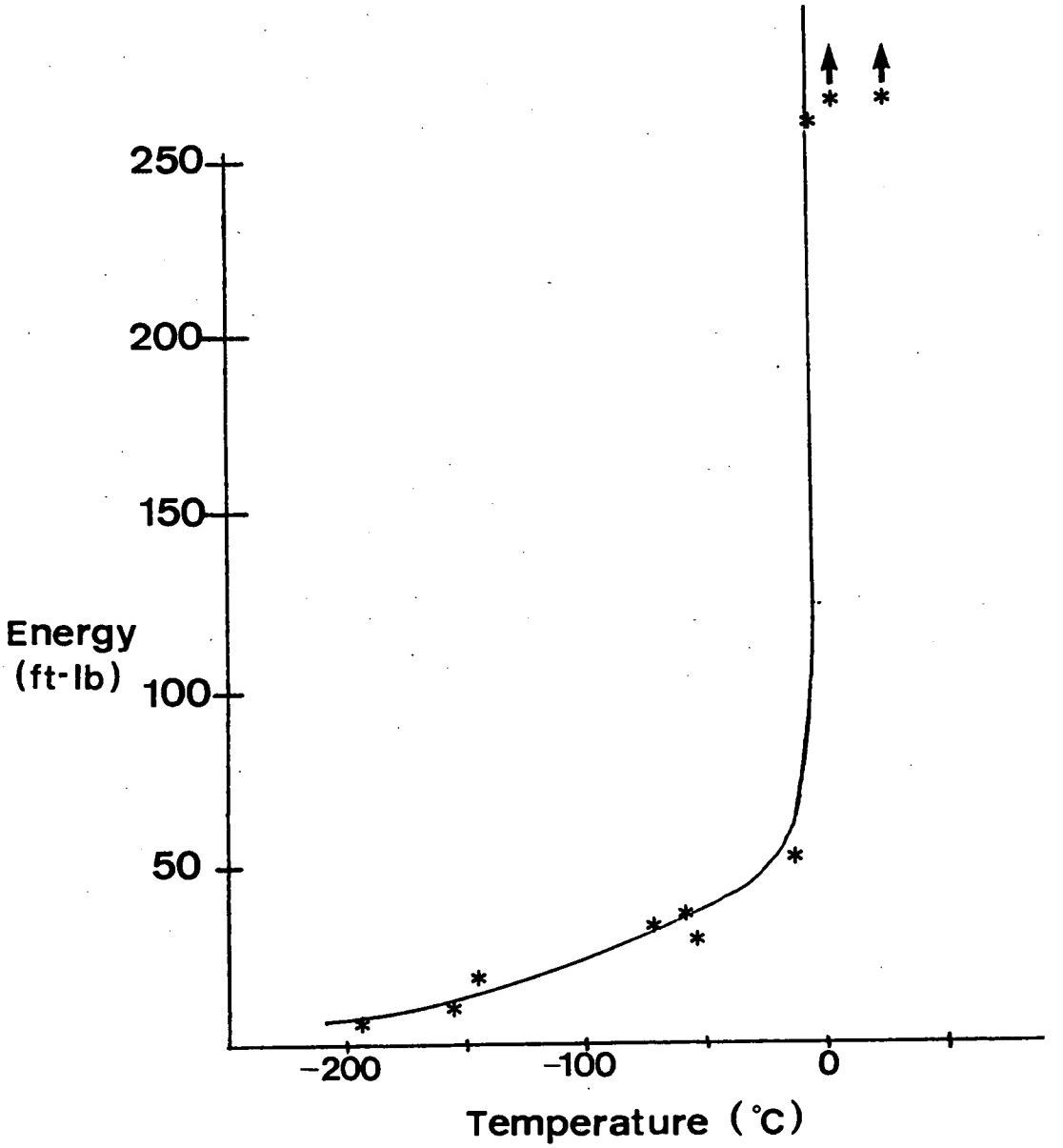

Figure 46. Ductile to Brittle Transition in Group 1 samples not exposed to hydrogen.

toughness or in other words, raised the DBTT by nearly 20K in both cases, Figure 47. The DBTT of the Tenelon plate was sensitive to inclusion orientation because early fracture along the inclusion matrix either helped crack growth (inclusion stringers perpendicular to the notch and also the crack front as in Group 2) or acted as crack arrestors (inclusion stringers parallel to the notch, Group 1). The difficulty in crack growth depended on the group of samples being tested at a certain temperature. Multiple cracking was evident in most Group 1 samples illustrated in Figure 48. These cracks formed along the inclusion-matrix interfaces and tended to blunt the propogating crack thus, the crack had to be reinitiated for continued crack growth. Reinitiation is evident in both the load time traces, (Figure 49a) and in fractography of the failed samples, (Figure 49b).

The tearing slope demonstrated an abrupt transition in its temperature dependence. During the low temperature tests, brittle fracture processes caused tearing to be much easier than during fracture at temperatures above the ductile to brittle transition, (Figure 50). When hydrogen effects were investigated, the studies showed that no hydrogen induced effects on the tearing slope occurred. Temperature plays the major

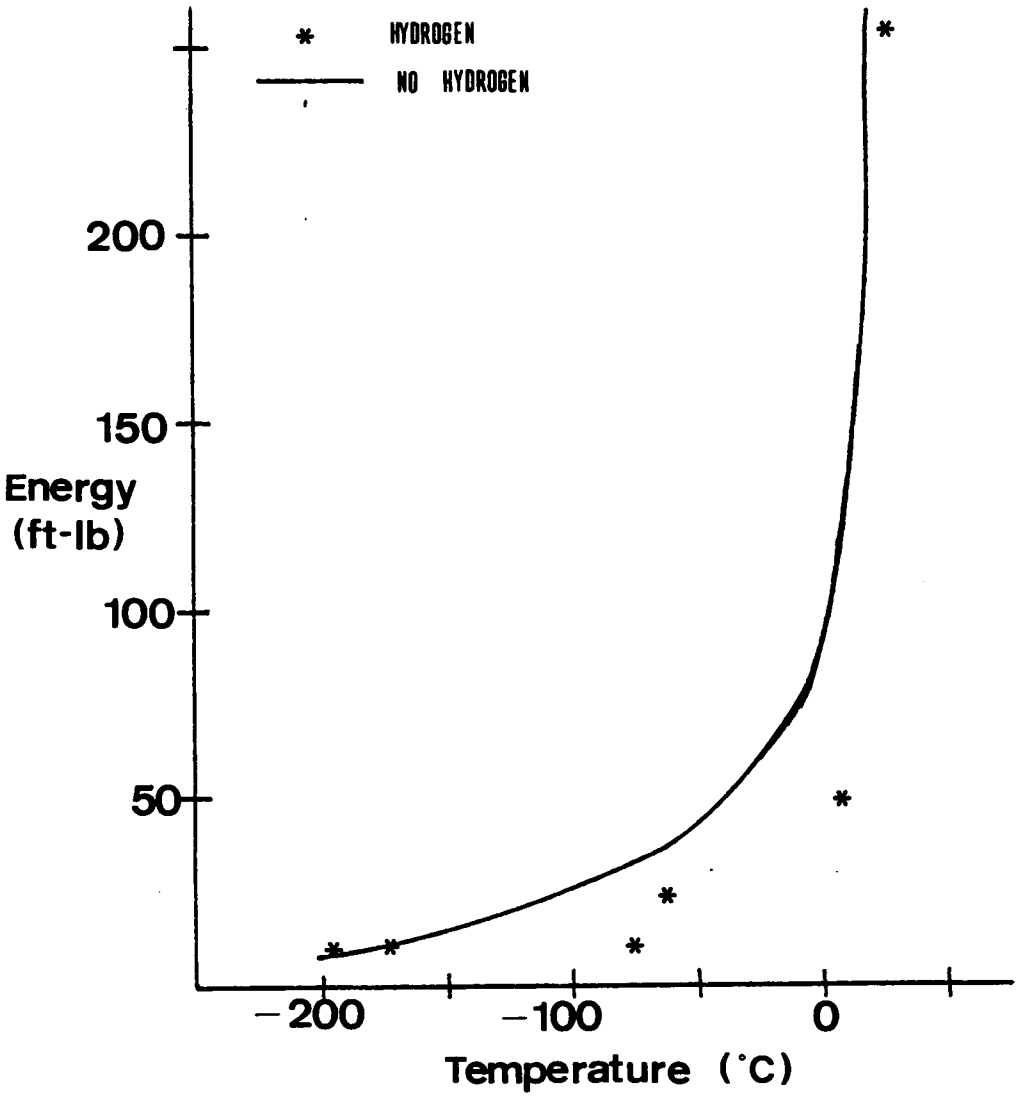

Figure 47. Effect of hydrogen on the impact behavior of Group 2 Tenelon. Note that the solid curve is the reference curve.

Figure 48. Micrograph showing crack arrest by fracture along inclusion matrix interface.

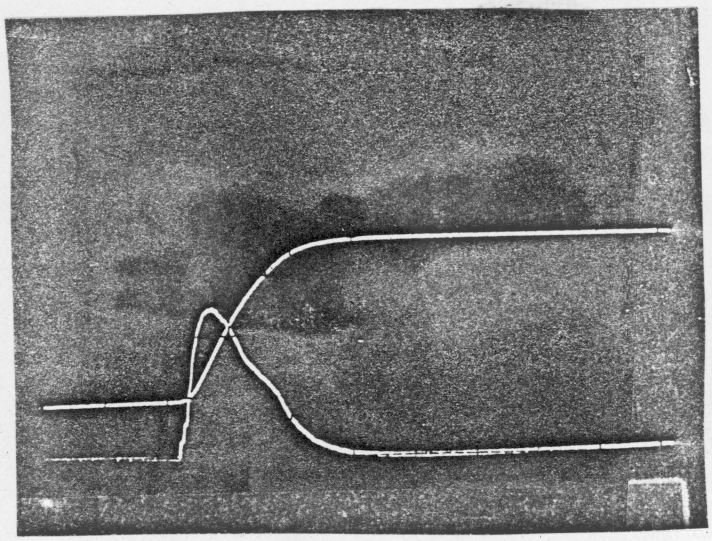

a) Load-time curve for crack reinitiation.

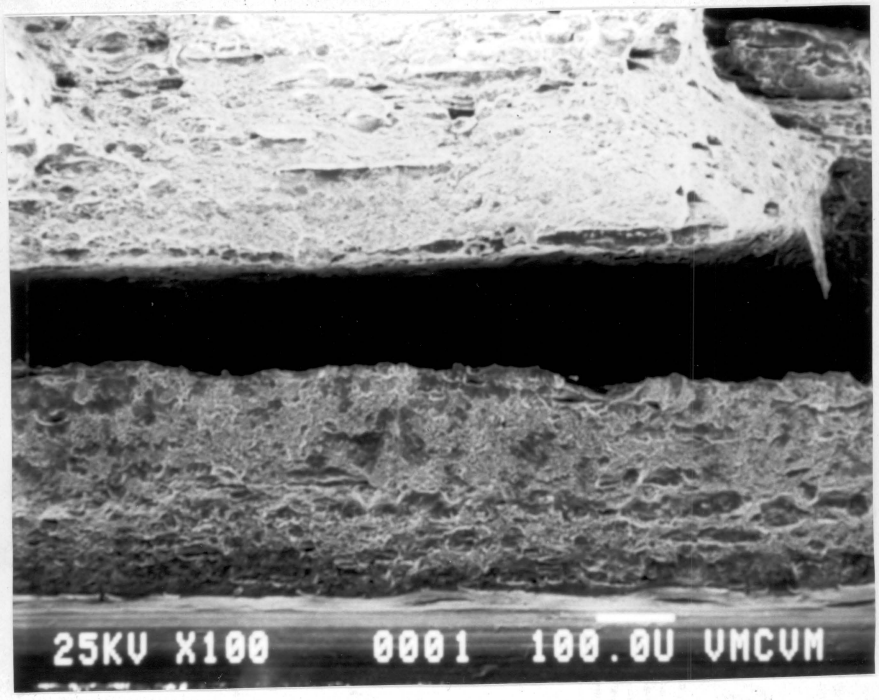

b) Crack blunting and reinitiation.

Figure 49. Crack reinitiation of Group 1 samples.

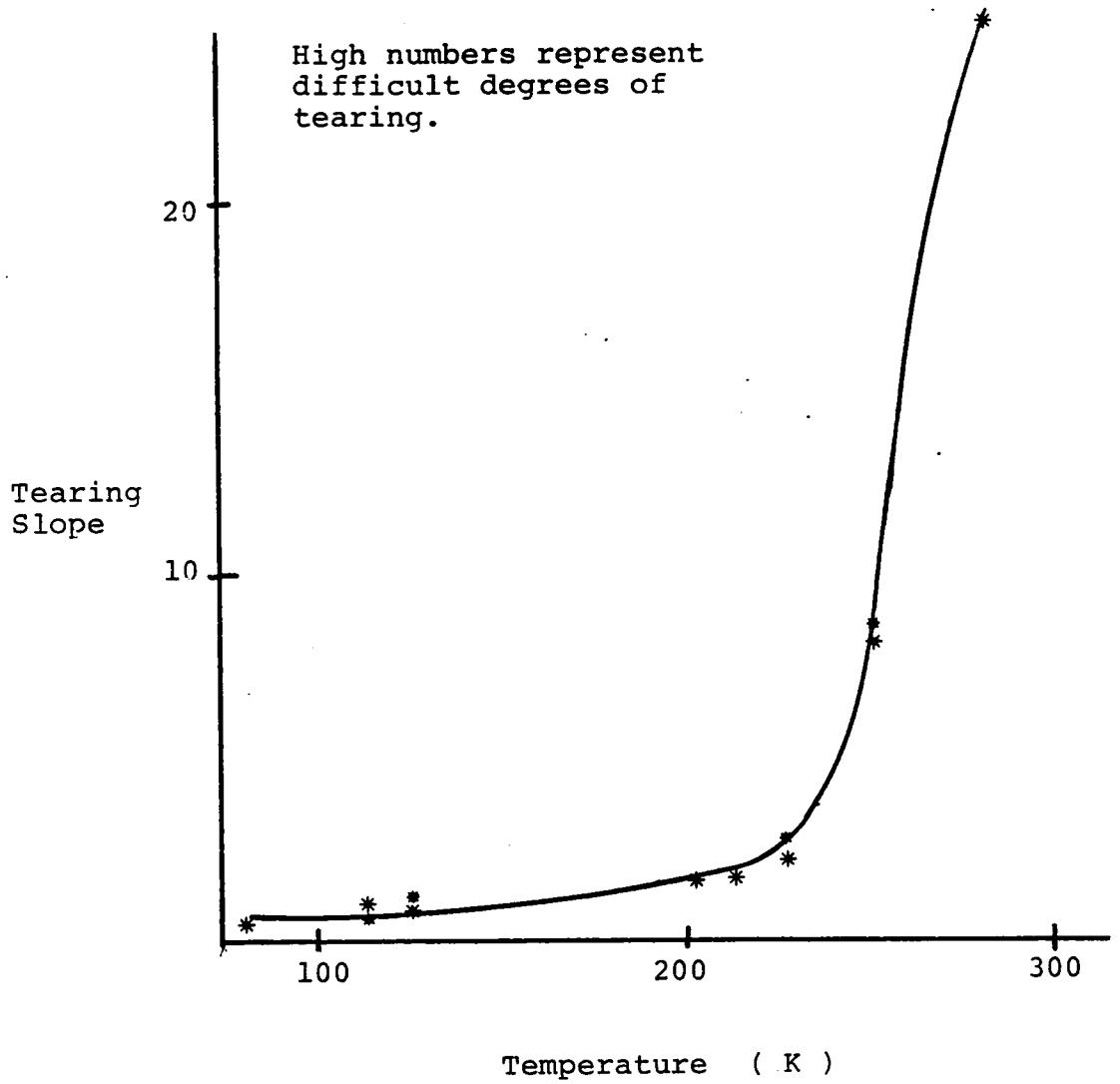

Figure 50. Effect of temperature on tearing slope for Group 1 samples. Very little hydrogen effect.

role in tearing slope effects.

Fractographic studies showed that failure above the DBTT occurred by microvoid coalescence (Figure 51a) while mixed mode fracture was noted at temperatures below the DBTT (Figure 51b). Above the DBTT the initiation region is stepped and irregular, and the propogation region for both charging conditions is extremely rough to the naked eye. The surface consists of waves and dimples with intermittant longitudinal splits resulting from intersection with large inclusion stringers (Figure 52). Below the DBTT the initiation region consists of combined stretch and dimple zones (Figure 53). The stretch zone is flat containing tear dimples which then leads into a region of equiaxed dimples which then becomes the propogation zone. In the propogation region twin boundary parting is common and ranges from 60% to 80% twin boundary separation. Hydrogen charging did not cause any new fracture modes to form, however hydrogen charging did promote the formation of the brittle fracture features. The hydrogen has the same result as lowering the temperature does and visa versa. This has an interesting application in industry. If a sample is typically used at 25 C, for example, and its hydrogen compatibility is of interest, instead of a

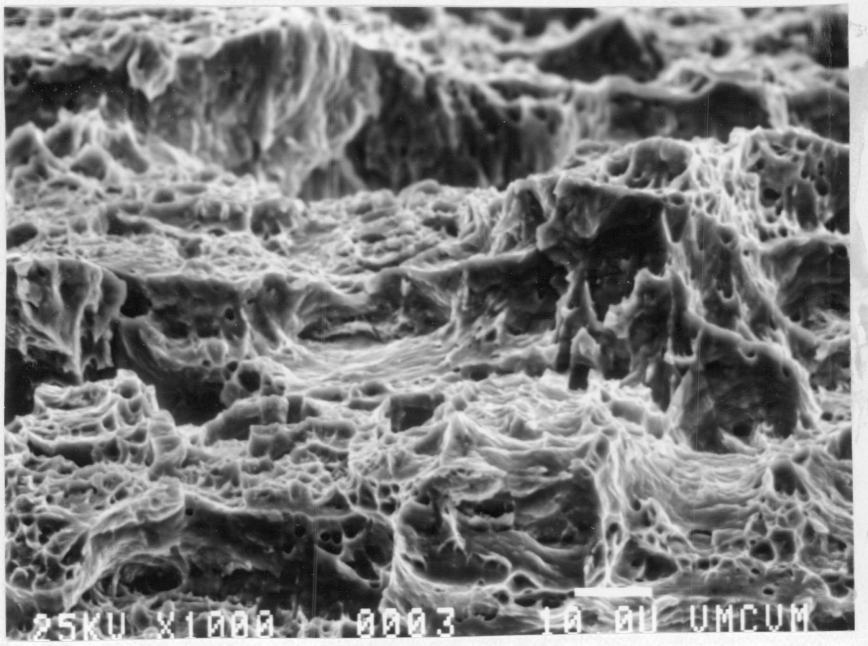

a) Microvoid coalescence at elevated temperatures (255K)

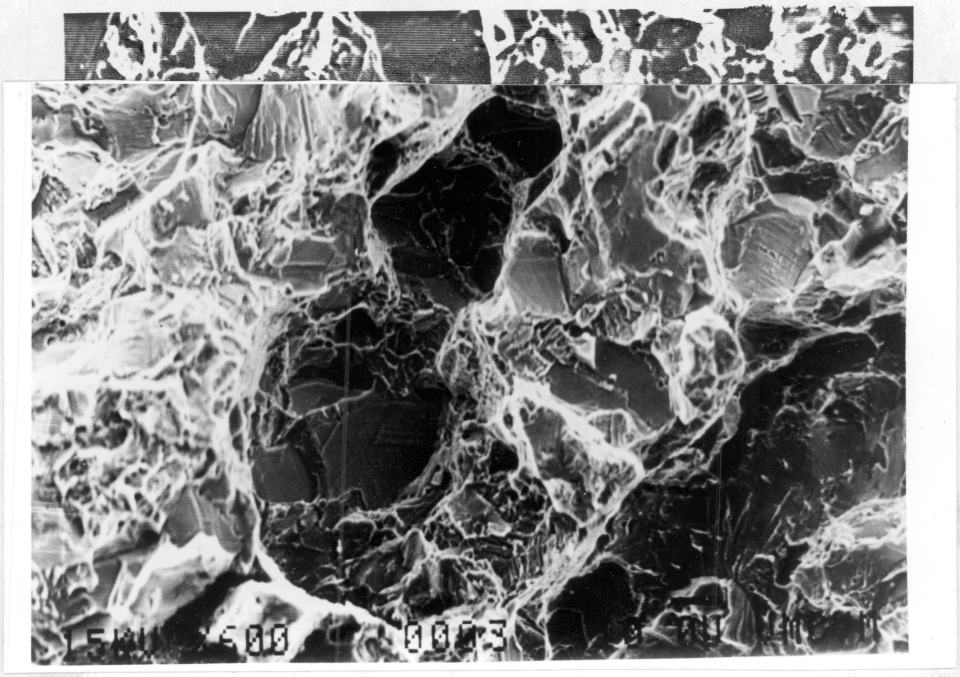

b) Mixed-mode at low temperature (77K)

Figure 51. Effect of temperature on typical fracture processes in Tenelon

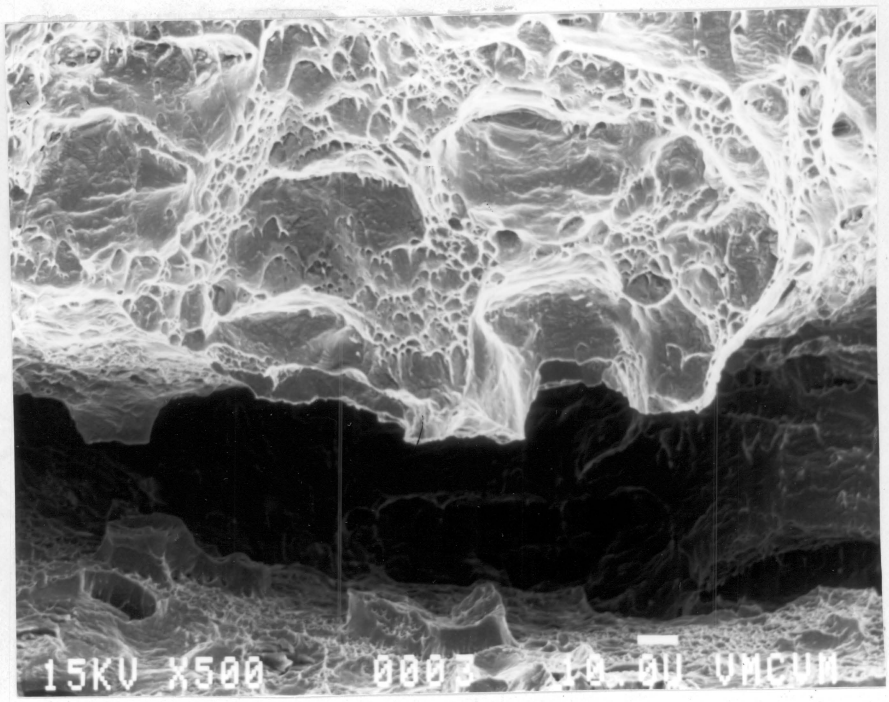

Figure 52. Fractograph of the cracks intersection with a large inclusion.

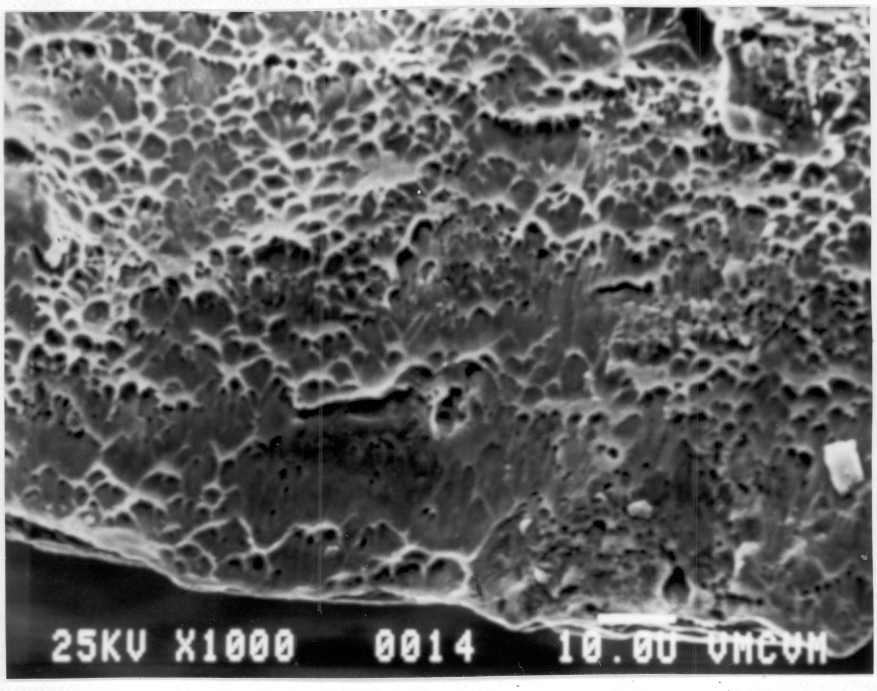

Figure 53. Fractograph demonstrating the stretch and dimple zone near the initiation of a crack.

complicated hydrogen charging procedure and then testing at 25°C, test the sample at -197°C. If the fracture process changes radically when the temperature is dropped, then hydrogen absorption may pose a problem. The hydrogen promotion of brittle facets can be seen by comparing the extent of brittle fracture in the propogation zone of a hydrogen charged and an as-received sample tested at 130K (Figure 54). The studies demonstrate that hydrogen absorption had little apparent effect on the strength of the inclusion-matrix interface, likely because the interface was primarily mechanical rather than metallurgical in nature. Yet, the impact data do demonstrate that hydrogen absorption lowers the fracture strength of the matrix and of metallurgical interfaces such as grain and twin boundaries. Hydrogen induced decreases in interfacial strength have been found in previous investigations (7, 15, 23, 41). Typically at low temperatures the hydrogen causes a greater degree of embrittlement that at the upper shelf temperatures (23). The concentration of hydrogen at an interface, C_I , is defined as:

$$C_I = C_L \exp - \left(\frac{G_B}{RT}\right)$$

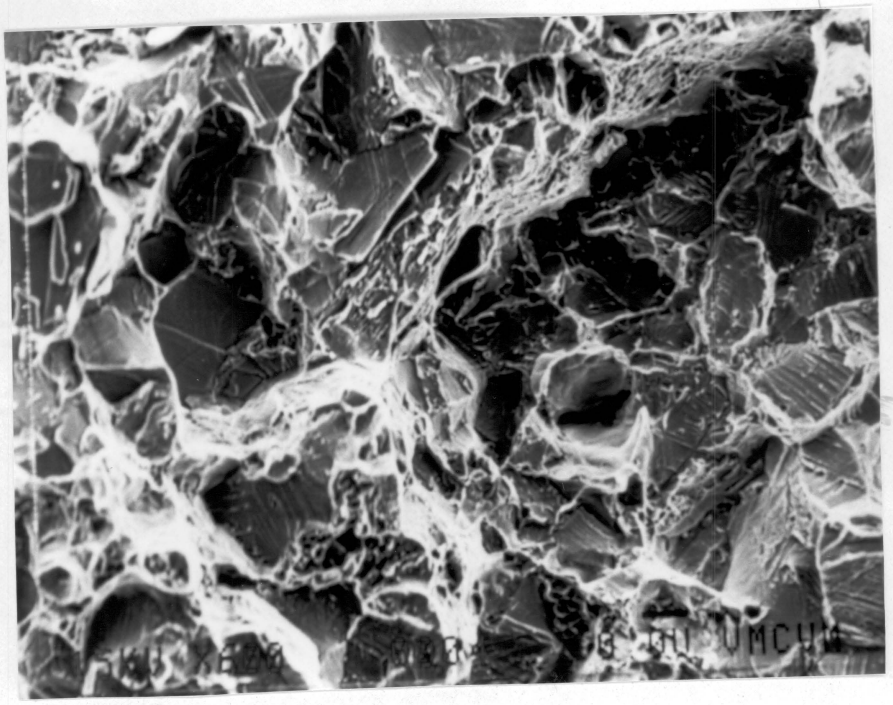

a) Hydrogen

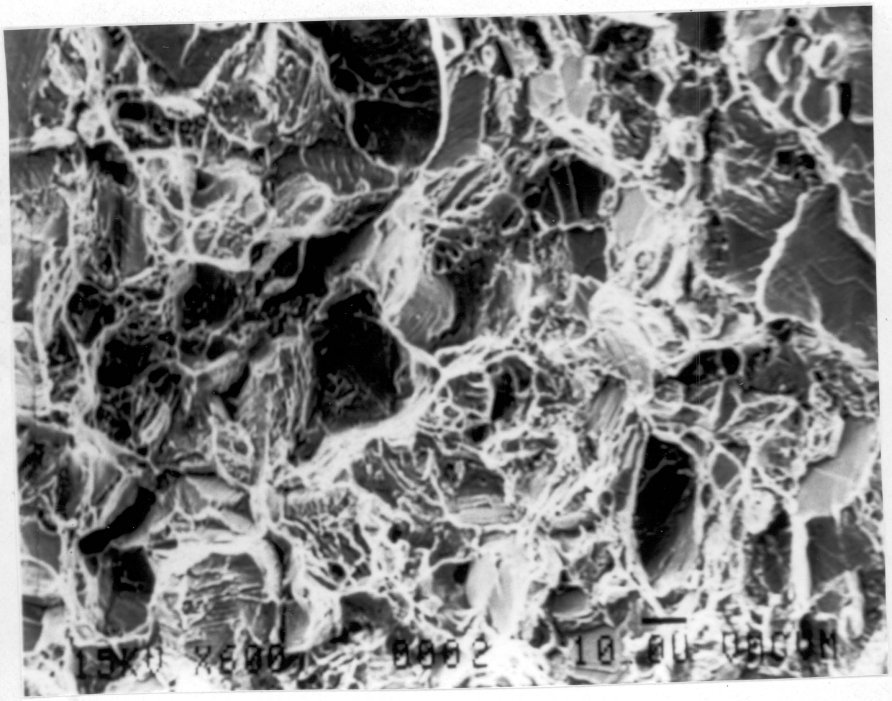

b) No Hydrogen

Figure 54. Hydrogen effects on the extent of brittle fracture during propogation of a crack during impact testing (77K).

where C_L is the concentration of hydrogen in the lattice and G_B is the binding energy of hydrogen to the interfaces which is negative for segregation. As a result, by decreasing the test temperature from room temperature to liquid nitrogen temperature (-198^{o}C), the concentration of hydrogen at an interface increases and is reflected in a greater reduction in energy absorbed in an impact test.

Earlier studies emphasized slow strain rate testing in which dislocation transport of hydrogen could promote interfacial fracture. The high strain rate of the current tests caused the hydrogen influence to be a result of hydrogen induced reductions in strength which existed before the load was applied. When tests are run at liquid nitrogen temperature, hydrogen's diffusivity is $<10^{-40}cm^2/sec$ therefore during high strain rate tests essentially no hydrogen movement occurs. In cases where hydrogen induced reductions in strength were observed, no dislocation or deformation induced rearrangement or localization is required to lower the austenite's strength. The hydrogen induced lowering of strength occurred along coherent twin boundaries and other {111} planes which are clearly evident from metallographic investigation (Figure 55).

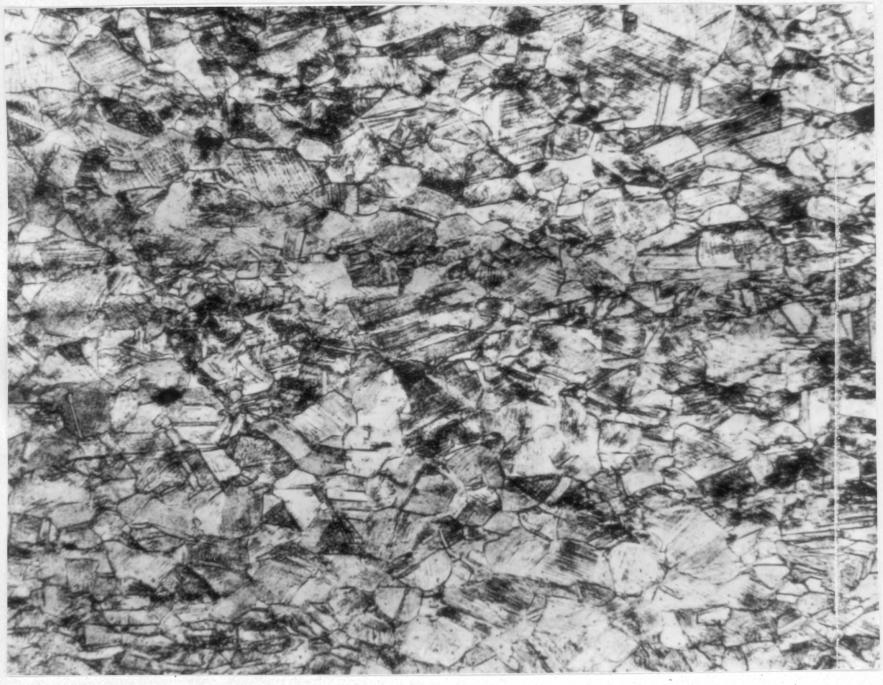

Figure 55. Metallograph demonstrating large degrees of annealing twins in the Tenelon microstructure.

Other investigators assume that the stacking fault energy and coplanar dislocation motion are of primary importance (24). Although strain induced martensite is unlikely in either Tenelon or Nitronic 40, the effect of stacking fault energy and coplanar dislocation motion may be important to discussion of hydrogen effects on this alloy. The low stacking fault energy associated with Tenelon and Nitronic 40 causes these materials to produce coplanar dislocation arrays during early stages of plastic strain. Therefore, plastic deformation leads to dislocation pile-ups at obstacles such as second phase particles, twin and slip lines or grain boundaries. These pile-ups cause localized stress concentrations. In addition, large lattice dilations will develop at the tip of the pile-up and the hydrogen concentration at that area will increase as hydrogen laden dislocations accumulate. This accumulation requires both plastic deformation and hydrogen diffusion which in this circumstance is slight and can explain the effect of hydrogen and strain rate on the fracture of many austenitic stainless steels.

Annealing twins are visible in the as-received microstructure and previous studies have found these twins to be the site of most of the hydrogen induced

decohesion (27). These would also be the most probable site for dislocation pile-ups. Deformation induced twin boundary parting was evident in this experiment (Figure 56). Also, extensive fracture on other {111} planes was visible (Figure 57). The parallel (111) traces are slip bands in the Tenelon. Investigators try to attribute the large amounts of twinning to extensive strain induced twinning, however, in a FCC structure the possibility is remote because the twinning shear exceeds one. Therefore, the trend for cracking along parallel (111) planes signifies that the hydrogen content representative of exposure to 10 ksi hydrogen is adequate to decrease the strength of the austenite lattice. This particular result, at such high strain rates, demonstrates that when austenitic stainless steels are employed in high pressure hydrogen environments, minimal lattice segregation is necessary for embrittlement.

Single surface stereographic analysis of the flat region found with the mixed-mode failure corroborated that fracture was usually along the {111} planes. X-ray diffraction scans confirmed this observation by showing that the relative {111} peak intensity was much greater than that obtained for polished samples of the same orientation. This relative increase in {111} peak

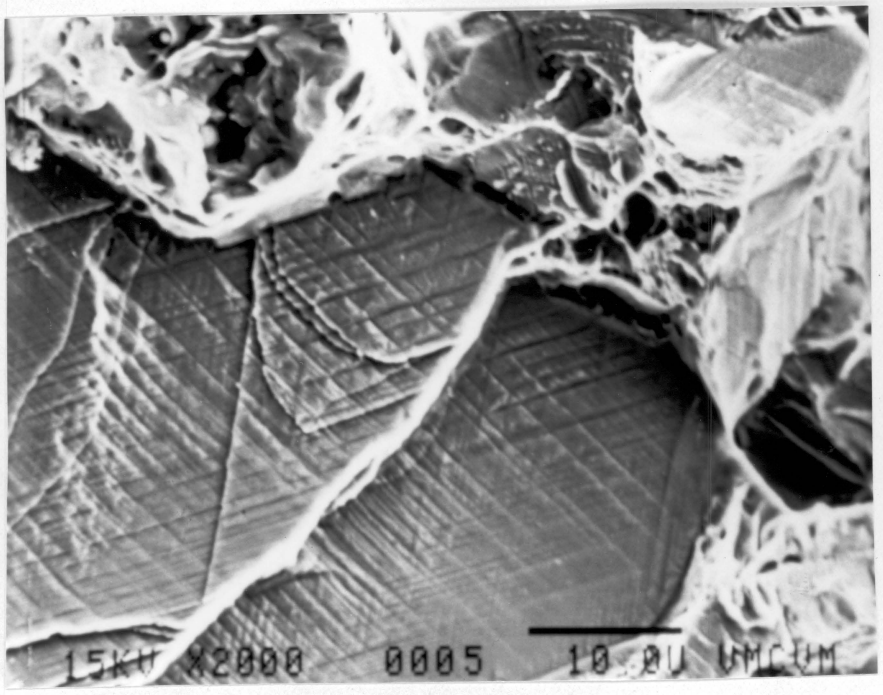

Figure 56. Deformation induced twin boundary parting in Impact Tested Tenelon

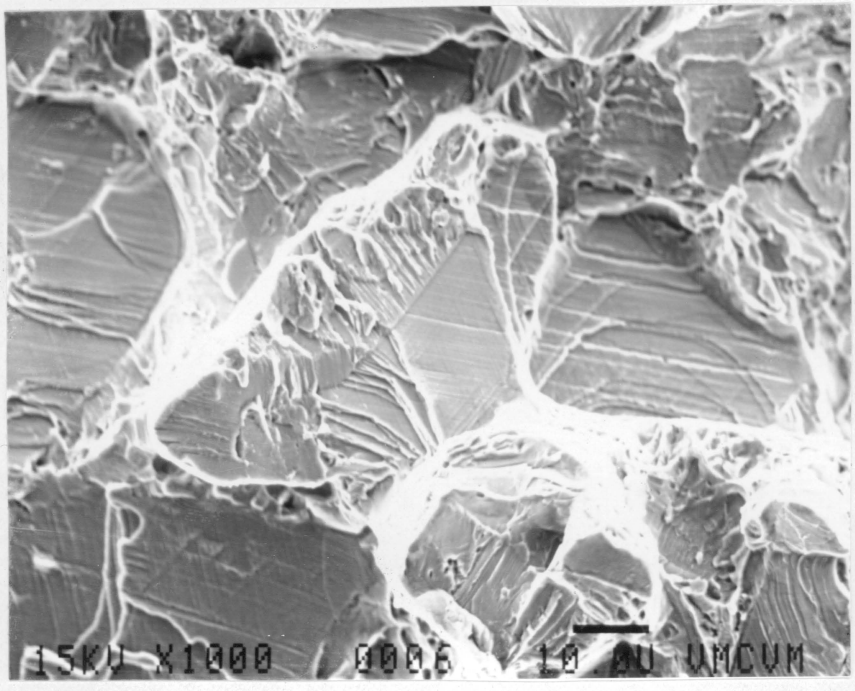

Figure 57. Fracture of Tenelon along other (111) planes.

intensity would only occur if fracture took place along the {111} plane. The X-ray studies also verified that little or not transformation to α or ε' martensite was associated with either the hydrogen charging or deformation process since only austenite peaks formed on the scan. This is consistent with earlier work stating that Tenelon is a stable austenitic stainless steel (41).

In addition to examining the fracture surfaces and analyzing the maximum energy absorbed values, the relationships between E_p, E_i, and temperature were also examined. The tests on Tenelon show a great deal of scatter because of the two types of samples (Figure 58) but a specific tendency is evident. The tendency in Tenelon is for absorbed hydrogen to greatly decrease the E_p with only slight effects on the E_i (Figure 59). This result is interesting when one thinks about hydrogen tests on notched versus smooth bar samples. The propogation results support previous work discovering that notched samples are more degraded by hydrogen exposure than the smooth samples (45). The reasoning behind the propogation-initiation changes goes back to the strain rate effect. Initiation is such a short term phenomena, no time is available for any movement of strain induced localization. The energy required for

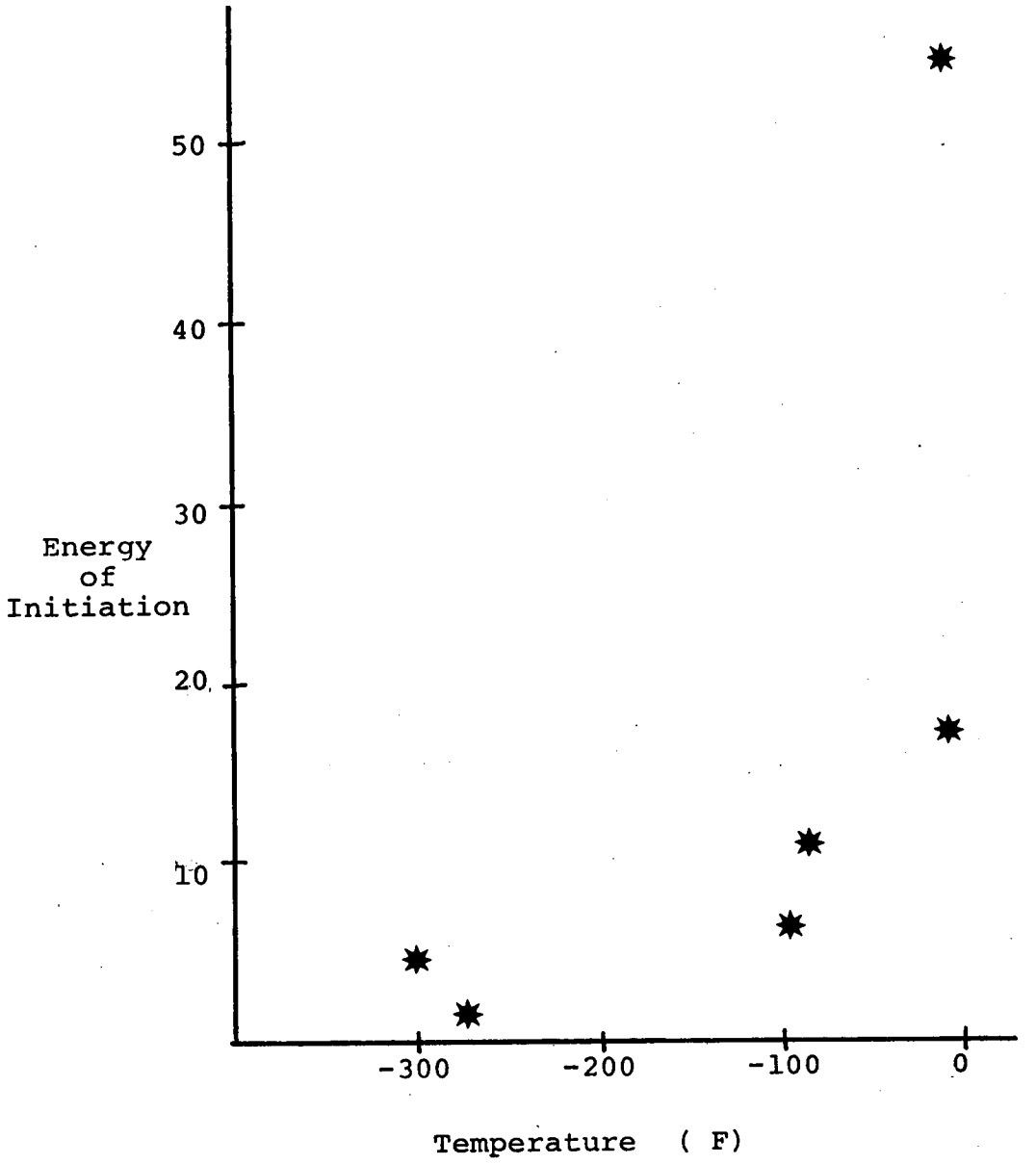

Figure 58. Typical scatter in the data for Tenelon.

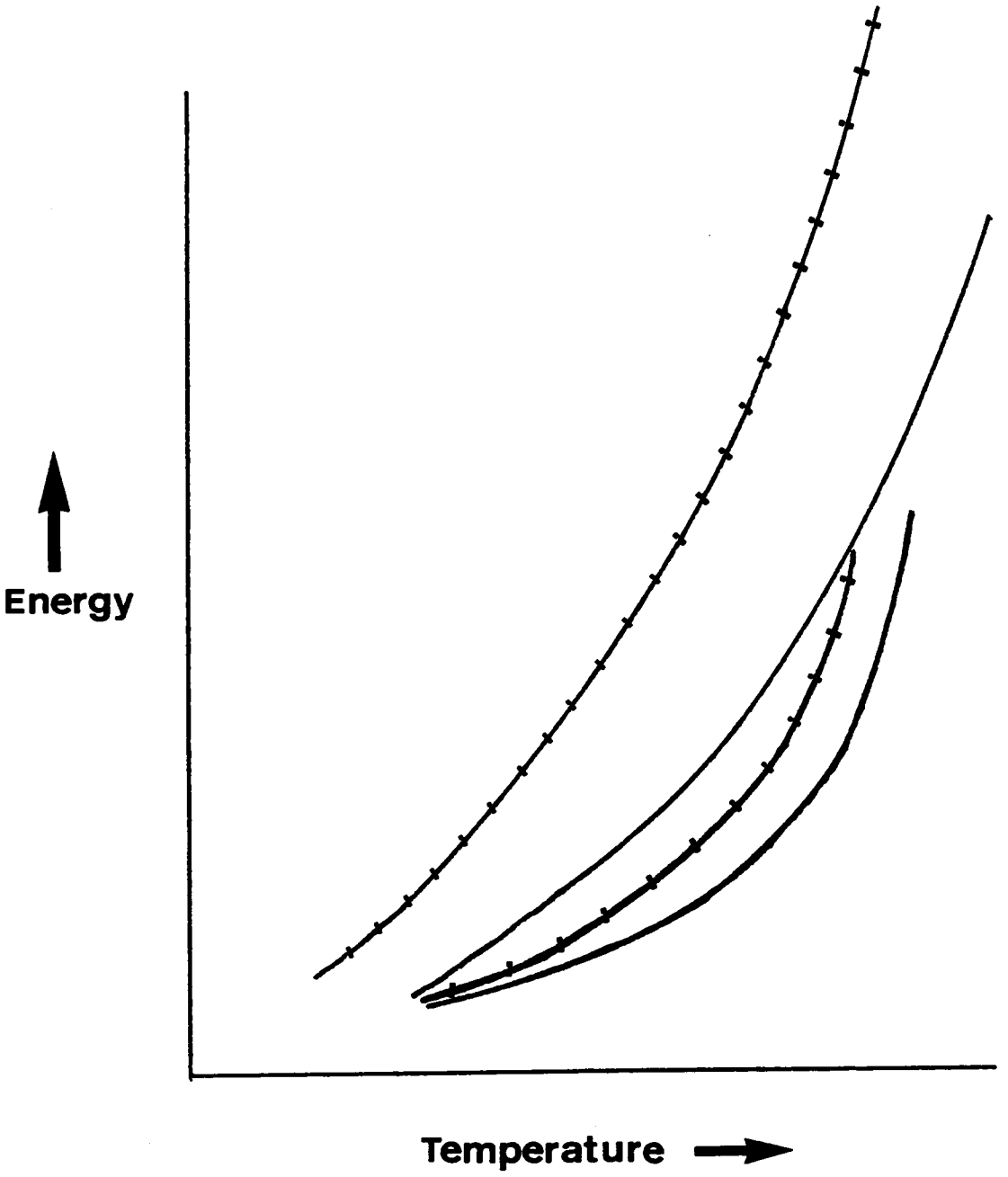

Figure 59. E_i and E_p curves for Tenelon with and without hydrogen exposure.

initiation is not able to change to any large degree because it is already so near its minimum. Propogation on the other hand takes more time to occur. Usually, investigators claim that since hydrogen embrittlement does occur during impact tests, this means that strain induced localization is not necessary. The fact that propogation is more affected by hydrogen than initiation tells us that strain rate may have a slight effect.

Now, a comparison of the two materials is in order. The results demonstrate that this heat of Tenelon is much more prone to hydrogen embrittlement than this particular heat of Nitronic 40. Both are nitrogen strengthen austenitic steels, however Tenelon contains ~.15% more nitrogen than the Nitronic 40 and an adverse effect of nitrogen on hydrogen embrittlement has been reported (10). A future outgrowth of these studies may be the development of a quick and easy test for hydrogen compatibility. From these two materials the possibility of using low temperature impact tests, instead of drawn out hydrogen charging and then ambient temperature tests to determine the compatibility is evident. Before hydrogen charging, liquid nitrogen tests on Nitronic 40 resulted in ductile fracture and on Tenelon resulted in mixed mode fracture. Absorbed hydrogen tends to simulate

low temperature behavior thus from the low temperature tests we could assume that Nitronic 40 would be safe and Tenelon may cause problems. The hydrogen charged tests verified this assumption. Future testing on a variety of steels would be useful to generalize this relationship.

CONCLUSIONS

This study has demonstrated that austenitic stainless steels are susceptable to hydrogen embrittlement under impact loading at liquid nitrogen temperatures. This embrittlement manifests itself in a reduction in the amount of energy required to fracture a hydrogen charged Charpy V-notched sample and in a change in fracture mode which results in tendency for failure along specific crystallographic planes and a shift in the DBTT. The hydrogen induced effects were dependent on the type of steel tested and were similar to effects induced by decreases in temperature. The temperature dependence of the fracture processes were greatly changed by the fabrication process used to produce the steel studied. The following specific points were established:

- HERFing Nitronic 40 improves the impact toughness and cuts down the detrimental effect of inclu-ions.
- An optimal level of HERFing exists in relation to impact toughness.
- Hydrogen embrittlement is dependent on the hydrogen charging pressure and thus the amount of hydrogen in the lattice.

- Hydrogen absorption in Tenelon lowers the cohesive strength of the austenite lattice and promotes fracture along the {111} planes.
- Hydrogen embrittlement can be manifested as a reduction in the amount of energy required to fracture a specimen.
- Dislocation transport and strain induced localization of hydrogen are not necessary for hydrogen embrittlement in austenitic stainless steels.

REFERENCES

1. H. W. Kirby and J. I. Morely, J. Iron Steel Inst., Vol. 158, p. 289 (1948).

2. J. P. Hirth, Scripta Metallurgica, Vol. 11B, p. 861 (1980).

3. L. Christodoulou, M. F. Stevens, J. J. Lewandowski, I. M. Berstein, and A. W. Thompson, Environmental Degredation of Engineering Materials in Hydrogen, edited by M. R. Louthan, Jr., R. P. McNitt and R. D. Sisson, Jr., p. 161, V.P.I. & S.U., Blacksburg, VA. (1981).

4. M. R. Louthan, Jr., Hydrogen in Metals, edited by I. M. Bernstein and A. W. Thompson, p. 53, The Metallurgical Society of AIME, N. Y. (1981).

5. M. R. Louthan, Jr., G. R. Caskey, Jr., J. A. Donovan and D. E. Rawl, Jr., Materials Science and Engineering, Vol. 10, p. 357 (1972).

6. M. R. Louthan, Jr., R. D. Sisson, Jr., R. P. McNitt, and P. E. Smith, p. 829, ibid. Ref 4.

7. G. G. Hancock and H. H. Johnson, Trans AIME, Vol. 236, p. 513 (1966).

8. Hannu Hanninen, Simo-Kekka Hannula, Seppo Tahtinen, "Hydrogen Effects in Austenitic Stainless Steels".

9. A. W. Thompson, "Applications of St. Steel in High Pressure Hydrogen", prepared for A Handbook of Stainless Steels.

10. A. W. Thompson, I. M. Bernstein, "The Role of Metallurgical Variables in Hydrogen Assisted Environmental Fracture", Advances in Corrosion Science & Technology, Vol. 7, Plenum Press, N.Y. (1970).

11. G. R. Caskey, Jr., "Hydrogen Induced Brittle Fracture of Type 304L Austenitic Stainless Steel", ASTM STP, Vol. 733, p. 86.

12. J. A. Brooks and A. J. West, "Hydrogen Induced Ductility Losses in Austenitic Stainless Steel Welds", Sandia Laboratories.

13. M. R. Louthan, Jr., D. E. Rawl, Jr., J. A. Donovan, and G. Holmes, "Hydrogen Embrittlement of Austenitic Stainless Steel", Presented at The American Nuclear Society Annual Meeting, June 8-13, 1975, New Orleans, LA.

14. T. L. Capeletti and M. R. Louthan, Jr., "Tensile Ductility of Austenitic Stainless Steel in Air and Hydrogen", Journal of Engineering Materials and Technology, April 1977, p. 153.

15. G. R. Caskey, Jr., "Hydrogen Effects in Stainless Steels", Proposed for publication in: Hydrogen Effects in Iron-Based Alloys.

16. M. R. Louthan, Jr., and R. P. McNitt, Effect of Hydrogen on Behavior of Materials, edited by A. W. Thompson and I. M. Bernstein, p. 496, The Metallurgical Society of AIME, N. Y. (1976).

17. A. R. Troiano, Trans ASM, Vol. 52, p. 54 (1960).

18. C. D. Beachem, Met. Trans., Vol. 3, p. 437, (1972).

19. J. A. Donovan, "Release of Hydrogen from Metals During Plastic Deformation", presented at the AIME 5th Annual Spring Meeting, May 29, (1979). Philadelphia.

20. M. R. Louthan, Jr., G. R. Caskey, Jr., J. A. Donovan and D. E. Rawl, Jr., Hydrogen Damage, edited by C. D. Beacham, p. 289, ASM, Metals Park, OH (1977).

21. J. M. Hyzak, D. E. Rawl, Jr., M. R. Louthan, Jr. "Hydrogen Affected Impact Behavior of Type 304L Stainless Steel", Scripta Metallurgica, Vol. 15 p. 937 (1981).

22. B. C. Odegard, J. A. Brooks, A. J. West, "The Effect of Hydrogen on the Mechanical Behavior of Nitrogen Strengthened Stainless Steel", p. 116 in Effect of Hydrogen on Behavior of Materials. Metallurgical Society of AIME, PA (1976).

23. J. A. Wagner, M. S. Thesis, Department of Materials Engineering, Virginia Tech (1982).

24. A. J. West and M. R. Louthan, Jr., "Dislocation Transport and Hydrogen Embrittlement", Met. Trans., Vol. 10A, p. 1675 (1979).

25. Beverly Lewis, Master's Thesis, V.P.I. & S.U.

26. G. R. Caskey, "Fractography of Hydrogen-Embrittled Stainless Steel", presented at the 106th AIME Annual Meeting, March 6-10, 1977, Atlanta, GA.

27. G. R. Caskey, Jr., "The Role of Twinning and Transformation in Hydrogen Embrittlement of Austenitic Stainless Steel", in Environmental Degradation of Engineering Materials, V.P.I., Blacksubrg, VA (1977).

28. A. J. West and J. H. Holbrook, "Hydrogen in Austenitic Stainless Steels: Effects of Phase Transformations and Stress State", Hydrogen Effects in Metals, ed. I. M. Bernstein and A. W. Thompson, (1980).

29. G. E. Dieter, Mechanical Metallurgy, 2nd edition, McGraw Hill Book Co., p. 555 (1976).

30. Henry Otto, A. R. Dowling, and R. W. Sullivan, "A Comparison of the Effects of Explosive Forming and Static Deformation on the Mech. Prop. of Pressure Vessel Steels", Met. Trans., Vol. 4, p. 657 (1973).

31. A. W. Thompson, "Ductility Losses in Austenitic Stainless Steels Caused by Hydrogen", Hydrogen in Metals Conference, Sept. 23-27, 1973, Seven Springs, Penn.

32. B. C. Odegard and A. J. West, "On the Thermo-mechanical Behavior and Hydrogen Compatability of 22-13-5 Stainless Steel", Mat. Sci. Eng., 19, p. 261 (1975).

33. M. R. Louthan, Jr., J. A. Donovan, and D. E. Rawl, Jr., Corrosion, Vol. 29, p. 108, (1973).

34. G. R. Caskey, Jr., "The Effect of Hydrogen on Work Hardening of Type 304L Austenitic Stainless Steel", proposed for publication in Scripta Met.

35. M. R. Louthan, Jr., Scripta Met., Vol. 17, p. 451, (1983).

36. A. W. Thompson and J. M. Bernstein, "Environmental Fracture of Aluminum Alloys and Stainless Steels as a Function of Composition and Microstructure".

37. C. L. Briant, "A Fractographic Study of Hydrogen Assisted Cracking in Austenitic Stainless Steels".

38. A. J. West, Jr. and M. R. Louthan, Jr., Met. Trans A, Vol. 13A, p. 2049 (1982).

39. Ray Wasielewski, Master's Thesis.

40. George R. Caskey, Jr., Hydrogen Compatibility Handbook for Stainless Steels.

41. George R. Caskey, Jr., "Fracture of Fe-Cr-Mn Austenitic Steel" paper presented at 108th Annual AIME Meeting, New Orleans, L.A. (1979).

42. F. W. Schaller and V. F. Zackay, "Low Temperature Embrittlement of Austenitic Cr-Mn-N-Fe Alloys", Trans. ASM 51, 609 (1959).

43. H. H. Uhlig and R. A. White, Trans. ASM 52, 830-847 (1960).

44. J. D. Defilippi, K. G. Brickmer and E. M. Gilbert, "Ductile to Brittle Transition inAustenitic Chromium Manganese-Nitrogen Stainless Steel", Trans. Met. Soc. AIME 245, 2141 (1969).

45. G. R. Caskey, Jr., "Notch and Hydrogen Effects on Sensitized 21-6-9 Stainless Steel", TMS-AIME Meeting, 9/16-20, (1979), Milwaukee, Wisc.

The vita has been removed from the scanned document

IMPACT PROPERTIES OF AUSTENTIC STAINLESS STEELS

by

Cindy Kornegay

(Abstract)

Austenitic stainless steels make suitable choices for use in aggressive environments. Both Tenelon and Nitronic-40 are high strength austenitic steels which have been tested for use in various environments. In impact tests of Nitronic-40 stainless steel, high energy rate forming (HERFing) the material prior to testing, caused a marked improvement in toughness up to a certain level. Hydrogen embrittlement studies show that hydrogen segregation to twins, and second pahse particles prior to testing adversely effect the mechanical properties of metal assuming a high enough hydrogen lattice concentration. Hydrogen embrittlement processes in austenitic stainless steels occur primarily by hydrogen induced weakening of specific metallographic interfaces. Impact tests of Nitronic-40 and Tenelon demonstrate that hydrogen effects manifest themselves as a promotion of faceted fracture along interfaces in the metal lattice. The extent of this weakening increases as the hydrogen content in the sample is increased as evidenced by

the negligible effect in the 10 ksi charged Nitronic-40 and greater effect in 20 ksi charged Nitronic-40. Tenelon also experienced a hydrogen induced increase in the DBTT. The combined results of these tests support a decohesion type embrittlement mechanism with the decohesion occurring at the interfaces, without the need for dislocation transport of hydrogen.